

# **Investigating Role of Tyrosyl-DNA Phosphodiesterase 1 (TDP1) In Non-Homologous End Joining (NHEJ)**

BY

JING LI

B.S., China Pharmaceutical University, 2010

THESIS

Submitted as partial fulfillment of the requirements for  
the degree of Doctor of Philosophy in  
Medicinal Chemistry in the Graduate College of the University of Illinois at  
Chicago, 2017  
Chicago, Illinois

Defense Committee:

Les Hanakahi, Chair and Advisor

John Nitiss, Department Of Biopharmaceutical Sciences

Joanna Burdette

Alexander Mankin

Douglas Thomas

This thesis is dedicated to my girlfriend, Katherine Zhen, without whom it would never have been accomplished.

## ACKNOWLEDGMENTS

First I would like to thank my advisor **Dr. Les Hanakahi**. It has been a great lifetime memory to be her first Ph.D. student graduated from University of Illinois at Chicago-Rockford. She has taught me how to be a motivated-, productive- and enthusiastic-woman scientist in the Ph.D. pursuit. I would also like to acknowledge my committee members, **John Nitiss, Joanna Burdette, Alexander Mankin, Douglas Thomas** for providing advises that helped me accomplish my research. Especially, I am very grateful for the help and collaboration provided by **Dr. John Nitiss** and **Dr. Karin Nitiss**. Working together with these fantastic scientists has been a great pleasure.

A special acknowledgment goes to my beloved girlfriend: **Katherine Zhen**. She has been extremely supportive to my life for 5 years. She gives me the motivation to be a better person in so many ways. **Matthew Summerlin** has been my lab mate for 5.5 years. He is a true friend and an amazing man. I appreciate his kind help and glowing personalities that brought me happiness in US. As a student came alone from China, I am truly grateful for the kindness and friendship all the **Ph.D. students** gave me. I want to specifically thank **Matthew Gilbertson**, his wife **Rachael Gilbertson**, and **Rachael's family**. They gave me a lot warm memories in the past 4 years. At last but not least, I want to thank my **parents** for their endless support and love.

JL

## TABLE OF CONTENTS

### CHAPTER 1

#### INTRODUCTION

Overview	1
1-1 DNA double-strand break repair (DSBR)	2
1-2 NHEJ required factors: protein structure, macromolecular interactions and roles in NHEJ	3
1-2-1 Ku	8
1-2-2 DNA-dependent protein kinase catalytic subunit (DNA-PKcs)	8
1-2-3 DNA ligase IV and XRCC4	10
1-2-4 XLF	13
1-3 The molecular mechanism of NHEJ	15
1-4 Tyrosyl DNA phosphodiesterase 1 (TDP 1)	23
1-4-1 Tyrosyl DNA phosphodiesterase 1 repairs Topoisomerase 1-mediated DNA damage and TDP1 enzymatic mechanism	27
1-4-2 TDP1 Structure	28
1-4-3 TDP1 is capable of processing a variety of DNA ends	30
1-4-4 Mutation of TDP1-H493 results in neurological diseases spinocerebellar ataxia with axonal neuropath (SCAN1)	32
1-4-5 Role of TDP1 in DNA double strand repair by NHEJ	34

### CHAPTER TWO

#### MATERIALS AND METHODS

	42
2-1 Plasmids, cell culture and antibodies used	44
2-2 Transformation of plasmid in E. coil	45
2-3 Growth of E. coil and induction of protein expression	46
2-4 Purification of his-tagged protein	47
2-5 Purification of Glutathione S-transferase (GST)-tagged proteins	49
2-6 Generate maltose binding protein (MBP)-tagged protein cell lysate	50
2-7 Affinity capture (pull-down) assay using His-TDP1 protein and Hi-NTA resin	50
2-8 Affinity capture (pull-down) assay using cell lysate expressing GST-tagged protein and GST-sepharose resin	51
2-9 Affinity capture (pull-down) assay using cell lysate expressing MBP-tagged protein and Amylose resin	52
2-10 Oligonucleotide 32p labeling reaction	53

## **TABLE OF CONTENTS (continued)**

2-11 TDP1 enzymatic activity assay	54
2-12 TDP1 Knockout by CRISPR/Cas9	55
2-13 Drug sensitivity assay	57
2-14 Clonogenic survival assay for ionizing radiation	57
2-15 Generate EJ5-GFP integrated HEK cell lines	58
2-16 End joining efficiency assay	58
2-17 End joining junction sequencing	59
2-18 Generate 100% perfect junction positive control	61
2-19 In vitro NHEJ activity assay	62
 <b>CHAPTER THREE</b>	
<b>TDP1 PHYSICALLY INTERACTS WITH XLF</b>	64
 Introduction	65
3-1 Expression and purification of his-TDP1 and GST-XLF	66
3-2 TDP1 physically interacts XLF	69
3-3 TDP1 mutants (TDP1- $\Delta$ N, TDP1-H263A, TDP1-H493R) retain the ability to interact with XLF	75
3-4 The C-terminal domain of XLF is required for interaction with TDP1	83
3-5 XLF stimulates TDP1 enzymatic activity on dsDNA, but not on ssDNA	89
 <b>CHAPTER FOUR</b>	
<b>TDP1 IS REQUIRED FOR EFFICIENT NON-HOMOLOGOUS END JOINING IN HUMAN CELLS</b>	99
 Introduction	100
4-1 Generation and characterization of TDP1-knockout cells	101
4-2 TDP1-knockout cells have reduced end joining efficiency	109
4-3 TDP1 is required for efficient NHEJ in vitro	116
4-4 TDP1-knockout cells have different end joining accuracy	120
4-5 Phosphorylation of TDP1 at serine-81 regulates TDP1 participation in NHEJ	124
 <b>CHAPTER FIVE</b>	
<b>DISCUSSION</b>	129
 5-1 Biochemical evidence for TDP1 participation in human NHEJ: TDP1 physically interacts with NHEJ required factor XLF and XLF stimulates TDP1 enzymatic activity on dsDNA but not ssDNA	130

## **TABLE OF CONTENTS (continued)**

5-2 Biological evidence for TDP1 participation in human NHEJ: TDP1 is required for efficient NHEJ in human cells	131
5-3 TDP1-deficiency changes the spectrum of end joining products: TDP1-knockout cells have different spectrum of end joining junctions	133
5-4 Role of TDP1 in NHEJ	134
<b>REFERENCES</b>	141
<b>VITA</b>	166

## SUMMARY

A study of the role of tyrosyl-DNA phosphodiesterase 1 (TDP1) in non-homologous end joining (NHEJ) was carried out using cell culture, biochemical, genetic assays. All the experiments were at least done in triplicate.

### Biochemical assays:

Human TDP1 physically interacted with the required NHEJ protein -XLF. This interaction also stimulated DNA binding for both TDP1 and XLF, and formation of TDP1:XLF:DNA complexes. TDP1-S81 phosphomimetic, TDP1-S81E, had 10-fold reduced XLF binding. TDP1 can remove adducts from DNA 3' ends, and TDP1:XLF interactions stimulated this activity on double-stranded, but not on single-stranded DNA.

### Cell culture:

CRISPR/Cas9-mediated genome editing was used to generate TDP1-knockout HEK 293 cells, which showed an expected increase sensitivity to Topoisomerase 1 poisoning and ionizing radiation. Using a chromosomally- integrated end-joining reporter substrate, we observed an average 4-fold reduction in repair of I-SceI-induced DSBs in TDP1-KO cells as compared to wild type cells. Ectopic expression of TDP1-S81E in TDP1-knockout cells failed to restore NHEJ activity.

## **SUMMARY (continued)**

Genetic assay:

NextGen sequencing of end-joining junctions generated in this reporter system showed that TDP1 deficiency resulted in increased use of microhomology in joining.

Our observations support the hypothesis that TDP1 participates in mammalian NHEJ, and contribute important details to our understanding of DNA repair.



## LIST OF TABLES

TABLE I. EFFECTS OF TDP1 DEFICIENCY IN DIFFERENT SPECIES	40
TABLE II. ANTIBODIES USED	44

## LIST OF FIGURES

Figure 1-1. Major DSBR repair pathways in mammalian cells	7
Figure 1-2-1. Structure of Ku	18
Figure 1-2-2. Structure of DNA-PKcs	19
Figure 1-2-3. Ligase mechanism and structure of ligase IV, XRCC4 and ligase IV-XRCC4 Complex	20
Figure 1-2-4. Structure of XLF	22
Figure 1-3. Required factors for non-homologous end joining (NHEJ)	26
Figure 1-4-1. Top1 and TDP1 enzymatic mechanisms	37
Figure 1-4-2. TDP1 structure	38
Figure 1-4-3. TDP1 can process a variety of DNA ends	39
Figure 3-1. Column purified his-TDP1 and GST-XLF	68
Figure 3-2A. MBP-XLF lysate used in affinity capture assay	72
Figure 3-2B. Purified, recombinant TDP1 used in affinity capture assay	73
Figure 3-2C. His-TDP1 physically interacts with MBP-XLF	74
Figure 3-3A. Diagrams of TDP1 proteins used in affinity capture assays	78
Figure 3-3B. Purified, recombinant TDP1 proteins used in affinity capture assays	79
Figure 3-3C. Diagram of substrate used for TDP1 enzymatic activity assay	80
Figure 3-3D-G. Enzymatic activity of purified, recombinant TDP1 proteins	80

## LIST OF FIGURES (continued)

Figure 3-3H. Physical interactions between active site and N-terminal deletion mutants of TDP1 and XLF	82
Figure 3-4A. C-terminal deleted MBP-XLF lysate used in affinity capture assay	85
Figure 3-4B. C-terminal domain of XLF is required for interaction with TDP1	86
Figure 3-4C. MBP-XLF-K293A lysate used in affinity capture assay	87
Figure 3-4D. XLF-K293A had reduced interaction with TDP1	88
Figure 3-5A. Single-strand substrate used in TDP1 enzymatic assay	92
Figure 3-5B. Sequencing gel provides suitable separation between ssDNA 3'-biotinylated substrate and the product generated by TDP1	92
Figure 3-5C. Double-strand substrate used in TDP1 enzymatic assay	93
Figure 3-5D. Denaturing sequencing gel can separate double-strand biotinylated substrate and TDP1 generated product	93
Figure 3-5E. Purified, recombinant his6-flag-XLF used in TDP1 activity assay	94
Figure 3-5F. XLF has no effect on TDP1 enzymatic activity on ssDNA	95
Figure 3-5G. XLF increased TDP1 enzymatic activity on dsDNA	95
Figure 3-5H. XLF increased TDP1 enzymatic activity on dsDNA (TDP1 titration)	96
Figure 3-5I. XLF increased TDP1 enzymatic activity on dsDNA but not on ssDNA (TDP1 titration)	97
Figure 3-5J. Summary of 3 independent TDP1 activity experiments	98
Figure 4-1A. Schematic representation of the CRISPR/cas9 strategy used to knockout TDP1 expression	104
Figure 4-1B. Mutations near CRISPR/Cas9 target site sequences in TDP1-KO cells	105
Figure 4-1C. TDP1-KO cells lack detectable TDP1 expression	106

## LIST OF FIGURES (continued)

Figure 4-1D. TDP1-deficiency dramatically increases camptothecin (CPT) sensitivity in TDP1 KO cells 7D1, 8A3 and 8A5	107
Figure 4-1E. TDP1-KO cells 7D1, 8A3, and 8A5 are sensitive to ionizing radiation (IR) as compared to WT cells	108
Figure 4-2A. Schematic diagram for the EJ5 end-joining reporter system	111
Figure 4-2B. Representative FACS analysis of WT HEK293 cells with EJ5-GFP end joining reporter system	112
Figure 4-2C. TDP1-KO cells have reduced end-joining efficiency	113
Figure 4-2D. Ectopic expression of catalytic inactive TDP1 in TDP1-KO cells partially restored end joining efficiency	114
Figure 4-2E. Ectopic expression of SCAN1 mutant TDP1 in TDP1-KO cells failed to restore end joining efficiency	115
Figure 4-3A. NHEJ in vitro assay is XRCC4 and DNA-PKcs dependent	117
Figure 4-3B. Extracts prepared from TDP1-KO cells have reduced NHEJ efficiency <i>in vitro</i>	118
Figure 4-3C. Summary of 4 independent NHEJ experiments	119
Figure 4-3D. NHEJ factors (Ku70, Ku80, ligase IV, XLF, XRCC4 and DNA-PKcs) in TDP-KO cells were equally expressed as compared to WT cells	119
Figure 4-4A. TDP1 affected end joining junctions in EJ5-GFP assay	121
Figure 4-4B. Detail of junction sequences from WT-EJ5GFP and TDP1-KO-EJ5GFP cells	122
Figure 4-5A. Ectopic expression of phosphor-mimetic TDP1 in TDP1-KO cells failed to restore end joining efficiency	126
Figure 4-5B. Ectopic expression of TDP1-WT, TDP1-S81A and TDP1-S81E proteins results in equal amounts of TDP1 proteins in TDP1-KO cells	126
Figure 4-5C. Effect of TDP1- S81 mutation on CPT resistance in TDP1-KO cells	127

## **LIST OF FIGURES (continued)**

Figure 4-5D. Mutation of TDP1-S81 reduces interaction with XLF	128
Figure 5. Role of TDP1 in NHEJ	137

## LIST OF ABBREVIATIONS

5'dRP	5'deoxyribose-phosphate
ACV	Acyclovir
altNHEJ	alternative NHEJ
AP	apurinic/apyrimidinic
APE1	AP endonuclease 1
APLF	aprataxin-and-PNK-like factor
APTX	aprataxin
Ara-C	cytarabine
ATM	ataxia-telangiectasia mutated
ATR	ATM- and Rad3-Related
AZT	zidovudine
BER	base excision repair
BFP	blue fluorescent protein
BRCT	BRCA1 C-terminal
BSA	Bovine Serum Albumin
CAM	chloramphenicol
cNHEJ	classical NHEJ
CPT	camptothecin
DDR	DNA damage response
DNA-PKcs	DNA-dependent protein kinase, catalytic subunit
DSBR	DSBs repair
DSBs	DNA double-strand breaks
dsDNA	double-strand DNA
DTT	Dithiothreitol
EDTA	ethylenediaminetetraacetic acid
EtBr	ethidium bromide
Exo1	Exonuclease 1
FACS	fluorescence activated cell sorting
FBS	Fetal Bovine Serum
GST	Glutathione S-transferase
HEAT	Huntington elongation factor 2, A subunit of protein phosphatase 2A and TOR1
HEK293	human embryonic kidney cell line 293
HPLB	hypotonic lysis buffer
HR	homologous recombination
HSB	high salt buffer
IP <sub>6</sub>	inositol hexakisphosphate
Ku	Ku70/80 heterodimer
LN	liquid nitrogen

## LIST OF ABBREVIATIONS (continued)

MBP	maltose binding protein
MRN	Mre11-Rad50-Nbs1
NHEJ	non-homologous end joining
PAXX	Paralog of XRCC4 and XLF
PIKK	phosphatidylinositol 3-kinase-like kinase group
PIKKs	phosphatidylinositol-3-kinase-like kinase
PMI	Personal Molecular imager phosphorimager
PMSF	phenylmethane sulfonyl fluoride
POT1	protection of telomeres 1
RT	room temperature
SAP	SAF-A/B, Acinus and PIAS motifs
SCAN1	spinocerebellar ataxia with axonal neuropathy
SCID	severe combined immune deficiency
SOC	Super Optimal broth with Catabolite repression
ss61-bio	biotinylated single-strand 61-mer oligonucleotide
SSBR	single strand break repair
ssDNA	single-stranded DNA
TDP1	Tyrosyl-DNA phosphodiesterase 1
TDP1-KO	TDP1 knockout
TIN2	TRF1-interacting nuclear factor 2
Top1	Topoisomerase 1
Top1cc	Top1 cleavage complexes
TRF1	telomeric repeat-binding factor 1
WRN	Werner syndrome helicase/exonuclease
WT	wild type
XLF	XRCC4-like factor protein
XRCC4	X-ray repair cross-complementing 4

## **Chapter 1**

### **Introduction**



## **Overview**

DNA double-strand breaks (DSBs) are one of the most toxic types of DNA damage [1]. DSBs can be generated by external DNA damaging agents or internal physiological DNA rearrangement processes. Efficient and accurate repair of DSBs is necessary to maintain genome integrity and cell survival. Failure to repair DSBs can lead to cell cycle arrest and apoptosis [2]. Misrepair of DSBs can introduce mutations at the site of repair, or cause chromosomal translocations [3]. To repair DSBs in a variety of circumstances, such as different phases of cell cycle, cells have developed multiple DSBs repair pathways. Among the pathways for DSBs repair (DSBR), homologous recombination (HR) and non-homologous end joining (NHEJ) are the best characterized and responsible for the majority of DSBR in mammalian cells [4, 5].

The focus of my research is NHEJ, which does not use a template to repair DSBs [6]. This allows cells to employ NHEJ throughout the entire cell cycle. This is particularly important, during G0, G1 and early-S phases of the cell cycle when a homologous DNA template is not available. Because NHEJ does not use an undamaged homologous DNA strand as a template, this pathway is generally error prone [7-11]. Yet the majority of NHEJ junctions are error free. The mechanism(s) by which NHEJ minimize error are not well known.

Tyrosyl-DNA phosphodiesterase 1 (TDP1) was found to regulate NHEJ fidelity on undamaged DNA ends in yeast [12]. Because TDP1 is conserved across species from yeast to humans, we hypothesize that TDP1 participates in NHEJ in human cells.

### **1-1 DNA double-strand break repair (DSBR)**

DSBs can arise during a variety of situations, such as during DNA replication when replication fork collides with a DNA lesion [13], during meiosis [14] and in non-replicating cells with oxidative damage [15, 16]. Cells will respond by sensing the DSBs, triggering cell cycle arrest, activating the appropriate DSBR pathway, or, in the event of persistent unrepaired DSBs, -initiating programmed cell death [17]. In eukaryotes, the DNA damage response (DDR) is regulated by the DDR signaling pathway. Among the proteins in signaling pathways, DDR kinases orchestrate the signaling cascade by phosphorylation of a variety of proteins which participate in a wide range of DNA processing [18]. The most upstream DDR kinases in mammalian cells include ATM (ataxia-telangiectasia mutated), ATR (ATM- and Rad3-Related), and DNA-PKcs (DNA-dependent protein kinase, catalytic subunit) [19, 20]. All three of them belong to phosphatidylinositol-3-kinase-like kinase (PIKKs) family of protein kinases, yet the roles of these kinases are distinct. ATM is mainly activated by DSBs, whereas ATR responds to variety DNA lesions, including DSBs and DNA forms of damage that can interfere with replication. Like ATM, DNA-PKcs is also activated by DSBs, and participates mainly in the non-homologous end joining (NHEJ) pathway of DSBR [21]. In DSBR, ATM is recruited to

the DSBs and activated by the Mre11-Rad50-Nbs1 (MRN) complex [22]. Activated ATM can then phosphorylate histone variant H2AX to form  $\gamma$ H2AX, which will rapidly spread on chromatin over 500 kb flanking the DSB [23]. Because my project focus on NHEJ, the role of ATM in NHEJ will be further discussed in the following sections.

Because DSBs are very dangerous lesions that can occur in all cell types (replicating and non-replicating), multiple repair mechanisms are necessary. In mammalian cells, there are two major DSBs repair pathways: -homologous recombination (HR) and non-homologous end joining (NHEJ).

HR employs extensive sequence identities (homology) to template repair, therefore it is considered to be the most accurate (or error free) form of DSBR. The source of the homologous template is the intact sister chromatid, and this requirement restricts HR to S/G2 phase of cell cycle [24]. The initiation step of HR is resection of the DNA ends to generate long 3' ssDNA. This end resection can be achieved by nucleases such as the endonuclease/ exonuclease Mre 11, the 5' to 3' exonuclease Exo1 and the helicase/endonuclease Dna2 in late S and early G2 [25]. The 3' ssDNA tail will first bind by abundant ssDNA-binding protein RPA and subsequently exchanged by Rad 51. Rad 51 (in mammalian cells), which is a DNA strand exchange protein, binds to the 3' ssDNA to form a nucleoprotein filament. This filament promotes strand invasion into a homologous double-strand DNA (dsDNA), serves as a primer, for copying the information from the donor chromosome by subsequent DNA synthesis [26]. The synthesized DNA

dissociates from the donor duplex DNA, then anneals to the other DNA end and the HR will be finished via ligation by DNA ligase I [27].

NHEJ, which includes classical NHEJ (cNHEJ) and alternative NHEJ (altNHEJ) [28] (Figure 1-1), directly and efficiently joins DNA ends without the use of a homologous template. The disadvantage of template-independent DSB repair is the increased likelihood of mutations at the repair junction [29, 30], making NHEJ more prone to error as compared to HR. Although classical NHEJ does not require DNA end resection and searching for template, it is not a simple end-to-end ligation. The challenges for NHEJ include detection of the DSB, tethering and alignment of the DNA ends to prevent translocation, and processing to remove any damage from the DNA.

(From now on, “NHEJ” in the thesis is referring to classical NHEJ.)

NHEJ incorporates a series of factors to resolve these challenges and finally ligate DSBs. Factors required for classical NHEJ in mammalian cells include the Ku70/80 heterodimer (Ku), the DNA-dependent protein kinase catalytic subunit (DNA-PKcs), the X-ray repair cross-complementing 4 (XRCC4)-ligase IV complex and the XRCC4-like factor protein (XLF, also as known as Cernunnos)[31-39]. The basic mechanism of NHEJ is conserved across all taxa, including bacteria, and the majority of the required factors are conserved from yeast to humans [40]. The structures, roles in NHEJ and protein-protein interactions of these required factors will be discussed in the next section.

NHEJ can repair DSBs caused by exogenous sources, such as ionizing radiation, and endogenous sources such as V(D)J joining and class switch recombination that generate programmed DSBs for the development of lymphocyte development [41]. The (V(D)J) recombination is a process to rearrange DNA that can generate diversity of antibodies [42]. To generate diversity, V(D)J recombination produces programmed DSBs, which are then repaired by NHEJ. Defects in V(D)J recombination in human or mouse result in severe combined immune deficiency (SCID) and T and B lymphocytes deficiency [43]. Study in SCID mice showed compromised immune system (alymphocytosis) along with increased cellular sensitivity to ionizing radiation, that will generate DSBs majorly repaired by NHEJ [44, 45]. Therefore, immunodeficiency and radiosensitivity, or sensitivity to radiomimetic drugs such as bleomycin, are associated with defects in NHEJ [46, 47] [48].

Figure 1-1

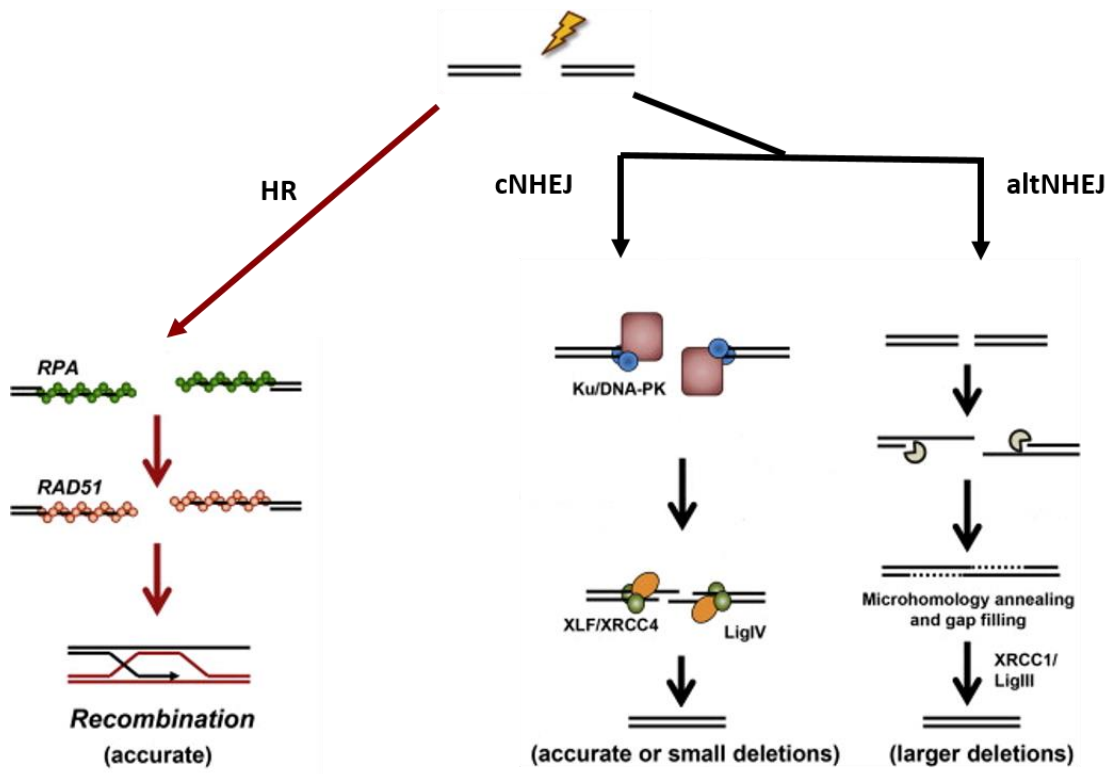


Figure 1-1 Major DSB repair pathways in mammalian cells

HR: -homologous recombination, NHEJ: -non-homologous end joining, cNHEJ: - classical NHEJ, altNHEJ: -alternative NHEJ.

Adapted from Shibata et. al., 2014 [49]

## **1-2 NHEJ required factors: protein structure, macromolecular interactions and roles in NHEJ**

### **1-2-1 Ku**

Human Ku is a heterodimer that is comprised of the Ku70 (70 kD) and Ku80 (86 kD) proteins. Humans Ku70 is encoded by the *XRCC6* gene located at position NC\_000022.11 on chromosome 22. Humans Ku80 is encoded by the *XRCC5* gene located at position NC\_000002.12 on chromosome 2.

The ring shape of Ku (Figure 1-2-1, lower panel) allows it to load specifically onto DNA ends, by threading the DNA through the central channel of the Ku protein to form an extremely stable Ku-DNA complex through the central channel and translocate on DNA strands [50-52]. In addition, Ku binding can protect the exposed DNA ends from nuclease attack (end resection). Because Ku is a ring-shaped protein that threads onto the DNA, it will be theoretically trapped on the DNA after final ligation step of NHEJ. Recent studies show that Ku can be removed from the DNA by ubiquitination and subsequent proteasomal degradation of the Ku80 subunit [53, 54]. However, the mechanism to remove Ku from DNA after DNA repair is not completely understood yet.

Ku70 and 80 share similar domain organization and structure (Figure 1-2-1, upper panel), but their terminal domains have different functions [55, 56]. The N-terminal (von Willebrand A (vWA) domain) of Ku70 has 5'dRP (5'deoxyribose-phosphate)/AP

(apurinic/aprimidinic) lyase activity [57] while N-terminal vWA domain of Ku80 can interact with the aprataxin-and-PNK-like factor (APLF), which is thought to promote assembly and activity of the required NHEJ factors [58]. The C-terminal domain of Ku70 (SAF-A/B, Acinus and PIAS motifs (SAP) domain) has DNA binding activity that is distinct from DNA binding mediated by the toroid structure of the heterodimer [59]. The C-terminal domain of Ku80, which has extended length as compared to Ku70 and lack of the SAP domain, mediates interaction with DNA-PKcs [60], and activates DNA-PKcs protein kinase activity [61]. The central domains of Ku70 and Ku80 facilitate heterodimerization and interaction with XLF [38].

The structure of Ku promotes a variety of protein-protein interactions with NHEJ factors and help characterizes Ku as the protein in the initiation step of NHEJ to recruit other parts of the NHEJ machinery [33, 34, 36, 38]. Both Ku70 and Ku80 knockout mice suffer from immunodeficiency caused by defects in V(D)J recombination, and radiosensitivity, indicating Ku is essential to NHEJ [62-65].

Ku is not just a scaffolding protein for NHEJ. The 5'dRP lyase activity [57] indicating an enzymatic end processing role of Ku in NHEJ. Ku is capable of removing abasic sites close to the DSB, especially at 5' overhang [66], suggesting Ku may contribute to the overall accuracy of NHEJ. A cluster of basic amino acids located between the base of N-terminal domain of Ku80 and central domain of Ku70 bind the small, phosphate-rich molecule inositol hexakisphosphate (IP<sub>6</sub>), which is a stimulatory factor in mammalian



NHEJ [67, 68]. This Ku-IP<sub>6</sub> interaction is important for efficient repair DSBs by NHEJ *in vitro* [69], while relevance of IP6 in NHEJ has yet to be demonstrated *in vivo*.

Beside participation in NHEJ, Ku also serves in DNA damage signaling. Mutation of serine 155 in Ku70's vWA domain leads to decreased DNA damage signaling and activation of apoptosis after ionizing radiation [70]. Ku70 is also implicated as an inhibitor of apoptosis by interaction and inhibition of Bax, which is a proapoptotic factor [71, 72]. In addition to NHEJ and DNA damage signaling, Ku also participates in protection at telomeres. Because telomeres are the DNA ends of chromosomes, they can be potentially recognized as DSBs, and acted upon by DSB repair pathways. To protect telomeres, the specific TTAGGG repeats at the end of telomeres are directly bind by shelterin subunits, telomeric repeat-binding factor 1 (TRF1), TRF2 and protection of telomeres 1 (POT1), which are connected by three additional shelterin proteins, TRF1-interacting nuclear factor 2 (TIN2), TPP1 and Rap1 to form a shelterin complex. This complex protects telomere from end resection and being recognized as site of damage [73]. Ku participates in maintaining telomere length in yeast [74-76]. Studies in mice also showed that Ku protects telomeres from end to end fusion and chromosomal aberration [77, 78]. The role of Ku in protecting telomeres appears to be separate from its function in classical NHEJ since -ligase IV deficient yeast did not show telomere defects [79].

### **1-2-2 DNA-dependent protein kinase catalytic subunit (DNA-PKcs)**

Human DNA-PKcs is encoded by *PRKDC* gene, located at position NC\_000008.11 on chromosome 8. Human DNA-PKcs is a 460 kD protein kinase comprised of 4128 amino acids, which requires interaction with both Ku and DNA ends for fully activity [80]. Physical interaction of DNA-PKcs with Ku assembles the DNA-PK holo-enzyme and increases protein kinase activity by 100-fold [81]. During assembly of NHEJ factors at the DSB, Ku will recruit DNA-PKcs to the DNA end, then translocate away from the DNA ends around one helical turn to make room for binding of DNA-PKcs to the exposed DNA end [82]. The interaction between Ku and DNA-PKcs is very stable and protects the DNA ends from nuclease attack and altNHEJ [83-85].

DNA-PKcs belongs to phosphatidylinositol 3-kinase-like kinase group (PIKK) which also includes DNA repair kinases ATM and ATR [86, 87]. Once DNA-PKcs binds to Ku, it stimulates end synapsis to increase the access of ligase [88]. DNA-PKcs can phosphorylate a variety of substrates that participate in NHEJ, including Ku [89, 90], XLF [91], XRCC4 [92] and DNA-PKcs itself (autophosphorylation) [93]. The autophosphorylation sites were mapped and identified a cluster of six sites within DNA-PKcs, named the ABCDE cluster [94]. Mutation of any one of the sites did not display increased sensitivity to ionizing radiation, while when all sites were mutated to alanine, cells showed high level radiosensitivity [95]. To date the ABCDE and PQR clusters are the best known autophosphorylation sites. Interestingly, autophosphorylation of DNA-PKcs at ABCDE cluster increase DNA end access to end processing enzymes,

phosphorylation of the PQR cluster decrease DNA access [96]. It is reasonable and meaningful for DNA-PK to regulate end processing factors access to DNA ends, because it can limit the altNHEJ, which frequently generates extensive deletions, and HR outside of S/G2 phase.

DNA-PKcs is required for NHEJ. Human radiosensitive cell line –MO59 was identified to be lack of DNA-PKcs expression and DNA-PK activity [97]. Subsequent study observed immunodeficiency in the DNA-PKcs-knockout mouse, indicating a role for DNA-PKcs in V(D)J recombination [98]. Inhibition of DNA-PKcs protein kinase activity, or mutation of the domain responsible for DNA-PKcs catalytic activity in human cells revealed that the protein kinase activity of DNA-PKcs is required for NHEJ and V(D)J recombination [99].

The structure of DNA-PKcs is a C-shape clamp consist of a domain containing HEAT (Huntington elongation factor 2, A subunit of protein phosphatase 2A and TOR1) repeats, a protein kinase domain, and a Ku interaction domain at the top of the clamp/opposite the gap of clamp [100] (Figure 1-2-2). Cryo-EM showed that the central cavity of DNA-PKcs is responsible for binding dsDNA [101]. The three dimensional structure of the DNA-Ku-DNA-PKcs ternary complex showed that DNA ends were brought into close proximity forming a possible synaptic complex [102]. Atomic force microscopy also, showed that DNA-PKcs can increase tethering of multiple DNA ends

[103]. These studies suggest that DNA-PKcs might facilitate minimize distance between DNA ends (DNA end bridging) during NHEJ.

### **1-2-3 DNA ligase IV and XRCC4**

Human DNA ligase IV is encoded by gene *LIG4*, located at position NC\_000013.11 on chromosome 13. Human XRCC4 is encoded by gene *XRCC4*, located at position NC\_000005.10 on chromosome 5. DNA ligase IV and XRCC4 are recruited to the DSB by Ku and DNA-PKcs as a preformed XRCC4-ligase IV complex during NHEJ [104-107].

Ligase IV is a 109 kD protein comprised of 911 amino acids. During ligation lysine 273 (human enzyme), which is located in the ligase IV catalytic domain, is adenylated (first step). The second step is transfer of the adenyl group to the 5'-phosphate of the DNA exposed ends with (Figure 1-2-3). In the final ligation step, the adenylated 5'-phosphate is used to attack 3'-hydroxyl terminus of the DSBs, and links the termini with a new phosphodiester bond [108]. One of the most important role of XRCC4 in NHEJ is to stabilize ligase IV by protein-protein interaction [109, 110].

Because the requirement of the XRCC4:ligase IV interaction in NHEJ, it is not surprising that loss of either XRCC4 or ligase IV in mice results in embryonic lethality [111-113]. In these experiments, massive apoptosis of newly generated neurons was observed throughout the nervous system of ligase IV-deficient embryos. It is important to

note that both embryonic lethality and neuron apoptosis of ligase IV- deficient mice were rescued by p53 knockout, indicating these two phenotypes of ligase IV deficiency are caused by p53-dependent DNA damage response and neuronal apoptosis [114]. Similarly, ATM deficiency also rescued embryonic lethality and neuron apoptosis in ligase IV-deficient mice [115].

The N-terminal domain of ligase IV is required for catalytic activity and highly conserved between all three mammalian ligases I, III and IV [116]. This N-terminal domain mediates DNA binding by wrapping around the DNA [108, 117, 118]. Ligase IV has two tandem BRCA1 C-terminal (BRCT) domains that are not found in ligase I or III. The linker between these BRCT domains interacts with XRCC4 [109, 110, 119, 120].

XRCC4, which forms a dimer in NHEJ, is a 36 kD protein consists of N-terminal globular head domain, a coil-coil domain and a C-terminal domain. XRCC4 forms stable homodimers by interaction of the globular head domain and the top of the coil-coil domain. The globular head domain also mediates interaction with XLF. The coil-coil domain interacts directly with BRCT domain of ligase IV [109, 121]. The C-terminal domain is flexible and possibly to fold close to the head domain, however is absent in the crystal structure [122] (Figure 1-2-3).

XRCC4 is well known to form homodimers, as well as tetramers [121], and to form complex with ligase IV most likely with one XRCC4 homodimer to one ligase IV ratio [123]. However, the molar ratio of XRCC4 dimers to ligase IV in the human nuclei is

around 3 to 1, indicating XRCC4 homodimer may present separately from ligase IV [124]. In addition to stabilizing ligase IV, XRCC4 was found to stimulate adenylation of ligase IV *in vitro*, which is the first step of ligase IV mechanism [125]. Another way that XRCC4 may promote NHEJ is by bridging two DNA ends for ligation, likely via interaction with Ku that present at the DSB [105]. In addition, *in vitro* study showed that purified XRCC4 can bind DNA with preference of nicked or broken ends, suggesting functions independent of DNA ligase IV [125].

### **1-2-4 XLF**

Human XLF is encoded by gene *NHEJ1*, located at position NC\_000002.12 on chromosome 2. XLF, also as known as Cernunnos, was identified as a factor required for NHEJ by both cDNA complementation of cells from an ionizing radiation sensitive human immunodeficiency patient [126] and by a yeast two-hybrid screen for XRCC4-interacting proteins [127].

XLF is a 33 kD protein comprised of 299 amino acids. The crystal structure reveals that XLF, is a dimer, with monomers consisting of an N-terminal globular head domain, a central coil-coil domain, and an unstructured C-terminal domain. The globular head domain interacts with head domain of XRCC4 and is required to form long XLF-XRCC4 filaments [128, 129]. The coil-coil domain mediates interaction between XLF monomers for homodimerization. And the C-terminal domain of XLF folds back toward the N-terminal

domain, -acts as the DNA binding domain, and also activates XRCC4-ligase IV complex [128-130] (Figure 1-2-4).

To date, no enzymatic activity has been identified for either XRCC4 or, XLF has not been found of any enzymatic activity. It appears that the major role of XLF in NHEJ is stimulation of ligase IV activity of XRCC4-ligase IV complex [131, 132]. Specifically, XLF stimulates ligation of noncohesive and mismatched DSBs, which are less favored by the XRCC4-ligase IV complex [130, 133]. XLF accumulates at DSBs within a few seconds. This response is mediated by interaction with Ku [36], which initiates NHEJ, and is not dependent on XRCC4. XLF binds dsDNA in a length dependent manner, and binds stably on DNA fragment longer than 83 bp [132, 134]. Interaction with Ku stimulates XLF binding to DNA shorter than 83bp [36]. The other role of XRCC4 is to form long and super-helical protein filaments with XLF *in vitro* [135-138]. It has been suggested that these filaments is suggested promote tethering and bridging of DSBs for final ligation in NHEJ [138]. Together, these study suggest XLF might participate early in NHEJ to increase DSBs sensing, and at a late stage to promote ligation.

Although XLF is one of the NHEJ required factor, we must note that, unlike Ku, DNA-PKcs, ligase IV and XRCC4, XLF is dispensable for V(D)J recombination in murine lymphoid cells. In contrast, patients with defective XLF were observed to have recurrent infections caused by immunodeficiency [126]. Fibroblasts from these patients failed to efficiently repair DSBs on extrachromosomal plasmid substrate, and were significantly

impaired for V(D)J recombination [126, 139]. Like XLF, the recently identified XRCC4-like NHEJ protein PAXX (Paralog of XRCC4 and XLF) [140, 141], was also not required for viability, normally growth or fertilization in mice. Surprisingly, PAXX/XLF double-knockout mice showed embryonic lethality with apoptosis in nervous system, and severely impaired lymphogenesis -phenotypes that closely resemble those of XRCC4- and ligase IV-deficient mice [142]. Similar to XLF and PAXX, ATM deficiency alone only results in very modest defects in V(D)J recombination and lymphocyte developmental, yet ATM-XLF- deficient mice showed severely impair of lymphocyte development caused by failed joining of V(D)J intermediates [143]. These studies identify XLF as an important participant in NHEJ, and V(D)J joining to be a special application of NHEJ with unique XLF requirements.



Figure 1-2-1

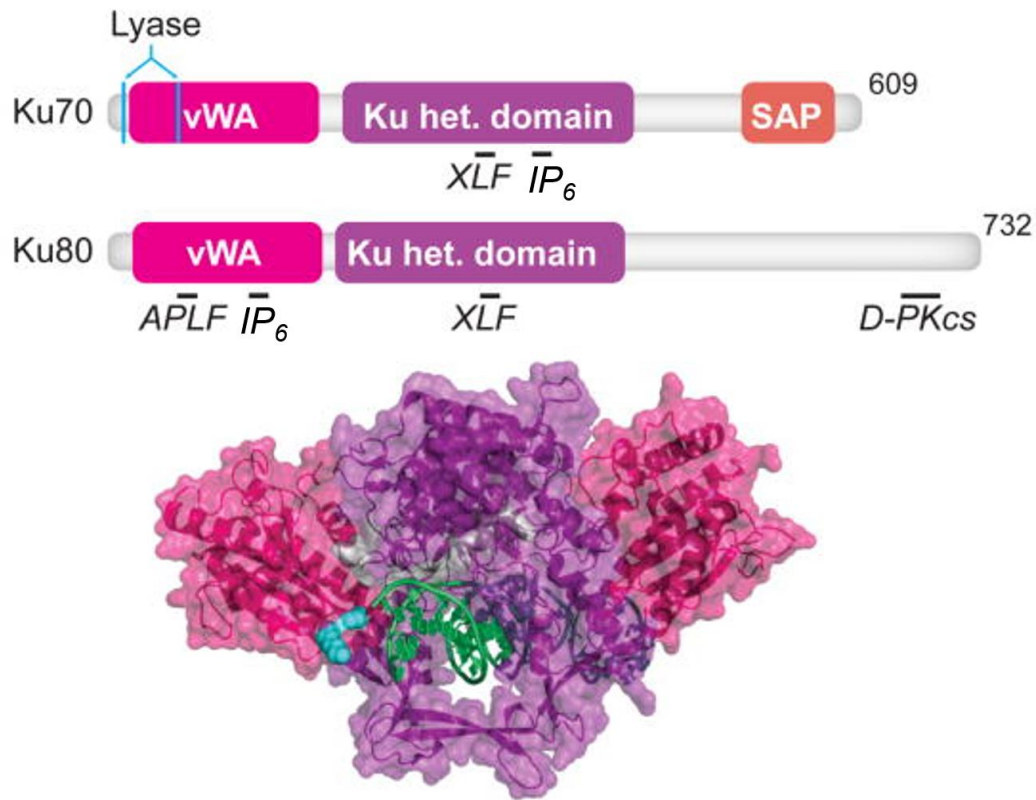


Figure 1-2-1 Structure of Ku

**Upper panel** shows the domain distribution of Ku70 (609 amino acids) and Ku80 (732 amino acids). Domains of Ku70 include the vWA (von Willebrand associated) domain (*pink*), the heterodimerization domain (Ku het. domain) (*purple*), and SAP (C-terminal SAF-A/B, Acinus and PIAS) domain (*orange*). Residues important for lyase activity in Ku70 are indicated (*cyan*). Domains of Ku80 include the vWA domain, and Ku het. domain. Ku-70/80 interactions with APLF, DNA-PKcs, and XLF are indicated.

**Lower panel** shows the crystal structure of Ku70/80 heterodimer. Color of the crystal structure corresponds to color in domain map (upper panel). DNA is shown in *green*.

Adapted from Waters et al., 2014 [144]

Figure 1-2-2

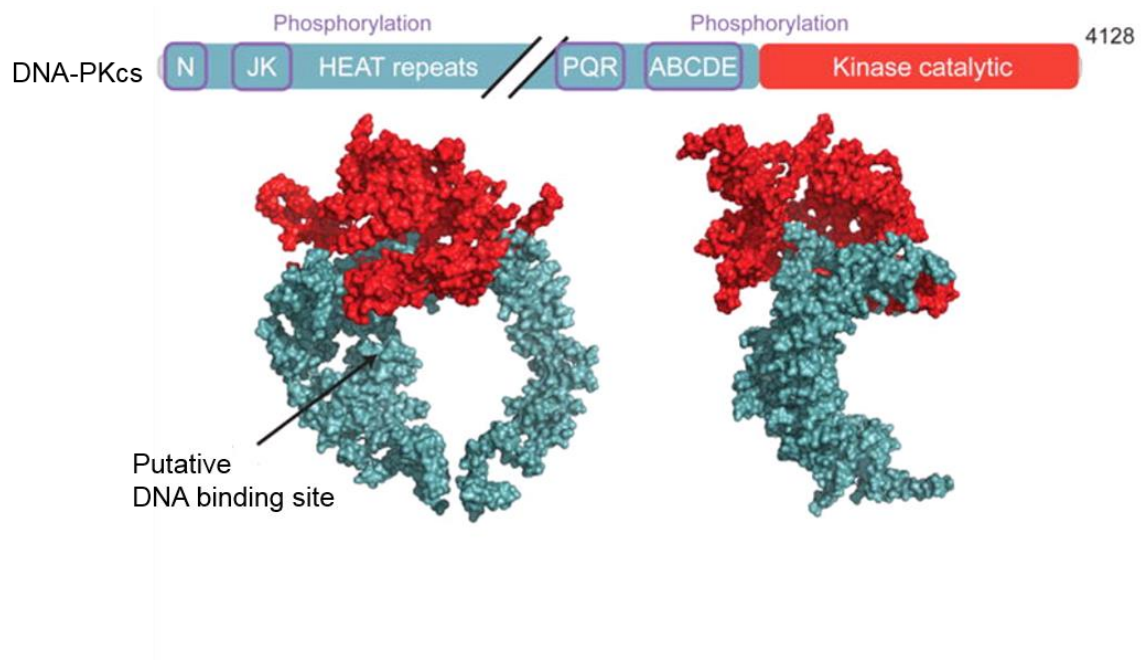


Figure 1-2-2 Structure of DNA-PKcs

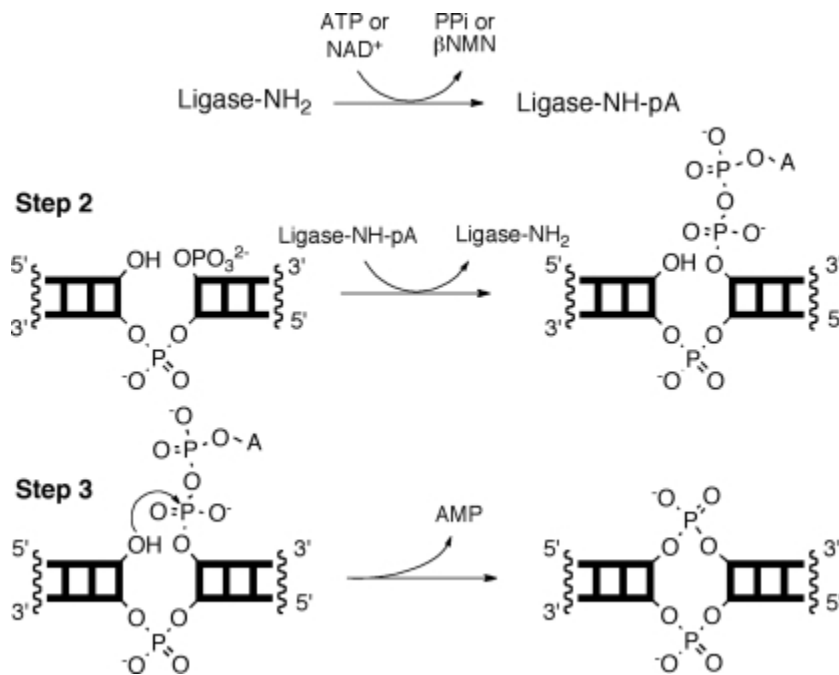
**Upper panel** shows domain distribution of DNA-PKcs (4128 amino acids). DNA-PKcs consists of an N-terminal domain (*blue*), and a relatively short protein kinase catalytic domain (*red*). Diagonal black lines represents omitted protein length. Autophosphorylation sites are shown in *boxes (purple)*. HEAT (Huntington elongation factor 2, a subunit of protein phosphatase 2A and TOR1) repeats are also indicated.

**Lower panel** shows the crystal structure of DNA-PKcs. Color of the crystal structure corresponds to color in domain map (upper panel). Putative DNA binding site is indicated by arrow. The on the right is the image on the left with 90° rotation.

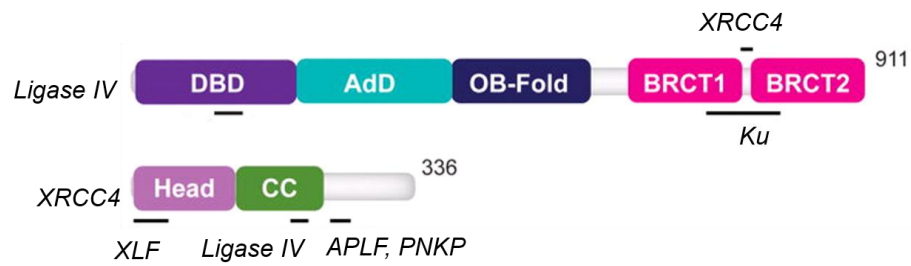
Adapted from Waters et al., 2014 [144]

Figure 1-2-3

A



B



C

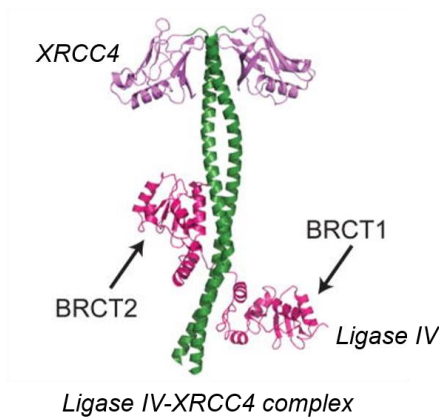


Figure 1-2-3 Ligase mechanism and structure of ligase IV, XRCC4 and ligase IV-XRCC4 complex

**(A)** shows ligase mechanism: Step 1: -the self-adenylation of an active site lysine using ATP or NAD<sup>+</sup>, depending on the ligase; Step 2: -the transfer of the adenylyl group to the 5'-phosphorylated terminus; Step 3: -the formation of the phosphodiester bond with loss of an AMP leaving group.  $\beta$ -NMN,  $\beta$ -nicotinamide mononucleotide; P, phosphate; A, 5'-adenosine.

Adapted from Lohman et al., 2011 [145]

**(B)** shows domain distribution of ligase IV (911 amino acids) and XRCC4 (336 amino acids). DNA ligase IV is consist of DNA binding domain (DBD) (*purple*), adenylation domain (AdD) (*teal*), oligonucleotide/oligosaccharide binding domain (OB-fold) (*dark blue*), and breast cancer carboxyl terminal (BRCT) domains (*pink*). Interaction sites of Artemis, Ku, and XRCC4 are indicated. XRCC4 is consist of Head domain (*lavender*), and the coiled-coiled domain (CC) (*green*). Interaction sites of XLF, ligase IV, APLF, APTX and PNKP are indicated.

**(C)** Shows the crystal structure of ligase IV-XRCC4 complex. Color of the crystal structure corresponds to color in domain map (upper panel). Only the BRCT domains are shown for ligase IV. C-terminal domain of XRCC4 is absent in the crystal structure.

Adapted from Waters et al., 2014 [144]

Figure 1-2-4

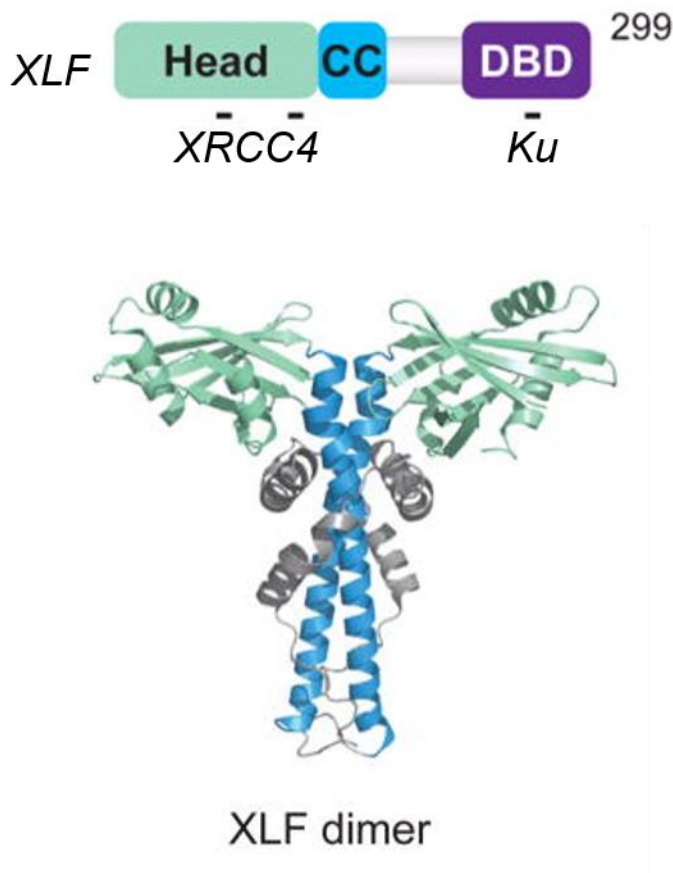


Figure 1-2-4 Structure of XLF

**Upper panel** shows domain distribution of XLF (299 amino acids). XLF is consists of a Head domain (*light green*), coil-coil domain (CC) (*cyan*), and a DNA binding domain (DBD) (*purple*).

Interaction sites of Ku and XRCC4 are indicated.

**Lower panel** shows the crystal structure of XLF homodimer. Color of the crystal structure corresponds to color in domain map (upper panel). The DNA binding domains is not shown.

Adapted from Waters et al., 2014 [144]

### **1-3 The mechanism of NHEJ**

The NHEJ pathway employs several proteins to sense the DSBs, bring the ends together in a synaptic complex, remove any of damage from exposed termini, and ligate the breaks. NHEJ is initiated by loading of the ring shaped Ku on DNA ends to form a platform onto which other Required NHEJ factors are recruited. Factors that participate in human NHEJ require DNA and Ku [146]. Using a laser system to introduce DSBs into the nuclei of Xrs6 (Ku-deficient) cells, Uematsu and colleagues found that while accumulation of DNA-PKcs at DSBs was Ku80 dependent, it did not require DNA-PKcs protein kinase activity or its DNA-PKcs autophosphorylation [147]. Interaction between Ku and DNA-PKcs is required for DNA-PKcs protein kinase activity [80] , which is required for NHEJ, and facilitates tethering the DNA ends into a synaptic complex [84]. Nick McElhinny and colleagues showed that XRCC4-ligase IV alone has very low DNA binding activity, and that Ku is required for recruitment of the XRCC4-ligase IV complex on DNA ends [106]. The interaction between Ku and XRCC4-ligase IV increases the ligation rate by 20 fold [106]. It is important to notice that between binding of Ku and initiation of NHEJ, and the final ligation reaction, the NHEJ mechanism is not well understood regarding the order of other factors recruitment.

After the initiation step, recruitment and assembly of the required NHEJ factors has been expected to proceed in a step-by-step fashion. This prevailing model for NHEJ predicts that Ku binds the DSB, recruits DNA-PKcs, and then XLF and XRCC4-ligase IV

can be recruited. Therefore, recruitment of XLF and XRCC4-ligase IV rely on DNA-PKcs binding to Ku and DSBs. However, the indirect immunofluorescence assay used for supporting the model lacks the ability to detect rapid events in cell. David Chen and his co-workers used live cell imaging to show that XLF and XRCC4 were recruited to DSBs independently of DNA-PKcs [35]. They also observed that XLF accumulated at DSBs in 5 seconds which is not likely be detected by using traditional indirect immunofluorescence method [35]. Similarly, XRCC4-ligase IV complex is recruited independent of XLF and DNA-PKcs [33]. Therefore, the recruitment of Required NHEJ factors depends only on Ku and DNA ends, and appears to proceed in the absence of a defined step-wise pathway (Figure 1-3) [6]. The flexible order of recruitment for the required NHEJ factors might be mechanistically beneficial. This flexibility may allow the NHEJ apparatus to recruit different sets of required factors to repair DSBs depending on the complexity of DNA damage (e.g. ligatable ends or not directly ligatable ends) at the exposed DNA ends [148].

Before ligation of the DNA ends, any damage at the ends must be removed to generate ligatable substrates (clean ends) e.g. 3'-hydroxyl and 5'-phosphate, that is named DNA end processing. So enzymatic DNA end processing is required in NHEJ. The end processing enzymes in NHEJ include nucleases such as Exonuclease 1 (Exo1), Mre11, Artemis [149-153], and tyrosyl-DNA phosphodiesterase 1 (TDP1) [12], aprataxin (APTX) [153], and the Werner syndrome helicase/exonuclease (WRN) [154]. DNA

polymerases (family X polymerases including Pol  $\mu$  and  $\lambda$  in mammalian cells) are also recruited to the DSBs to fill the gap prior the final ligation [155-158]. The end processing and DNA polymerization steps that can generate sequence alteration, might contribute to error in NHEJ.

Studies in yeast and mammalian cells discovered a backup end-joining system that joins DNA ends when cells lack one or more of the required classical NHEJ factors [159, 160]. This mechanism, which is characterized by use of ligase III, is now referred to as alternative NHEJ [161]. There are at least 3 characteristics of alternative NHEJ differs from that of classical NHEJ. First, alternative NHEJ frequently uses microhomology to direct joining. Second, ends joined by alternative NHEJ contains more excessive deletions. Third, the low accuracy of alternative NHEJ commonly results in chromosome translocations [162-164]. Microhomology-mediated end joining is a subset of alternative NHEJ in which use of microhomology to promote end joining is apparent at repair junctions [165, 166]. Microhomology indicates short fragments (usually 1-10 nucleotides) of DNA sequence identity. Evidence that alternative NHEJ take place in classical NHEJ-proficient cells indicated that it is not just a backup pathway that is used when classical NHEJ is not available [9].



Figure 1-3

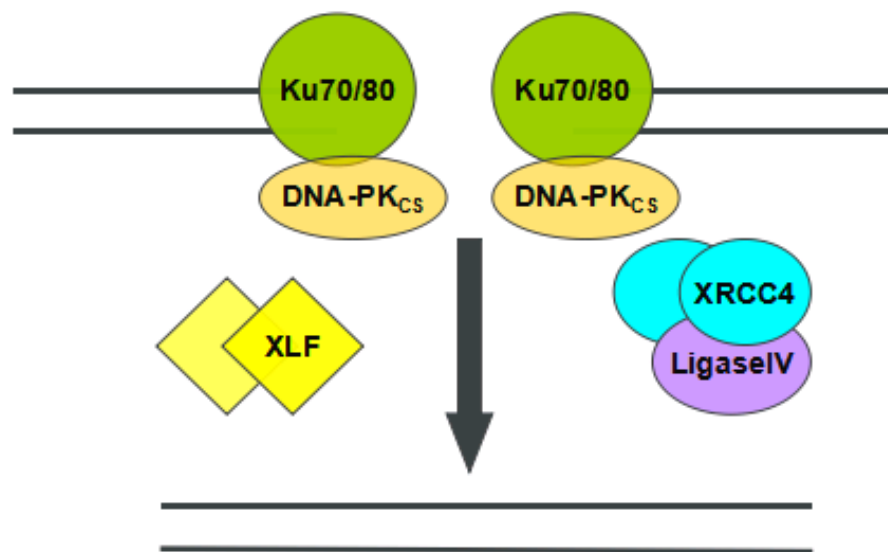


Figure 1-3. Required factors for non-homologous end joining (NHEJ)

The heterodimer Ku80/70 first binds to the DNA ends and recruit DNA protein kinase catalytic subunit (DNA-PKcs), XRCC4-ligase IV complex and XLF to ligate the ends.

## **1-4 Tyrosyl DNA phosphodiesterase 1 (TDP1)**

### **1-4-1 Tyrosyl DNA phosphodiesterase 1 repairs Topoisomerase 1-mediated DNA damage and enzymatic mechanism**

Topoisomerase 1 (Top1) regulates the topological state of DNA during replication and transcription by relaxing both positive and negative DNA supercoils [167-169]. To untwist DNA, Top1 generates a transient single-strand break by covalently linking tyrosine to the DNA 3' end to form Top1 cleavage complexes (Top1cc). The Top1cc is a transient intermediate and the Top1 protein will be released from the DNA after relaxation of the DNA supercoil and DNA strands religation (Figure 1-4-1A). DNA modification generated by endogenous sources, such as base mismatch and 8-Oxoguanosine, and by exogenous sources, such as UV lesions, can result in trapping Top1cc on the DNA [170-174]. Top1 poisons such as camptothecin (CPT) and its derivatives can also generate trapped Top1cc on DNA ends by stabilizing Top1-DNA complex [175, 176]. Unrepaired Top1cc will result in damage in genome by generating DSBs through replication and transcription fork collisions [177].

Nash and his colleagues observed protein in *Saccharomyces cerevisiae* that has unique activity to hydrolyze phosphotyrosyl bonds at 3' DNA ends. This study led to identification of TDP1 in yeast [178]. TDP1 can remove 3' tyrosine from oligonucleotide substrate, which mimicking Top1-DNA covalent complex, indicating that TDP1 participates in repair of Top1 mediated DNA damage [179, 180]. It is important to note that

TDP1 cannot remove intact full length Top1. Proteolytic digestion or denaturation of Top1 is required prior to removal by TDP1 [167, 181, 182].

The enzymatic mechanism of TDP1 involves 2 invariant histidines, which in human TDP1 are-histidine 293 (H293) and histidine 493 (H493) (Figure 1-4-1B). Removal of covalently linked 3'-phosphotyrosine begins with nucleophilic attack of the phosphodiester bond between Top1 and DNA by H293. This releases the tyrosine residue and result in formation of a TDP1-DNA covalent intermediate at the DNA 3' end. H493, which acts as a general base, will then active water molecule to hydrolyze the covalent TDP1-DNA intermediate. This releases TDP1 and leaves DNA with 3'-phosphate that will be processed by polynucleotide kinase phosphatase to restore 3'-hydroxyl [183-185].

#### **1-4-2 TDP1 Structure**

The human TDP1 protein contains 608 amino acids and is encoded by gene *TDP1*, located at position NC\_000014.9 on chromosome 14. It consists of an N-terminal domain, which is dispensable for TDP1 catalytic activity, and a C-terminal catalytic domain (Figure 1-4-2, upper panel). Interthal and colleagues observed that C-terminal catalytic domain of TDP1 is conserved between different species, while the N-terminal domain (1-150 amino acid) is poorly conserved and varies in both length and sequence

between [183]. Highly conserved amino acids are those between 262–289 and 492–522 of the human protein, which suggested that these amino acids are likely to be important for TDP1 catalytic activity. These two regions contain the highly conserved HxK(x)4D(x)6GSxN sequence, termed the HKD motif, and identified TDP1 as a member of the phospholipase D superfamily [183]. This understanding helped them identify two histidines in human TDP1, histidine 263 (H263) and histidine 493 (H493), that are important for catalytic activity. Mutation of H263 or H493 to alanine decreased TDP1 catalytic activity by more than 4 orders of magnitude or by 3,000 folds respectively. This mutational analysis suggested that TDP1 enzymatic mechanism could be similar to other members of PLD family.

The crystal structure of the C-terminal domain of human TDP1 with single-stranded DNA (ssDNA) revealed that TDP1 function as a monomer [184]. The catalytic site of TDP1, which is composed of the two HKN motifs, is located in the asymmetric substrate binding channel [184, 186]. This channel is narrow and positively charged to bind ssDNA (Figure 1-4-2 lower panel). Binding of ssDNA neutralizes the positive charge of the substrate binding channel causing it to widen. TDP1 interacts DNA substrate in a sequence nonspecific manner [187, 188], that allows TDP1 to process DNA ends at different genomic sites.

### **1-4-3 TDP1 is capable of processing a variety of DNA ends**

TDP1 is well known for its ability to repair Top1ccs, but TDP1 is not limited to this substrate. TDP1 can remove a variety of adducts from both the 3'- and 5'- ends of DNA (Figure 1-4-3), and can cleave undamaged nucleotides at an exposed DNA or RNA 3' end (3' nucleosidase activity, Figure 1-3-3) [179, 182, 189-194]. Further, TDP1 can process apurinic/apyrimidinic (AP) sites, and can serve as an alternative to the enzyme of AP endonuclease 1 (APE1) [195-201]. TDP1 orthologs are found in all organisms, where TDP1 is found in the nucleus and mitochondria [192, 202, 203]. Study in chicken, mouse and human cells have shown that TDP1 deficiency, or a defect in TDP1 function, results in increased sensitivity to a variety of DNA-damaging agents that produce lesions at DNA ends (Table 1).

Most of forms of DNA damage that can be removed by TDP1 are at the 3' of DNA. Other than Top1cc, one well recognized 3' substrate for TDP1 is the 3'-phosphoglycolate (3'-PG) (Figure 1-4-3). 3'-PG is commonly generated by ionizing radiation through oxidative DNA damage [189, 204]. Studies of radiation-damaged DNA have shown that nearly half of the DNA strand breaks induced by ionizing radiation have 3'-PG [189]. DNA containing a 3'-PG cannot serve as a substrate for DNA polymerases or ligases, and represents an impediment to replication and repair. Therefore, removal of 3'-PG following exposure to ionizing radiation is important for maintenance of genomic integrity. Povirk and co-workers also showed that TDP1 knockdown in HeLa cells result in hypersensitivity

to Calicheamicin [205], which generates DSBs with 3'-PG [206]. In addition, TDP1 deficient cells have reduced capacity to repair 3'-PG in both nuclear and mitochondrial DNA [202, 207].

Lebedeva et. al. observed that human TDP1 can also process AP sites (or abasic sites), which is a DNA damage that has neither a purine nor a pyrimidine base. AP sites are among the most frequent occurring of DNA damage, and can be generated by DNA glycosylase during base excision repair, or through spontaneous hydrolysis of the N-glycosidic bond [200]. The capacity of TDP1 to process AP sites is consistent with its interaction with ligase III and its role in base excision repair [208]. As mentioned at the beginning of this section, TDP1 has 3' nucleosidase activity on DNA ends, which allows TDP1 to remove 3' damage caused by chain terminating analogs. Huang and colleagues showed TDP1 can remove a variety of 3' nucleoside analogs generated by commonly used anti-viral and anti-cancer chain-terminators, including acyclovir (ACV), zidovudine (AZT) and cytarabine (Ara-C) [193]. Chain terminating nucleoside analogs exert their cytotoxic effect through generation of 3'-blocking lesions that impair DNA polymerization during replication. This study suggests that TDP1 may participate in repair of DNA damage during replication.

The role of TDP1 in removal DNA 5' end damage is less understood. Nitiss and coworkers discovered that TDP1 can remove a peptide bound to the DNA 5' end via a covalent phosphotyrosyl linkage [191]. This study also showed that, in yeast cell

overexpressing Top2, TDP1 catalytic inactive mutants can cause hypersensitivity to Top2 targeting drugs. These observations suggest that TDP1 is capable of repairing of Top2 mediated DNA damage in yeast. Yeast and human TDP1 share substantial sequence homology, especially in the highly conserved catalytic domain [183]. Over expression of human TDP1 in human embryonic kidney cell line 293 (HEK293) resulted in a dramatic increase of cell viability in cells treated with camptothecin, which is Top1 poison. This result is expected base on the well-known role of TDP1 in repair of Top1cc. Importantly, similar result was obtained with VP-16, which is Top2 poisons [192]. This study also showed that over expression of the catalytically inactive mutant, TDP1-H263A, had no impact on levels of DNA damage. Taken together, these observations show that TDP1 contributes to removal of Top2-mediated DNA damage.

#### **1-4-4 Mutation of TDP1 H493 results in neurological disease spinocerebellar ataxia with axonal neuropathy (SCAN1)**

The biological importance of TDP1 is illustrated by the fact that mutation of TDP1 at H493 to arginine (R, H493R) is correlated with the very rare human autosomal recessive neurodegenerative syndrome called spinocerebellar ataxia with axonal neuropathy (SCAN1) [209]. SCAN1 patients demonstrate increased cerebellar atrophy that leads to ataxia in late childhood (13-15 years) [209, 210]. The human TDP1-H493R (H432R in yeast) mutation has been demonstrated to increase the lifespan of the TDP1-DNA

covalent intermediate, and decrease phosphodiesterase activity (Figure 1-4-1, step 3 and 1 respectively) in both human and yeast proteins [211-215].

If TDP1 is expressed in all soft tissues [216], then why is presentation of the SCAN1 phenotype neurological? The reason might be that neurons accumulate more DNA damage requiring TDP1 for repair. DNA breaks generated by oxidative stress are a major threat to genome stability in post-mitotic neurons [217]. These oxidative damages, such as 8-Oxoguanosine and 5-Hydroxycytosine could result in accumulation of trapped Top1 [174]. Indeed, Nitiss and colleagues showed that TDP1-deficient mice showed increased levels of Top1ccs during embryonic development in cortical and cerebella tissue, and little to no accumulation of Top1ccs in control cells or other tissues [167, 218]. This study showed increased Top1cc accumulation in neuronal tissues during development. Top1cc and the TDP1-DNA covalent intermediate have enormous potential interfere with replication and transcription, and could therefore trigger apoptosis [212, 214].

Lymphoblastoid cells isolated from SCAN1 patients showed a defect in repair of single-strand breaks induced by oxidative species and CPT [212, 219, 220]. By using alkaline comet assay, El-Khamisy and colleagues observed defects in single-strand break repair in SCAN1 Lymphoblastoid cells following exposure to ionizing radiation [221]. Together, these studies shows that TDP1 significantly contributes to neuronal protection during development.

#### **1-4-5 Role for TDP1 in DNA double strand repair by NHEJ**



Removal of 3' lesions by TDP1 to facilitate single-strand break repair is well established [222]. Recently, it has been recognized that TDP1 not only acts as an end processing factor, but also may participate during the early stages of single strand break repair (SSBR), by interacting with some key proteins in SSBR, such as DNA ligase III, XRCC1 and poly(ADP-ribose)polymerase-1 (PARP1) [208, 223, 224]. As mentioned before, ATM and DNA-PKcs orchestrate the DNA damage response through phosphorylation of variety of downstream proteins. Human TDP1 is phosphorylated by both ATM and DNA-PKcs phosphorylation at serine 81 (S81), which located in the soluble, N-terminal domain [223]. Phosphorylation of TDP1 at S81 has been shown to increase TDP1 stability, accumulation at DSBs, and facilitate TDP1 interaction with XRCC1 and ligase III [208]. Human TDP1 also interacts with PARP1 through the N-terminal domain [224]. XRCC1, ligase III and PARP1 are implicated in repair of DNA single-strand breaks as part of the base excision repair (BER) pathway [225]. Taken together, these studies suggests that TDP1 most likely participates in BER/SSBR to remove 3' lesions at SSBs.

Little is known about the role of TDP1 in DSBR. Bahmed and colleagues provided the first evidence linking TDP1 with DSBR by NHEJ in yeast [12]. They used restriction enzymes to generate ligatable DSBs with 3'-, or 5' overhangs-, or blunt ends as substrates for NHEJ. In TDP1-deficient yeast, 23/100 colonies showed misrepair of DSBs with 5'-extensions, whereas in wild type (WT) cells, the frequency of inaccurate repair

was 4/100. The major form of inaccurate repair in TDP1 deficient cells was 2-4 nucleotide insertions. Insertions required Ku80, ligase IV, and DNA polymerase IV, which suggested that insertions were formed through gap filling by DNA polymerase IV during NHEJ. In contrast, TDP1-deficiency had no effect on the fidelity of NHEJ on DSBs with 3'-extensions or blunt ends. Increased inaccuracy of NHEJ on 5'-extension was not detectable in cells expressing catalytic inactive TDP1, indicating a key role for TDP1 catalytic activity in maintenance of NHEJ accuracy. Nitiss and colleagues proposed that, in yeast, the 3'-nucleosidase activity of TDP1 prevents erroneous insertion by DNA polymerase. TDP1 can act at an undamaged 3' end to remove the nucleoside and leave a 3' phosphate, which acts as a block to polymerases or ligases. They observed that overexpression of Tpp1, which is a yeast DNA 3' phosphatase, also resulted in increased frequency of insertions. This observation supported the model, and suggesting that generation of 3' phosphate is a key step to minimize error in NHEJ mediated by TDP1.

TDP1 catalytic activity is central for TDP1 regulation of NHEJ accuracy in yeast that mentioned above. The TDP1 catalytic domain is highly conserved across all species. Like TDP1, the basic molecular mechanism of NHEJ is conserved between yeast and humans. Therefore, we hypothesize that the role of TDP1 is likely to be conserved between species. To understand the role of TDP1 in NHEJ in mammalian cells, we generated TDP1 deficient HEK293 cells by using CRISPR/cas9. We observed that TDP1 is required for efficient NHEJ in human cells, and that physical interaction with the

required NHEJ factor XLF mediates participation of TDP1 in NHEJ. Further, we show that a mutation that mimics phosphorylation of TDP1-S81 inhibits TDP1 participation in NHEJ, which suggests that PI3K-family protein kinases may regulate participation of TDP1 in NHEJ. Our data contribute to a more profound understanding of the molecular mechanism of NHEJ in human cells.



Figure 1-4-2

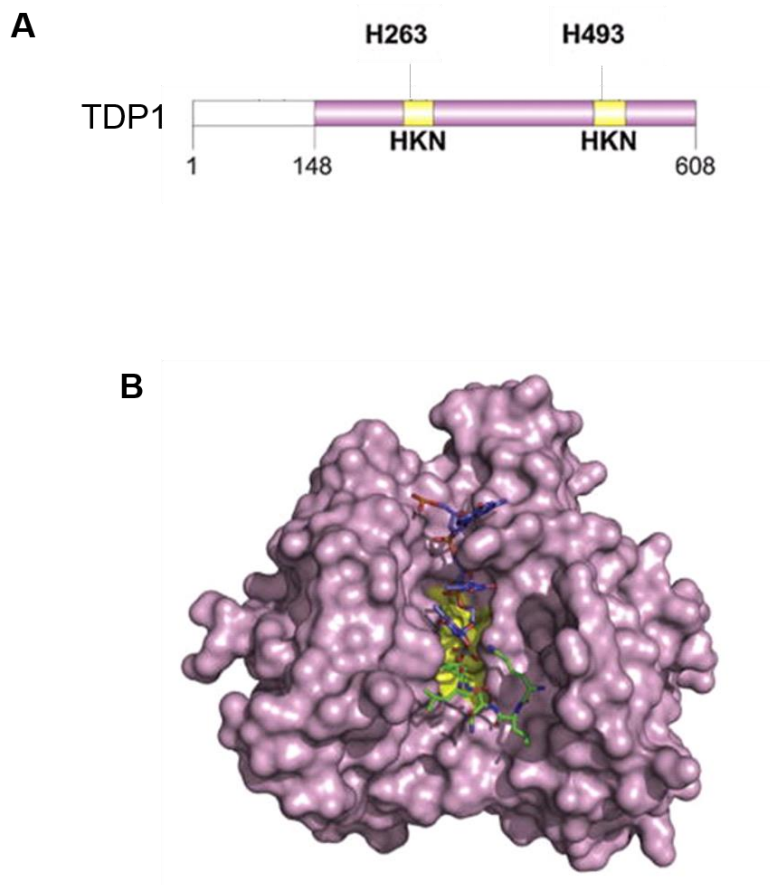


Figure 1-4-2 TDP1 structure

**Upper panel** Domain distribution of human TDP1 (608 amino acids). TDP1 consists of a variable N-terminal domain (*white*), and a highly conserved C-terminal catalytic domain (*purple*), which houses two HKN domain (*gold*) that contain the two invariant catalytic histidines (H263 and H493 in human).

Adapted from Pommier et al., 2014 [222]

**Lower panel** shows the crystal structure of TDP1. Color of the crystal structure corresponds to color in domain map (upper panel). The DNA binding domains is not shown.

DNA is in blue sticks. Peptide is in green sticks. Both sticks colored by element (N, blue; O, red; P, orange; Vanadate, grey)

Adapted from Davies et al., 2002 [184]

Figure 1-4-3

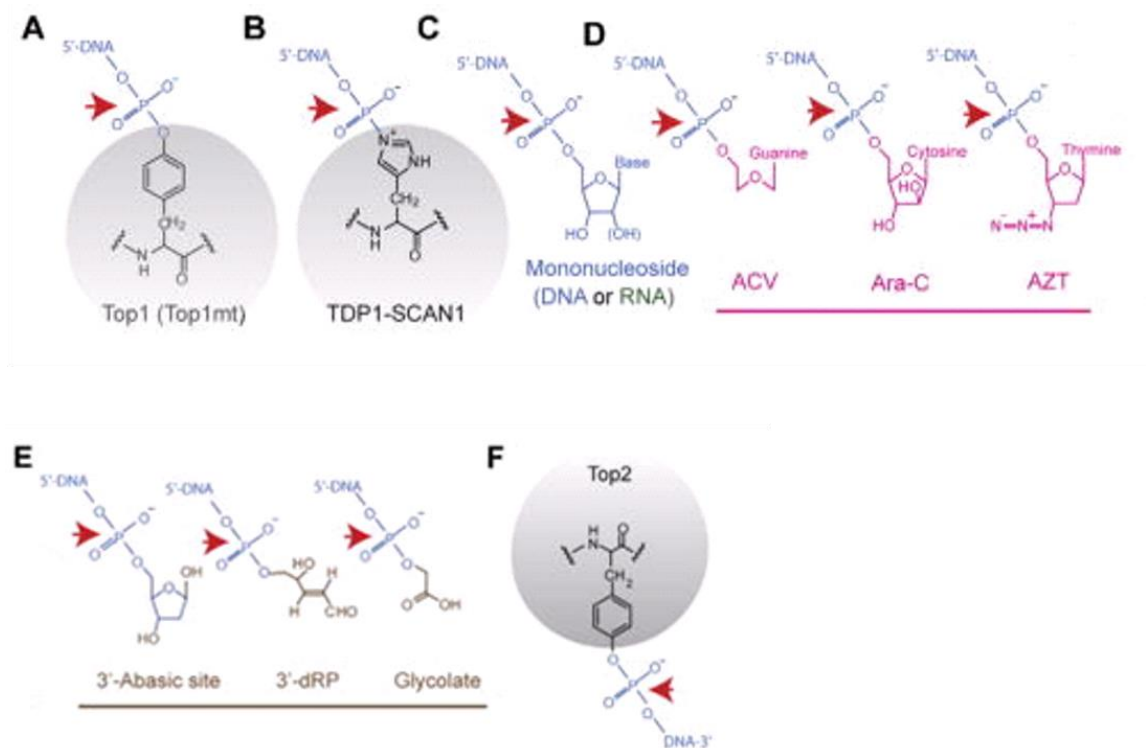


Figure 1-4-3 TDP1 can process a variety of DNA ends

**(A)** Classical substrate corresponding to Top1 and mitochondrial Top1 (Top1mt).

**(B)** TDP1 can also hydrolyze 3'-phosphoamide groups such as those generated by mutated TDP1 with the SCAN1 mutation.

**(C)** TDP1 can also excise 3'-base (3'-nucleosidase activity).

**(D)** TDP1 is involved in the excision repair of 3'-chain-terminating anticancer and antiviral nucleosides (pink) including acyclovir (ACV), cytarabine (Ara-C) and zidovudine (AZT).

**(E)** TDP1 excises 3'-blocking lesions (brown) resulting from base alkylation: 3'-abasic and 3'-deoxyribose phosphate ends [45,53,58] or oxidation (3-glycolates).

**(F)** Yeast TDP1 and human TDP1 can hydrolyze 5'-tyrosyl ends.

The red arrows indicate the cleavage sites.

Adapted from Pommier et al., 2014 [222]

TABLE I. EFFECTS OF TDP1 DEFICIENCY IN DIFFERENT SPECIES

TDP1 mutant	Species/Cell lines	DNA Damaging Agent	Cellular Phenotype
Knockout	Murine quiescent primary cortical astrocytes Murine cerebellar granule neurons	hydrogen peroxide, methyl methanesulfonate (MMS)	Kinetics of removal of single-strand breaks was delayed. High levels of single DNA strand breakage were accumulated in TDP1 knockouts [207]
Knockout	Extracts of murine embryonic fibroblasts	SCAN1	TDP1 deficient fibroblasts showed deficiencies in processing 3' phosphotyrosyl single-strand breaks and 3'-phosphoglycolate double-strand breaks[226]
Knockout	Mouse	Topotecan	TDP1 deficient mice treated with topotecan showed significant loss of intestinal and hematopoietic progenitor cells[227]
TDP1 gene ortholog glait knockdown	Drosophila	Bleomycin, CPT, or non-camptothecin Top1 inhibitor NSC-725776	Reduced lifespan and diminished climbing ability in females. [228]
Enzymatically inactive mutation	Yeast	Bleomycin, CPT	Hypersensitive to Bleomycin and CPT[192]

TABLE I. EFFECTS OF TDP1 DEFICIENCY IN DIFFERENT SPECIES (CONTINUED)

TDP1 mutant	Species/Cell lines	DNA Damaging Agent	Cellular Phenotype
H493R (SCAN1 mutant)	Human lymphoblastoid cells from SCAN1 patients	Non-protein chromophore of neocarzinostatin	3'-PG accumulation in cells with TDP1 H493R [229]
Knockout	Human glioblastoma-resistant cancer cells (T98G)	Temozolomide	Hypersensitive to Temozolomide [194]
Knockout	Chicken bursal lymphoma (DT40)	CPT, bleomycin, etoposide, MMS, H <sub>2</sub> O <sub>2</sub> , and IR	Hypersensitive to CPT, bleomycin, etoposide, MMS, H <sub>2</sub> O <sub>2</sub> , and IR [192]



## **Chapter 2**

### **Materials and Methods**

## **2-1 Plasmids, cell culture and antibodies used**

Plasmids pET15b.FLAG.hTDP1, pET15b.hTDP1.H263A and pET15b.hTDP1.H493R were derived from pET15b.hTDP1 by site directed mutagenesis (Quickchange II, Stratagene) using oligonucleotides summarized in the following section. Plasmid pMAL-XLF was cloned as follows: pGEX-XLF was digested with BamHI and HindIII to release the XLF cDNA, which was gel purified and ligated into pMAL-c2 (NEB) that had been digested with BamHI and HindIII. Plasmid pMAL-XLF-1-224 was derived from pMAL-XLF by site directed mutagenesis (Quickchange II, Stratagene). Plasmid pCl-Puro-Myc-hTDP1 was a generous gift from Sherif El-Khamisy (University of Sussex, Brighton, UK). All cDNA sequences were confirmed by direct DNA sequence analysis.

Site-directed mutagenesis oligonucleotides:

hTDP1.FLAG:

CATATGCTCGAGGTCGACTACAAGGATGACGACGATAAGCCAATGTCTCAGG

TDP1.H263A.K: TATTGCGTTTGGTACCCACGCCACGAAAATGAT

TDP1.H493R: AATGCCATGCCACGTATTAAGACATATATGAGACCTTCTCCAGAC

hTDP1.S81A.ApaI: AGGCAGAAAAGCGGGGCCAGGAGGACCTC

XLF225stopStuI: CAGTCACCACACAATAGGCCTAAGTGGGACAGAAG

HEK-293 cells (ATCC CRL-1573), and TDP1-knockout derivatives, were cultured at 37°C in 5% CO<sub>2</sub> atmosphere in DMEM (contains 4 mM L-glutamine) with 10% Fetal Bovine Serum (FBS), or 10% FB Essence (FBS alternative).

TABLE II. ANTIBODIES USED

Antibody	Dilution	Vendor, catalog number
Anti-TDP1	1:800	Proteintech, 10641-1-AP
Anti-MBP	1: 10,000	NEB, E8032S
Anti-beta-actin	1:1000	Abcam, ab3280
Anti-DNA-PKcs	1:2000	Serotec, AHP318
Anti-Ku70	1:500	Described in Hanakahi, 2007 [230]
Anti-Ku80	1:200	NeoMarkers, Ab-2
Anti-XRCC4	1:1000	Serotec, AHP387
Anti-ligase IV	1:1000	Novus Biologicals, NB100-92452
Anti-XLF	1:2000	Described in Hanakahi, 2011 [231]

## **2-2 Transformation of plasmid in *E. coli***

LB agar plates were prepared with antibiotics two days before use. The plates were stored at 4 °C and place on bench at room temperature one day before use.

To prepare competent cells (BL21(DE3)pLysS and Rosetta2™ *E. coli* cells (EMD Biosciences), BL21(DE3) or Rosetta2 were incubate in a 5 ml LB culture with 25 µg/ml chloramphenicol (CAM) at 37°C for overnight. 1 ml of cell culture with 25 µg/ml chloramphenicol (CAM) was added into 50 ml LB broth in a 250 ml flask next day and incubated at 37 °C, 250 rpm shaking for 1 h until the culture reached OD 0.1, which was detected by Nanodrop 2000. The 50 ml cell culture was added into pre-chilled 50 ml falcon tube and centrifuge the tube at 4 °C, 5000 xg for 20 min. The supernatant was discard. The pellet was resuspended in 2 ml pre-chilled 10% glycerol and the tube was refilled with the 10% glycerol followed by centrifugation at the same condition. The pellet was resuspended in the glycerol in the tube after pouring, aliquoted by 90 µl. Aliquots were frozen by liquid nitrogen (LN) and stored at -80 °C.

To transform TDP1 or XLF plasmid into *E. coli*, 1 ng of plasmid was added into 40 µl bacteria in ice-chilled 1 mM cuvette. Plasmid was transformed by electroporation (preset bacteria 1.8 KV). 800 µl Super Optimal broth with Catabolite repression (SOC) was pipetted into the cuvette to move out the electroporated bacteria and add it to 14 ml falcon tube. Bacteria recovered by incubation at 37 °C, 250 rpm shaking for 1 h. Cell culture was spread on the LB agar plated and incubate the plates at 37 °C for overnight.

LB broth: Tryptone 10 g, NaCl 10 g and yeast extract 5 g dissolved in 1 L H<sub>2</sub>O.

LB agar: agar 15 g dissolved in 1 L LB broth

LB broth and LB agar were sterilized by autoclaving for 45 min at 15 psi on liquid cycle.

### **2-3 Growth of E. coli and induction of protein expression**

To grow the bacteria, two colonies from plate with reasonable colony numbers were picked and incubate separately in 5 ml (10 ml for large growth) LB broth in 50 ml falcon tube with appropriate antibiotics at 37 °C for overnight. 0.1 ml (10 ml for large growth) of cell culture was added into 5 ml (500 ml for large growth) LB broth in 50 ml falcon tube (250 ml flask for large growth) with appropriate antibiotics at 37 °C for 1 h until OD-600 reach 0.1, then chilled on ice. 1 ml cell culture was pipetted into 1.5 ml tube and spun down the pellet for 5 min at 5000 xg. The supernatant was discarded and the pellet was frozen at -80 °C as “not induced” sample. To induce expression of TDP1 or XLF, 0.25 mM isopropyl β-D-1-thiogalactopyranoside was added into the culture and incubated at 18 °C, 250 rpm shaking for 16 h. OD-600 was then record. 1 ml of the culture was pipetted into 1.5 ml tube and spun down the pellet for 5 min at 5000 xg. The supernatant was discarded and the pellet was frozen at -80 °C as “induced” sample. The rest culture was centrifuged for 30 min at 5000 xg at 18 °C. The pellet was stored at -80 °C.

To determine whether the induction was successful, the pellet from 1 ml culture was resuspended in protein sample buffer (80 mM Tris-pH 6.8, 0.2% SDS, 10% glycerol, 0.0006% Bromophenol blue) with 10% 2-mercaptoethanol (2xPSB+β-ME) (0.1 ml beta

ME+0.9 ml PSB), sonicated (Branssen Digital Sonifier) (2 sec pulse, 2 sec pulse off, 10% amplitude and sonicate for 10 cycles), and then chilled on ice. The sample was boiled for 3 min and 18  $\mu$ l was loaded on sodium dodecyl sulfate polyacrylamide gel electrophoresis (SDS-PAGE) gel. The gel was run at 150 v for 1 h, and then stained with coomassie blue solution (1 g of coomassie brilliant blue is diluted in 1 liter solution with 50% methanol [v/v], 10% glacial acetic acid [v/v] and 40% H<sub>2</sub>O [v/v]) for 1 h. To destain, the gel was rinse and boil the in deionized water for 3 min. The destain step was repeated until the protein band was detectable.

#### **2-4 Purification of his-tagged protein**

To lyse cells expressing his-TDP1 and its mutants, cell pellet (from 250 ml culture) was resuspended in lysis buffer (500 mM NaCl, 5 mM imidazole, 20 mM Tris-pH7.9) at 3 % original culture volume and transferred in prechilled 50 ml centrifuge tube. The tube was then rinsed with lysis buffer at 2 % original culture volume and the solution was combined in the 50 ml centrifuge tube. Dithiothreitol (DTT) and phenylmethane sulfonyl fluoride (PMSF) were added to 2 mM and 1 mM final concentration respectively. Lysozyme was then added (final concentration 2 mg/ml) in the resuspended cell. The cells were then incubated at room temperature (RT) on rotor for 30 min with gentle end-to-end turning, followed by sonication for 8 rounds with 10% amplitude, 20 sec on, 40 sec off. Cell lysate was collected after centrifugation at 4 °C, 14,000 xg for 30 min.

To purify his-tagged protein, Ni-NTA column (Qiagen) was packed with resin volume of 0.2% of original culture volume (0.5 ml resin if use 250 ml culture). 0.5 mM DTT was added in column buffer (250 mM NaCl, 15 mM imidazole, 20 mM Tris-pH7.9). Column was equilibrate with 10 column volume column buffer. The cell lysate was added on the column and the flow through was collected as “unbound”. Column was washed with 10 column volume column buffer. His-tagged protein was eluted from the column by 2.5 ml elution buffer (250 mM NaCl, 917.5 mM imidazole, 20 mM Tris-pH7.9). 10 fractions of elution were collected. 10  $\mu$ l of each fraction with 10  $\mu$ l beta-ME was loaded on SDS-PAGE gel to determine which fractions can be combined. The combined fractions were dialyzed in dialysis buffer (50 mM NaCl, 1 mM ethylenediaminetetraacetic acid (EDTA), 50 mM Tris-pH7.9, 2 mM DTT, 5% glycerol) for overnight, aliquoted, frozen by LN and stored at -80 °C.

For his-tagged TDP1 proteins used in affinity capture assay with MBP-XLF, the protein was further purified with hi-Trap Q column after Ni-NTA purification. The eluate from Ni-NTA was diluted in 10 ml of loading buffer (100 mM NaCl with 20 mM Tris pH 7.9). The diluted elute was loaded onto a 1 ml hi-Trap Q column (GE) that had been equilibrated with 50 mM NaCl in Q buffer (50 mM Tris pH 7.9, 1 mM EDTA, 2 mM DTT, 5% glycerol). The column was washed with 10 column volume Q-buffer and eluted with a 50 mM to 1 M NaCl linear gradient in Q buffer. 30xcolumn volume fractions of elute from hi-Trap Q column were collected and that OD 280 was monitored to identify

protein-containing fractions. 10  $\mu$ l of each fraction was resolved on SDS-PAGE gel and his-tagged TDP1 proteins was observed by using coomassie blue staining. The fractions with the most his-tagged TDP1 were peak fractions and then combined in one tube. The combined fraction was dialyzed in dialysis buffer (50 mM Tris pH 7.9, 50 mM NaCl, 1 mM EDTA, 2 mM DTT, and 10% glycerol) for 16 h at 4°C, aliquoted, and frozen by LN and store the protein at -80 °C. This 2-step purification of TDP1 was generously done by Matthew Summerlin in our lab.

### **2-5 Purification of Glutathione S-transferase (GST)-tagged proteins**

The method for preparing and purification of GST-tagged protein was similar to that of his-tagged protein, but with different buffer and resin. Briefly, the cell pellet (from 250 ml cell culture) was lysed with 12.5 ml lysis buffer (1mM DTT and 1mM PMSF in GST buffer (800 mM NaCl, 5 mM EDTA, 50 mM Tris-pH8.0, 0.1% Triton x-100)), followed by sonication for 8 rounds with 10% amplitude, 20 sec on, 40 sec off. Centrifuge at 4 °C, 14,000 xg for 30 min. The supernatant (cell lysate) was collected and the pellet was discard. The cell lysate was bound to (GST)-sepharose (2 ml with 50% slurry, GE 17513201) for 1h at 4°C with gentle end-to-end mixing. The resulting mixture was transferred to a column and washed with 10 column volume of GST buffer. The GST-tagged protein was eluted with 40mM glutathione in 5 column volume of GST buffer.



## **2-6 Generate maltose binding protein (MBP)-tagged protein cell lysate**

The method for preparing cell lysate expressing MBP-tagged protein was similar to that of his-tagged protein, but with different buffer and resin. Briefly, the cell pellet (from 250 ml cell culture) was lysed with 12.5 ml MBP column buffer (200 mM NaCl, 20 mM Tris-HCl pH 7.4, 1 mM EDTA, 1 mM DTT) with 1mM PMSF, followed by sonication for 8 rounds with 10% amplitude, 20 sec on, 40 sec off. Cell lysate was collected after centrifugation at 4 °C, 14,000 xg for 30 min, aliquoted and frozen at -80 °C.

## **2-7 Affinity capture (pull-down) assay using His-TDP1 proteins and Ni-NTA resin**

100 µl Ni-NTA resin (with 50% slurry) was pipetted in 1.5 ml tube. Resin was washed in 1 ml water. 100 µg of purified his-tagged protein and 100 µg of non-his-tagged protein were added to the resin and the tube was filled to 500 µl with binding buffer (50mM tris-HCl pH8.0, 50mM KOAc, 1mM EDTA, 5% glycerol, 2 mM DTT). The tube was incubated at 4 °C for 1 h with gentle end-over-end mixing. Resin was collected by centrifugation (4300 xg, 1 min, RT) and the supernatant was removed. The resin was washed with 3x1 ml binding buffer. During the wash step, the resin was first resuspend in 1 ml binding buffer and collected by centrifugation (4300 xg, 1 min, RT) and the supernatant was removed. 25 µl 2xPSB+β-ME was added in the resin and boiled for 3 min to elute proteins from the resin. Elution was collected by centrifugation at 4300 xg for 1 min and then resolved on SDS-PAGE gel (100 v for 80 min). Separated protein samples

were transferred to PVDF membrane (Immobilon P) and individual proteins were detected by Western blot analysis.

## **2-8 Affinity capture (pull-down) assay using cell lysate expressing GST-tagged protein and GST-sepharose resin**

The GST-tagged protein was bound to the GSH-sepharose resin by incubating 250  $\mu$ l cell lysate expressing GST-tagged protein with 32.5  $\mu$ l GSH-sepharose (50% slurry) at 4°C for 1h with gentle end-over-end mixing. The resin was collected by centrifugation at 4300 xg for 1 min and the supernatant was removed. The resin was washed with 3x1 ml of GST buffer and 1 ml of binding buffer. Resin was collected by centrifugation at 4300 xg for 1 min and the supernatant was removed. 100  $\mu$ g of non-GST-tagged protein diluted in 300  $\mu$ l binding buffer was then added and incubate at 4 °C for 1h with end-over-end mixing. Resin and the bound protein were collected by centrifugation at 4300 xg for 1 min and the supernatant was removed. Resin was washed 3x1 ml of binding buffer and the protein was eluted by resuspension the resin with 50  $\mu$ l 2xPSB+ $\beta$ -ME and 3 min boiling. 12.5  $\mu$ l protein sample was loaded on 8% SDS-PAGE and run at 100v for 80min (200v for 45min). Separated protein samples were transferred to PVDF membrane and individual proteins were detected by Western blot analysis.

## **2-9 Affinity capture (pull-down) assay using cell lysate expressing MBP-tagged protein and Amylose resin**

For MBP pull down, 100  $\mu$ l amylose resin (50% slurry, NEB E8021S) was washed with 500  $\mu$ l MBP column buffer (200 mM NaCl, 20 mM Tris-HCl pH 7.4, 1 mM EDTA, 1 mM DTT). The amylose was collected by centrifugation (at 4300 xg for 1 min, RT). 250  $\mu$ l of cell lysate expressing MBP-tagged protein was added to the resin pellet and incubated at 4 °C for 1h with end-to-end mixing. The unbound fraction was removed after centrifugation (at 4300 xg for 1 min, RT). The resin was washed with 2x1 ml MBP column buffer and 1ml binding buffer (50 mM tris-HCl pH 7.4, 100mM KOAc, 1mM EDTA, 5% glycerol, 2 mM DTT). The resin and the bound MBP-tagged protein was collected by centrifugation (at 4300 xg for 2 min, RT). 100  $\mu$ g of non-MBP-tagged protein diluted in 300  $\mu$ l binding buffer with non-specific competitor -1mg/ml Bovine Serum Albumin (BSA) were added to the resin pellet and incubated at 4 °C for 2 h with end-to-end mixing. The resin and the bound protein were collected by centrifugation (at 4300 xg for 2 min, RT). The bound protein was eluted from the resin by incubation the resin with 50  $\mu$ l elution buffer (10 mM maltose in MBP column buffer) at 4 °C for 10min with gentle mixing. The resin was removed after centrifugation (at 4300 xg for 1 min, RT). The supernatant was diluted in 50  $\mu$ l 2xPSB+ $\beta$ -ME and 20  $\mu$ l protein sample was resolved on SDS-PAGE gel (150 v for 60 min). Protein samples were transferred to PVDF membrane and individual proteins were detected by Western blot analysis.

## **2-10 Oligonucleotide $^{32}\text{P}$ labeling reaction**

HPLC purified oligonucleotide with 3' tyrosine at the end (5' GATCTAAAAGACTT-Y 3', gift from Karin Nitiss, University of Illinois at Chicago, Rockford, IL, US) was labeled using  $\gamma\text{-}^{32}\text{P}$  ATP (PerkinElmer, NEG002A250UC) and T4 polynucleotide kinase. One reaction included 1  $\mu\text{l}$  of 20  $\mu\text{M}$  oligonucleotide, 2  $\mu\text{l}$  of 10x PNK reaction buffer, 2  $\mu\text{l}$  of  $\gamma\text{-}^{32}\text{P}$  ATP (3000 or 6000 Ci/mmol), and 1  $\mu\text{l}$  PNK (T4 Polynucleotide Kinase, 3'-phosphatase free, Roche 709 557) in 20  $\mu\text{l}$  final volume. The reaction was incubated at 37 °C for 30 min, cooled on ice and diluted in 20  $\mu\text{l}$  water to bring the final volume to 40  $\mu\text{l}$ .

A G-25 quick-spin oligonucleotide column (Roche 11814397001) was used to remove the incorporated radioactive nucleotides. To remove preservative from the column, we resuspend the column matrix by tapping, removed the top cap, snapped off the bottom, centrifuged (1000 x g for 1 min, RT), washed the column with 300  $\mu\text{l}$  water and packed the matrix using centrifugation (1000 x g for 2 min, RT). The reaction sample was pipetted to the middle of the column in a fresh collection tube and centrifuged (1000 x g for 4 min, RT). The radioactivity was counted by using scintillation counter (count  $^{32}\text{P}$  for 1 min) with 1  $\mu\text{l}$  diluted in 2 ml scintillation cocktail.

To label 3'-biotinylated oligonucleotide (Kpn1 and Pst1 Top-strand), the method was the same. Double-strand 3'-biotinylated oligonucleotide was generated by annealing Kpn1 and Pst1 bottom-strand after labeling of TS. To anneal, a final volume of 100  $\mu\text{l}$

reaction with 40  $\mu$ l of labeled top strand (20 pmol), 2  $\mu$ l of bottom strand (40 pmol), 20  $\mu$ l of 5x hairpin buffer ( 50 mM Tris-HCl pH 7.4, 12.5mM  $MgCl_2$ , 100 mM NaCl) was incubated at 95  $^{\circ}C$  for 2 min. The heat block was then turned off and cooled down until it reached RT (6 h). To collect dsDNA, a 10% (29:1) acrylamide gel was poured. The dsDNA sample was run on the gel at 150 V, in the cold room, for 5.5 h. The gel was then exposed to X-ray film overnight (mark the position of the film). The film was developed and the position of dsDNA on the gel was determined. The gel containing dsDNA was cut out and mince the gel with some NTE buffer (50 ml NaCl, 50 mM Tris-HCl pH 8.0, 1 mM EDTA). The minced gel was transferred to an Eppendorf tube, filled with NTE buffer and DNA was eluted by end-over-end mixing for 24 h at 4  $^{\circ}C$ . To collect the labeled DNA, the gel was centrifuged (14,000 xg, 5min, 4 $^{\circ}C$ ) and the supernatant was saved. The DNA was then ethanol precipitated from the gel supernatant and the radioactivity was measured by using scintillation counter.

### **2-11 TDP1 enzymatic activity assay**

For 1 TDP1 reaction, a 10  $\mu$ l reaction containing 25 fmol labeled oligonucleotide, 2  $\mu$ l of 5x TDP1 reaction buffer (50 mM Tris-Cl, pH 8.5, 100 mM NaCl, 25  $\mu$ g/ml BSA, 0.5 mM EDTA), 1  $\mu$ l TDP1 (with different amount of TDP1) was incubated at 37  $^{\circ}C$  for 15 min. 10  $\mu$ l of TBE-Urea sample buffer (Invitrogen, LC6876) was added to stop the reaction.

The sample was boiled for 5 min and 4 µl was loaded on a 15% denaturing acrylamide gel.

For making 15% denaturing acrylamide gel, 50 ml 30% (19:1) acrylamide solution (BioRad), 10 ml 10x TBE buffer (54 g of Tris base, 27.5 g of boric acid, 20 mL of 0.5 M EDTA pH 8.0, 500 ml final volume), 4 ml water, 600 µl 10% APS and 42.5 g urea was mixed. The mix was heated to help urea dissolve and added with 40 µl TEMED at last. The gel was run at 120 V for 2 h and then dried, exposed for 30 min and bands were detected using a BioRad Personal Molecular imager phosphorimager (PMI).

For reactions with 3'-biotinlated oligonucleotide as substrate, the reactions were the same as the reactions using oligonucleotide with 3' tyrosine as substrate that described above. The sample was boiled for 5 min and 4 µl was loaded on a 7.5% urea-acrylamide gel. The gel was run at 1800 volt for 2.5 h, then dried, exposed overnight and bands were detected using Personal Molecular imager phosphorimager.

## **2-12 TDP1 Knockout by CRISPR/Cas9**

Cas9-sgRNA expression plasmids (TDP1 guide 1, TDP1 guide 2) were generated by the Genome Editing Core of the University of Illinois Cancer Center. The plasmids were constructed by ligating oligonucleotide duplexes with the sequences 5'-TCTTTGGGCAGTGCCGTCAT-3' and 5'-GACATCTCTGCTCCCAATGA-3' to target

TDP1 exon 3. Two wells of HEK 293 cells were seeded in a 6 well plate with concentration of  $3 \times 10^5$  cells/ ml. TDP1 guide 1, TDP1 guide 2 with/without pcDNA3.1.hygro were transfected into two wells respectively by Lipofectamine® 2000 Transfection Reagent (Thermo Fisher Scientific, 11668027) 24 h after seeding.

For transfection, 4 µg plasmid (with hygromycin resistant plasmid: 40%TDP1 guide 1, 40% TDP1 guide 2 and 20% hygromycin resistant plasmid, without hygromycin resistant plasmid: 50%TDP1 guide 1, 50% TDP1 guide 2) and 10 µl lipofectamine® 2000 (Thermo Fisher Scientific, catalog number 31985062) were used according to the manufacture's instruction. After 2 days, cells were split into 3 wells. 250 µg/ml hygromycin were added after 24 h and incubated for 3 days, then the cells were incubated in media without hygromycin. Cells transfected with hygromycin were seeded into 96-well plates at concentration of 111 cells/ ml, 333 cells/ ml and 1000 cells/ ml. 5 plates were seeded for each concentration. Cells transfected without hygromycin were seed into 5 96-well plates with concentration of 1000 cells/ ml. The plates were wrapped with plastic wrap and incubated at 37°C for 2 weeks.

Single colonies were picked and seeded in 48 well plate. 12 colonies were picked and used for further analysis. Chromosomal DNA of these 12 colonies were extracted by QIAGEN QIAamp DNA Blood Mini Kit (catalog number 51104). CRISPR/Cas9 targeted sequenced were amplified by PCR, cleaned by QIAquick PCR Purification Kit and

sequenced. 3 colonies (7D1, 8A3 and 8A5), which lacked detectable TDP1 western blot signal, were selected and cultured as TDP1 knockout (TDP1-KO) cell lines.

### **2-13 Drug sensitivity assay**

Each cell line was seeded at  $3 \times 10^5$  cells/ ml in one well of 6-well plate. Plasmids, which encoded complementary proteins, were transfected into each cell line on the next day. 48 h after transfection, 7 cell lines (HEK WT, 3 TDP1-KO cell lines and 3 TDP1-KO cell lines with ectopic expression of TDP1) were seeded at 3000 cells/ well into 7 wells of 96-well plate and incubated for 24 h and then the media was removed. For each cell line, drugs were added in a final volume of 100  $\mu$ l media. The plates were incubated for 3 days and then the media was removed. 100  $\mu$ l media with 10  $\mu$ l WST-1 (Sigma 5015944001) was added into each well and incubated for 2.5 h. Signal was detected by Synergy 2 Multi-Mode Reader (BioTek) and analyzed by Gen5 Data Analysis Software (BioTek).

### **2-14 Clonogenic survival assay for ionizing radiation**

HEK293 cell lines (WT, TDP1-KO) were treated with a range of ionizing radiation (0 Gy, 0.5 Gy, 1 Gy, 2 Gy and 4 Gy) (Radiation Machinery Corp. Gammator 50  $^{137}\text{Cs}$  source irradiator (Northern Illinois University)). Cells were seeded in 6-well plates at  $0.1 \times 10^3$  cells/ ml,  $0.2 \times 10^3$  cells/ ml,  $0.4 \times 10^3$  cells/ ml,  $2 \times 10^3$  cells/ ml and  $2 \times 10^6$  cells/ ml for 0 Gy, 0.5 Gy, 1 Gy, 2 Gy and 4 Gy respectively. Cells were incubated at 37°C for 14



days. Media was aspirated from the plates and 1 ml of Crystal violet was added in each well. Crystal violet was removed after 20 min. The plates were submerged in a container full of water, then dumped the water and refilled with it for several times until the dye stopped coming off. Cells were dried in a fume hood at room temperature for overnight. The colonies were imaged by ChemiDoc™ XRS+ System with Image Lab™ Software and quantified by Quantity One®. Cell viability of 0 Gy was normalized to 100%.

### **2-15 Generate EJ5-GFP integrated HEK cell lines**

Each cell line (WT, TDP1-KO cell lines (7D1, 8A3, 8A5)) was seeded at  $3 \times 10^5$  cells/ ml in 24 well plate. PimEJ5GFP (add gene plasmid number 44026) was linearized by XhoI.

Linear pimEJ5GFP plasmid was transfect into each cell line with lipofectamine® 2000. After 2 days, the media was removed and cells were incubated in media with 2 µg/ml puromycin for 14 days. Media was changed when there was too much dead cells. EJ5GFP integrated cell lines were expanded and stored.

### **2-16 End joining efficiency assay**

8 cell lines (WT, 7D1, 8A3, 8A5, WT EJ5-GFP, 7D1EJ5-GFP, 8A3EJ5-GFP and 8A5EJ5-GFP) were seeded at  $3 \times 10^5$  cells/ ml in two wells of 6 well plate.

pEX.sEF1a.Kozak.HA.NLS.Sce.T2A.BFP (AddGene 45565), which can express I-SceI and blue fluorescent protein (BFP), was transfected into one well of each cell line by lipofectamine® 3000 (Thermo Fisher Scientific, catalog number L3000008) and incubate for 72 h. BFP signal was detected by Synergy 2 Multi-Mode Reader (BioTek) and analyzed by Gen5 Data Analysis Software (BioTek). Cells in each well were then harvested, washed with PBS and resuspend in 1 ml of PBS. Cells with GFP signal were counted by FACS Calibur (Becton-Dickinson). NHEJ efficiency was normalized to WT EJ5-GFP cells' GFP cell percentage.

For cells that needed ectopic expression of TDP1 or TDP1 mutants, pCL-puro-myc-TDP1/TDP1 mutants plasmid was transfected into one well cells of 6 well plate by lipofectamine® 3000 24 h after seeding. pEX.sEF1a.Kozak.HA.NLS.Sce.T2A.BFP was transfected by lipofectamine® 3000 24 h after TDP1 plasmid transfection.

## **2-17 End joining junction sequencing**

6 wells of 6 well plate were harvested 72 h after transfection of pCVL SFFV-EF1s HA.NLS.Sce. Cells were resuspended in 1x Phosphate Buffered Saline (PBS) with 5% BSA and 2mM Ethylene diamine tetra acetic acid (EDTA). GFP cells were sorted in UIC RRC and chromosomal DNA was extracted by QIAGEN QIAamp DNA Blood Mini Kit. Junction sequence was amplified by primers JL.3327.P3F.CS1 and

JS.5518.P2R.CS2. and the PCR reaction (25  $\mu$ l) included 1x Go Taq buffer (Promega™ M8901), 1.5 mM MgCl<sub>2</sub>, 0.2 mM dNTP, 0.6 mM each primers, 1  $\mu$ l of 1:50 homemade Taq polymerase and 16 ng of chromosomal DNA as template. The thermocycler condition we used was 94 °C 3 min, cycle 32 times (94 °C 45 s, 63 °C 45 s, 68 °C 1min 45 s), 68 °C 7 min, store at 4 °C. 10  $\mu$ l PCR product was run on 1.2% agarose gel to verify generation of amplicon with correct size and enough amount.

The correct amplicons were sent to UIC RRC DNA service to do NextGen sequencing. In detail, an 8-cycle PCR amplification was performed to add a unique 10-base barcode (Access Array Barcode Library for Illumina, Fluidigm). Final PCR products were purified using SequalPrep plates (Life Technologies) according to manufacturer's instructions. Pooling of the amplicons was performed after quantification of each amplicon using a Quant-iT PicoGreen dsDNA assay kit (Life Technologies). After pooling, libraries were sequenced on an Illumina MiSeq sequencer using standard V3 chemistry with paired-end, 300 base reads, and with a 20% spike-in of phiX. Fluidigm sequencing primers, targeting the CS1 and CS2 linker regions, were used to initiate sequencing. De-multiplexing of reads was performed on instrument. Library preparation was performed at the DNA Services facility at the University of Illinois at Chicago. Sequencing was performed at the W.M. Keck Center for Comparative and Functional Genomics at the University of Illinois at Urbana-Champaign. Forward and reverse reads were merged using PEAR [232]. Ambiguous nucleotides were trimmed from the ends and

reads with internal ambiguous nucleotides were discarded. Primer sequences were identified using Smith-Watermann alignment and trimmed from the sequence. Reads that lacked either primer sequence were discarded. Sequences were then trimmed based on quality scores using a modified Mott algorithm with PHRED quality threshold of  $p = 0.01$ . All sequences were then dereplicated to produce a list of unique sequences. All sequences that had an abundance of at least 10 counts were designated seed sequences and all other sequences, i.e. less than 10 counts, were considered non-seed sequences. USEARCH was then used to find the nearest seed sequence for any non-seed sequence with a minimum identity threshold of 98%. For any non-seed sequence that matched a seed sequence, its counts were added to the seed sequence counts. For any non-seed sequence that did not match a seed sequence it would remain an independent sequence and counted separately. All counts were then tabulated into a single file and sequences for seeds and independent non-seeds were then combined into a single FASTA file.

## **2-18 Generate 100% perfect junction positive control**

PimEJ5GFP plasmid was digested by I-SceI and loaded on 0.7% agarose gel. PimEJ5GFP will be digested into two pieces (10 KB and 2 KB). The larger piece was extracted and purified by QIAquick Gel Extraction Kit (Qiagen 28706). 10 KB pimEJ5GFP was ligated and transformed into XL10-Gold Ultracompetent cell (Agilent Technologies,

catalog number: 200314). Four colonies were picked, cultured and miniprep DNA by GeneJET Plasmid Miniprep Kit, Thermo Fisher Scientific, catalog number K0503). One colony's plasmid, which showed 10 KB on agarose gel, was picked and diluted with HEK 293 chromosomal DNA. 26.7 fg plasmid was used as template in PCR reaction as positive control.

### **2-19 In vitro NHEJ activity assay**

To prepare whole cell extracts from each cell line, 2x 100% confluent 15 cm dishes of cells ( $2 \times 10^7$ ) were harvest by scraping. The plates were then washed twice with PBS and combined with cells harvested from last step. The cells were packed by centrifugation (700 x g, 5min, RT) and the pellet volume was determined. Cells were then lysed with 2 pellet volumes of hypotonic lysis buffer (HPLB) (10 mM Tris pH 8.0, 1 mM EDTA), and incubated on ice for 20 min. Cells were opened by dounce lysis, then 0.25 pellet volumes of high salt buffer (HSB) (83.5 mM Tris, pH 8.0, 1.65 M KCl, 3.3 mM EDTA) was slowly added with mixing. The lysate was incubation on ice for 10 min. Cell extract (supernatant) was collected by centrifugation (16,500 x g, 30min, 4°C) and dialyzed against 2 liter of dialysis buffer (20 mM Tris, pH 8.0, 0.1 M KOAc, 0.5 mM EDTA, 20% glycerol) for 4 h at 4°C.

To prepare substrate for *in vitro* NHEJ assay, pBluescript DNA was digested with HindIII. The linearized plasmid was labeled with  $\gamma$ - $^{32}\text{P}$  ATP at 5' end by using the same labeling method as described in Oligonucleotide  $^{32}\text{P}$  labeling reaction.

One *in vitro* NHEJ reaction was 10  $\mu\text{l}$  with HindIII-linearized 5'- $^{32}\text{P}$ -labeled pBluescript DNA (10 ng) and 25  $\mu\text{g}$  of WCE in NHEJ buffer (50 mM HEPES pH 8.0, 100 mM KOAc, 0.5 mM  $\text{Mg}(\text{OAc})_2$ , 1 mM ATP, 1 mM DTT, and 0.1 mg/ml BSA). Where indicated, reactions included the DNA-PKcs inhibitor Nu7026 (KuDos Pharmaceuticals, 50  $\mu\text{M}$ ), or neutralizing anti-XRCC4 antibodies (Serotec #AHP387 1:500). NHEJ reactions were incubated at 37°C for 2 h, after which 0.2 reaction volumes of protease solution (0.1 M Tris, pH 7.5, 50 mM EDTA, 10 mg/ml Proteinase K, 2.5% SDS) was added and the reactions were incubated at 37°C for 30 min. NHEJ products were separated by 0.6% agarose gel electrophoresis, after which the gel was dried for 2 h.  $^{32}\text{P}$  labeled bands were detected by PMI and densitometry was carried out using BioRad Quantity One software. For each cell line, a minimum of 2 independent extracts were prepared. NHEJ activity was independently tested for each extract at least twice, and each test was performed in triplicate.

## **Chapter 3**

### **TDP1 physically interacts with XLF**

## **Introduction**

Yeast study showed that TDP1 affected the efficiency and accuracy of NHEJ to repair restriction enzyme generated DSB [12]. NHEJ junctions in TDP1-deficient yeast showed increased frequency of gap filling by DNA polymerase 4, which required NHEJ proteins Ku70, Ku80 and ligase IV. In addition, Akopiants and colleagues observed that NHEJ junctions in XLF-deficient human cells showed reduced gap filling by DNA polymerases [233]. Taken together, these findings indicate that TDP1 participates in NHEJ, and that TDP1 and NHEJ proteins might collaborate to regulate NHEJ efficiency and accuracy. We hypothesize that, in human cells, TDP1 interacts with NHEJ protein XLF, or maybe XRCC4 which interacts with end processing enzymes, such as PNKP [124]. And the interaction between TDP1 and NHEJ required factor might affect TDP1 activity.

To determine whether there is physical interaction between the human TDP1 and XLF proteins, affinity capture (pull down) was carried out using purified recombinant human TDP1 and XLF. We observed that his-tagged TDP1 was retained by MBP-tagged XLF on the MBP-affinity amylose resin, indicating a physical TDP1:XLF interaction. We also determined that the TDP1:XLF interaction requires the C-terminal domain of XLF. To assess the effect of TDP1:XLF interactions on TDP1 catalytic activity, we assessed the ability of purified recombinant TDP1 to remove a 3' phosphotyrosine or a 3' biotin from oligonucleotide substrates. In this assay, TDP1 enzymatic activity assay showed that XLF



can stimulate TDP1 activity by 2-3 fold on dsDNA (dsDNA), but has no effect on ssDNA (ssDNA).

### **3-1 Expression and purification of his-TDP1 and GST-XLF**

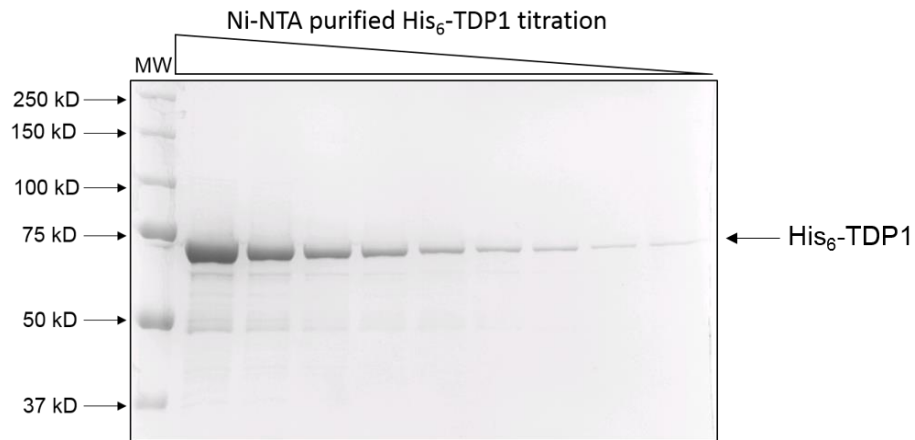
To express human TDP1 in *E. coli*, we transformed plasmid pET-15b-hTDP1 and pET-23b-hTDP1 in BL21(DE3), which is a commonly used chemically competent cell line for protein expression, and Rossetta2 cells. Rossetta2 strain supplies tRNAs for 7 rare codons (AGA, AGG, AUA, CUA, GGA, CCC, and CGG) which could be required for human TDP1 expression, this could be the reason that Rossetta2 can be used for efficient expression of human TDP1. We compared expression from pET-23b-hTDP1, which includes bacterial vector carrying N-terminally T7-tag sequence, and pET-15b-hTDP1, which includes bacterial vector carrying N-terminally his-tag sequence, and found that optimal expression from pET-15b hTDP1 in Rosetta2 cells. We transformed pET-15b-hTDP1 and pEGX-XLF into Rossetta2 cells to express his6-tagged TDP1 (his-TDP1) and GST-tagged XLF (GST-XLF), respectively.

We used Ni-NTA and GSH affinity resins to purify his-TDP1 and GST-XLF, respectively, as described in chapter 2, used SDS-PAGE to identify elution fractions of highest purity. Selected elution fractions were pooled, dialyzed, and protein concentration was measured by Bradford (BioRad) assay. Purified proteins were aliquoted, frozen on liquid nitrogen, and stored at -80 °C. To ensure scientific rigor and minimize possible

artifacts from overexpression and purification, at least two batches of each recombinant protein were independently overexpressed and purified, and all assays were carried out using proteins from at least two independent purifications. Single-step affinity-chromatography of his-TDP1 and GST-XLF yielded proteins of approximately 70% purity (Figure 3-1). Subsequent purification on Hi-trap Q column increased protein purity to more than 90% (Figure 3-2B).

Figure 3-1

A.



B.

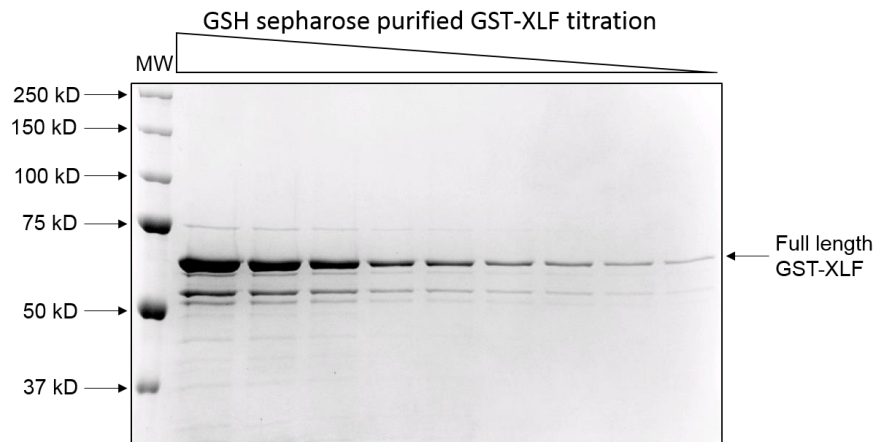


Figure 3-1 Column purified his-TDP1 and GST-XLF

**(A)** Ni-NTA purified his-TDP1 titration from 50 µg to 0.195 ng (1:2 dilution).**(B)** GST-sepharose purified GST-XLF titration from 50 µg to 0.195 ng (1:2 dilution).

### **3-2 TDP1 physically interacts XLF**

To determine whether his-TDP1 physically interacts with GST-XLF, we used Ni-NTA resin which should specifically bind his-TDP1, and retain GST-XLF through TDP1:XLF interactions. We began by loading purified, recombinant his-TDP1 on the Ni-NTA resin, thoroughly washed away any unbound protein, and then loaded purified, recombinant GST-XLF. After thorough washing to remove any unbound GST-XLF, proteins were eluted with imidazole, resolved on SDS-PAGE, western transferred, and membranes were probed with anti-XLF antibodies to determine whether his-TDP1 facilitated retention of GST-XLF on Ni-NTA. Reactions containing both his-TDP1 and GST-XLF showed affinity capture of significant amounts of GST-XLF, which suggested that TDP1 and XLF physically interact. Control reactions containing his-TDP1 alone lacked detectable XLF, which indicated that the anti-XLF antibody did not cross-react with his-TDP1. However, in control reactions containing GST-XLF alone, significant amounts of GST-XLF were retained by Ni-NTA in the absence of his-TDP1 (data not shown). Based on this non-specific retention of GST-XLF by Ni-NTA we abandoned the use of this combination of reagents.

As an alternative, we used GSH-sepharose to specifically capture GST-XLF, and any associated proteins. Unfortunately, we observed non-specific retention of his-TDP1 on GSH-sepharose (data not shown) and abandoned the use of the GST-XLF and GSH-sepharose system.

We moved to the maltose-binding protein (MBP) system, which utilizes amylose resin for affinity capture. Expression of MBP-XLF was successfully induced in Rossetta2 cells (Figure 3-2A). We used amylose resin to bind specifically capture and purify MBP-XLF. After thorough washing to remove any unbound proteins, we added purified recombinant his-TDP1, washed thoroughly to remove unbound proteins, and eluted maltose. The purity of TDP1 used in these assays is shown in Figure 3-2B (91% purity). Retention of his-TDP1 was detected via western blot using a monoclonal anti-his antibody to detect his-TDP1, and we observed XLF-dependent affinity capture of his-TDP1. Importantly, we no longer saw non-specific retention of his-TDP1 on the amylose resin (Figure 3-2C). TDP1-WT showed interaction with MBP-XLF (Figure 3-2C). We were unable to detect his-TDP1 in binding reactions that contained MBP alone, as compared to MBP-XLF, which indicated that his-TDP1 was captured through interaction with XLF, and not with the MBP affinity tag. His-TDP1 and MBP-XLF might bind to the same strand of DNA, that can also lead to false positive result. To determine whether the interaction was mediated by DNA, we performed the affinity capture assay in the presence of ethidium bromide (EtBr). EtBr can intercalate in DNA to impair some protein:DNA interactions, and is frequently used in protein:protein interaction assays to reduce false positive results mediated by DNA [234, 235]. His-TDP1:MBP-XLF interactions were unchanged by the addition of EtBr, indicating that the interaction between TDP1 and XLF was not likely mediated by DNA (Figure 3-2C). By using electrophoretic mobility shift assay, Dr. Heo in

our lab observed ternary complex composed of TDP1, XLF and DNA [236]. It is likely that the TDP1:XLF interaction mediates formation of the TDP1:XLF:DNA complex.

Figure 3-2A

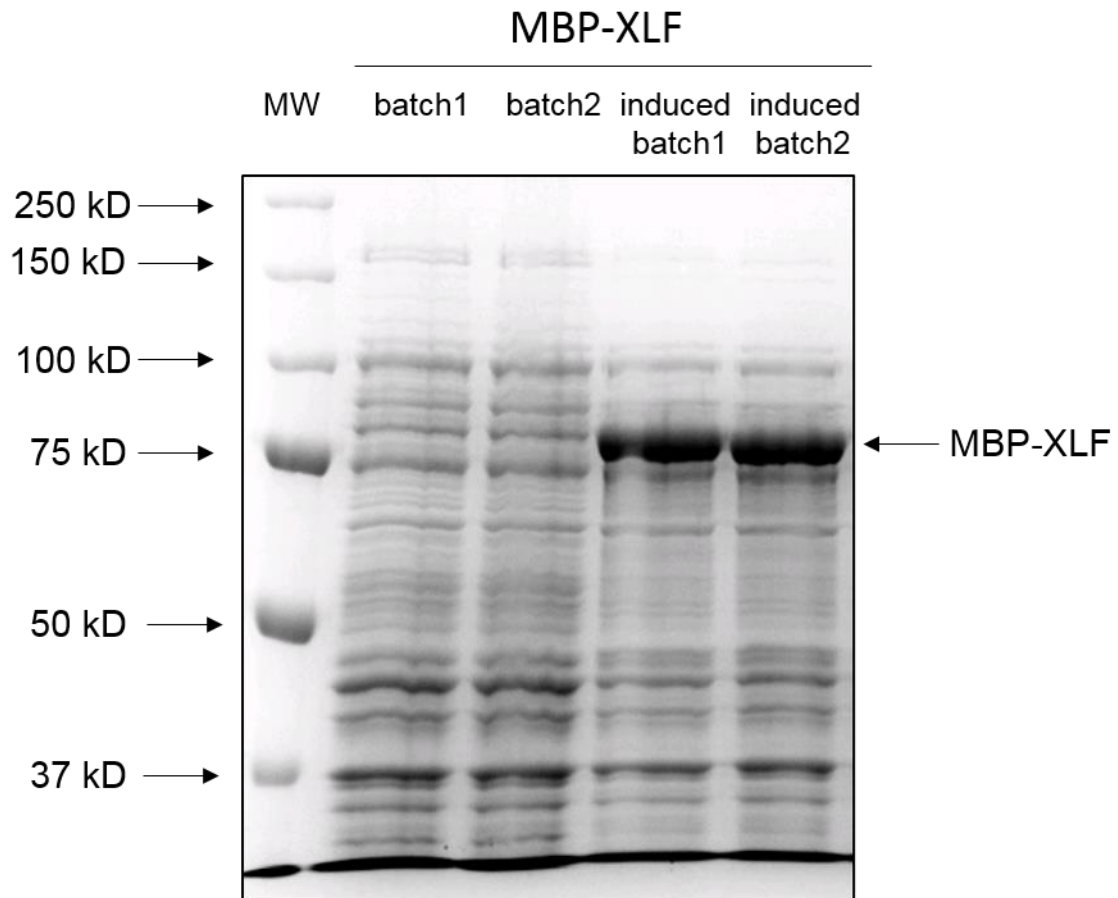


Figure 3-2A MBP-XLF lysate used in affinity capture assay

MBP-XLF was expressed Rossetta2 cells at 18°C for 16 h as described in chapter 2. MBP-XLF is 75 kD (MBP: 42 kD, XLF: 33 kD, which usually observed around 37 kD to 40 kD). Both induced batch 1 and 2 had significant MBP-XLF induction compare to not induced batches. Samples were separated by SDS-PAGE and stained by coomassie brilliant blue.

Figure 3-2B

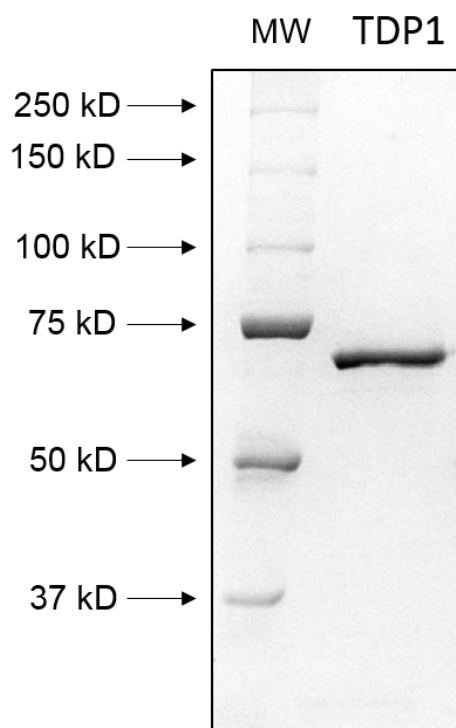


Figure 3-2B Purified, recombinant TDP1 used in affinity capture assay

His<sub>6</sub>-TDP1 was purified by using Ni-NTA column followed by Hi-trap Q column as described in (methods chapter). The purity of His<sub>6</sub>-TDP1 is estimated to be 91%.



Figure 3-2C

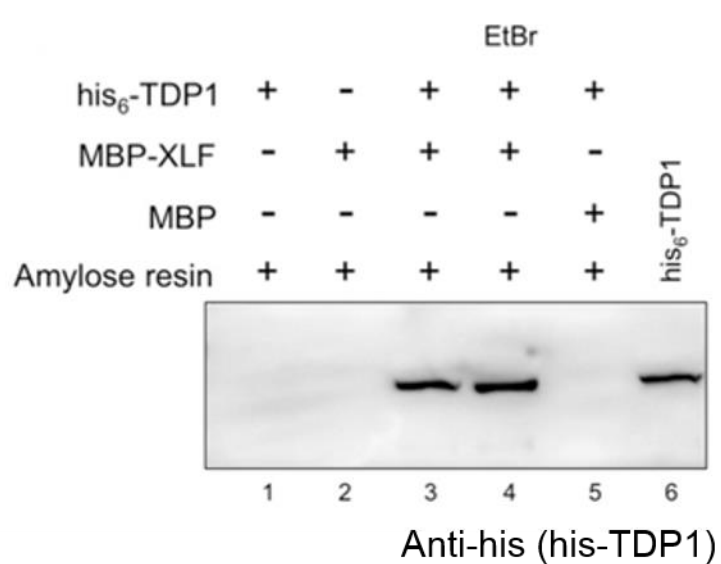


Figure 3-2C His-TDP1 physically interacts with MBP-XLF

MBP-XLF, or MBP alone, was used to pull down his-TDP1 on amylose resin as described in materials and methods. Lane 4, EtBr (100 µg/ml) was added to pull down reaction. Lane 6, his-TDP1 protein positive control for Western blot. Samples were separated by SDS-PAGE, Western transferred and his-TDP1 was detected using anti-his monoclonal antibodies.

### **3-3 TDP1 mutants (TDP1-ΔN, TDP1-H263A, TDP1-H493R) retain the ability to interact with XLF**

To identify the determinants of TDP1:XLF interaction, we first carried out mutational analysis of TDP1 to determine how well TDP1 mutants interacted with full length XLF. As described in chapter 1, TDP1 is composed of a poorly conserved N-terminal domain (1-148aa) and a well conserved catalytic domain (149-609) [183, 184, 222]. The N-terminal domain of TDP1 mediates interaction with several DNA repair proteins [208, 223, 224, 237], making it plausible that the TDP1:XLF interaction might also be mediated by the TDP1 N-terminal domain. To test this, we generated his-TDP1-ΔN mutant and used it in the further pull down assay. To determine whether TDP1 enzymatic activity is required for XLF interaction, we generated TDP1 proteins in which the invariant catalytic histidines were mutated. Mutation of H263 to alanine (A) produced the catalytic inactive mutant TDP1-H263A [183]. Substitution of H493 with arginine (R), TDP1-H493R, which is the mutation found in the human SCAN1 disorder, results in a protein with 25-fold reduced enzymatic activity and accumulated the TDP1-H493R:DNA covalent reaction intermediate [182, 190, 209, 212] (Figure 3-3A).

His-tagged TDP1-ΔN, TDP1-H263A, and TDP1-H493R were all expressed in Rosetta2 cells and purified essentially as described in chapter 2. When we purified TDP1-ΔN on Ni-NTA resin, we observed formation of an obvious precipitate after dialysis. Subsequent purifications of TDP1-ΔN used Hi-trap Q ion exchange chromatography after

Ni-NTA to further purify the TDP1- $\Delta$ N, and additional glycerol was added to the dialysis buffer to promote TDP1- $\Delta$ N solubility. Following these changes, TDP1- $\Delta$ N was purified to 93% purity as estimated by silver stained gel (Figure 3-3B). We purified other TDP1 mutants (TDP1-H263A and TDP1-H493R) and TDP1-WT by using Ni-NTA followed by Hi-trap Q with 10% glycerol during dialysis. All TDP1 proteins showed more than 90% purity, and lacked evidence of protein precipitation (Figure 3-3B).

To determine whether the various TDP1 mutant proteins that we produced retained or lacked enzymatic activity, we carried out TDP1 enzymatic activity assays *in vitro*. In this assay, we used a 5'-<sup>32</sup>P labeled DNA oligonucleotide with a 3'-phosphotyrosine as substrate. The 3'-phosphotyrosine can be removed by TDP1 to produce an oligo with 3'-phosphate, has a lower molecular weight, and runs faster on denaturing PAGE (Figure 3-3C). As expected (Figure 3-3D), TDP1- $\Delta$ N, which retained the TDP1 catalytic domain, exhibited enzymatic activity that was comparable to that of TDP1-WT (Figure 3-3E). Also as predicted, TDP1-H263A showed significant reduction in TDP1 catalytic activity (Figure 3-3F). TDP1-H493R also had significant reduced enzymatic activity, and the accumulation of TDP1-H493R:DNA covalent reaction intermediate was observed as a band of very low mobility, possibly stuck in the wells of the gel (Figure 3-3G).

To determine whether TDP1 mutants physically interact with XLF, we carried out the same affinity capture assay as previously described. Both TDP1- $\Delta$ N and TDP1-H263A bound XLF as well as TDP1-WT. In contrast, the SCAN1 mutant, TDP1-H493R, had 4

times reduced, but detectable, retention by MBP-XLF on amylose resin (Figure 3-3H).

Heo and colleagues showed these same TDP1 mutants had dramatically reduced DNA-binding activity as compared to TDP1-WT [236]. That TDP1-ΔN and TDP1-H263A lack DNA-binding activity, but retain the ability to physically interact with XLF, provide additional evidence that the interaction between TDP1 and XLF is not entirely mediated by DNA.

Figure 3-3A

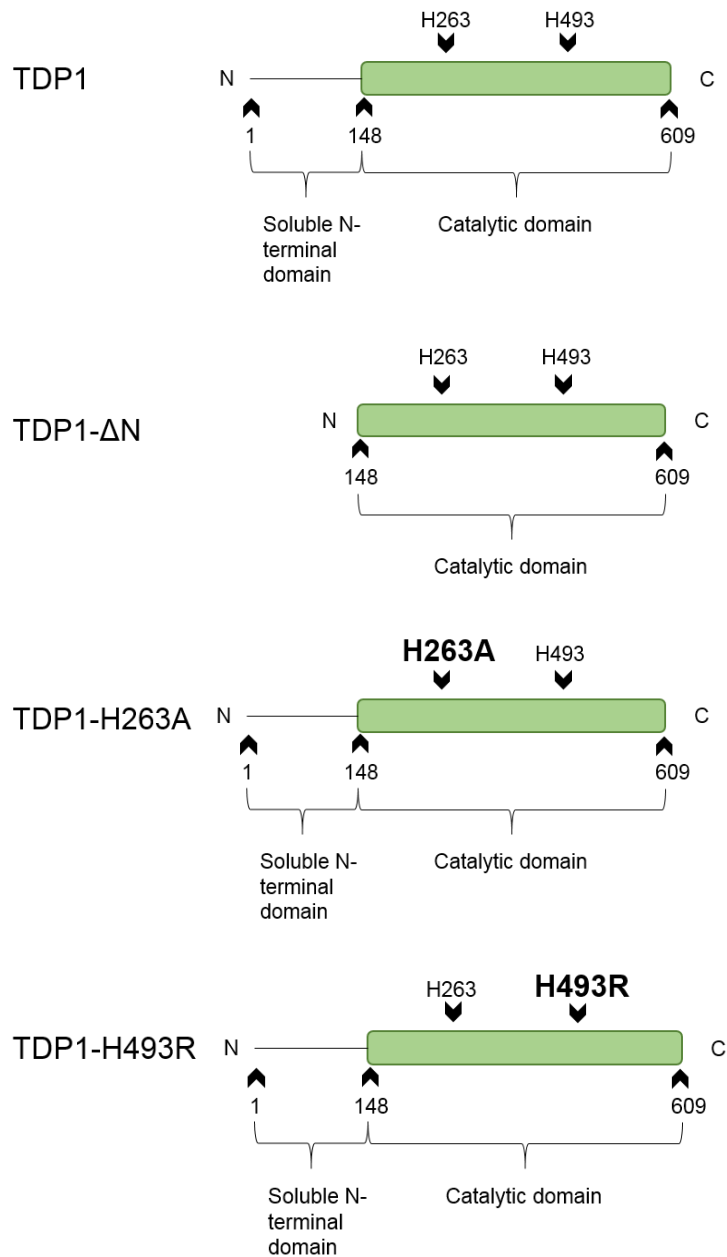


Figure 3-3A Diagrams of TDP1 proteins used in affinity capture assays

From Top to bottom, TDP1 WT (TDP1), N-terminal deleted TDP1 (TDP1-ΔN), catalytically inactive TDP1 (TDP1-H263A), and SCAN1 TDP1 (TDP1-H493R) are showed.

Figure 3-3B

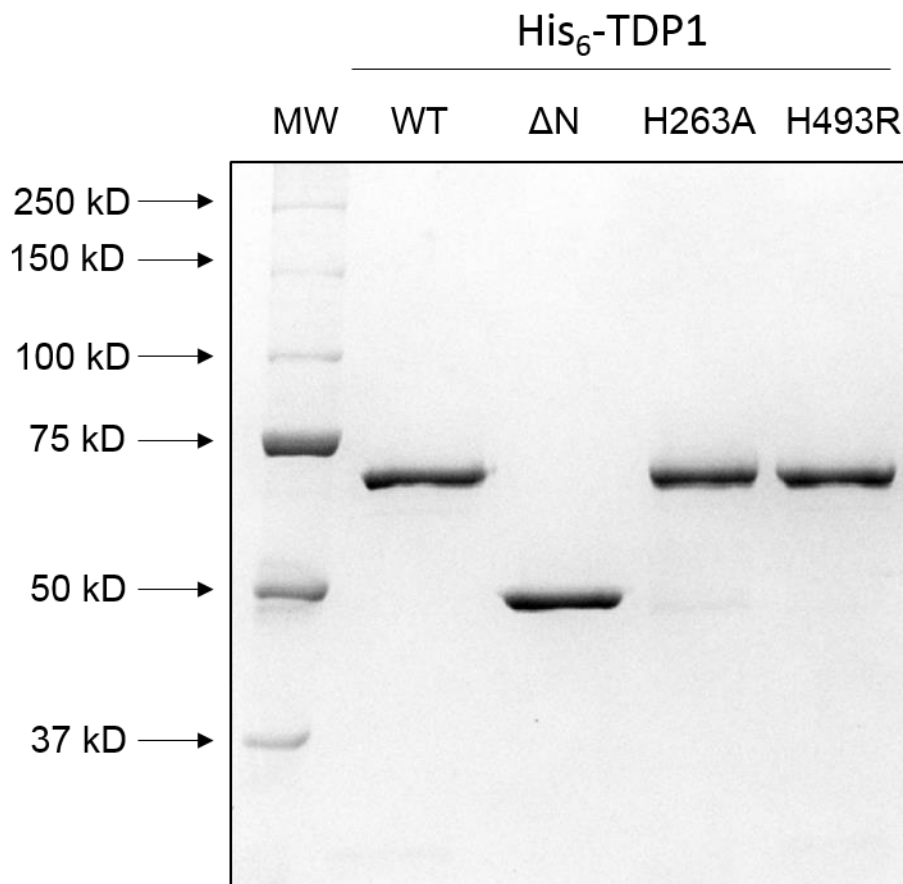


Figure 3-3B Purified, recombinant TDP1 proteins used in affinity capture assays

Purified, recombinant TDP1-WT, TDP1-ΔN, TDP1-H263A and TDP1-H493R on silver stained gel. Purity of TDP1, TDP1-ΔN, TDP1-H263A and H493R were estimated to be 91%, 93%, 91% and 94%, respectively.

Figure 3-3C

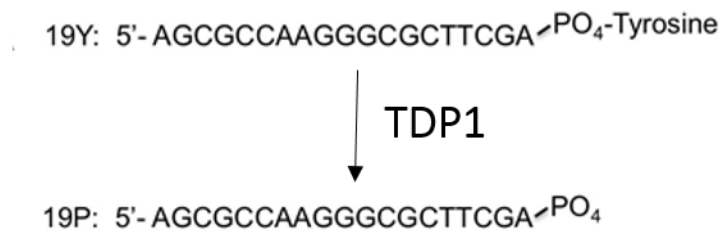
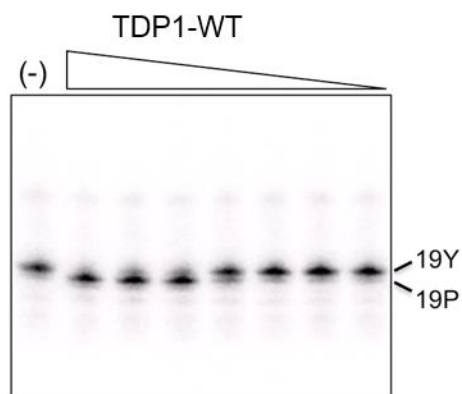


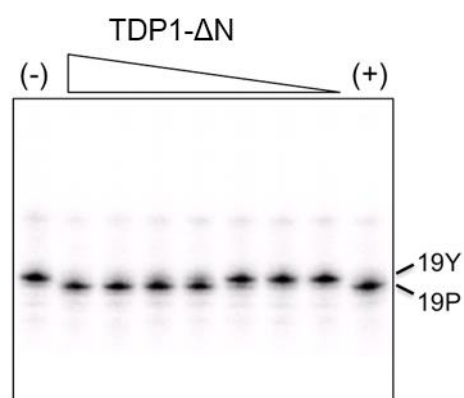
Figure 3-3C Diagram of substrate used for TDP1 enzymatic activity assay  
 19Y: 19-mer oligo was  $^{32}\text{P}$  labeled at 5' end and has tyrosine at 3' end.  
 19P: Expected product generated by TDP1 action on 19Y.

Figure 3-3D-G

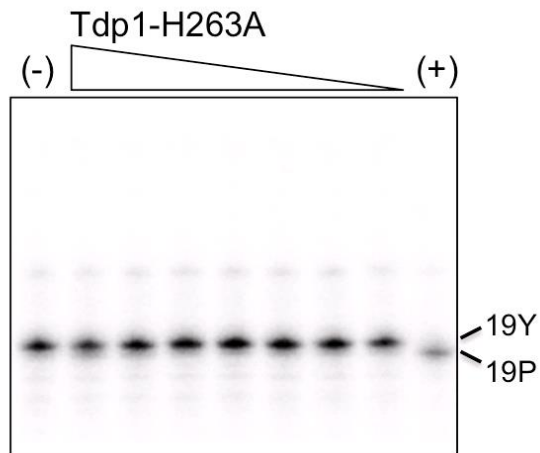
D



E



F



G

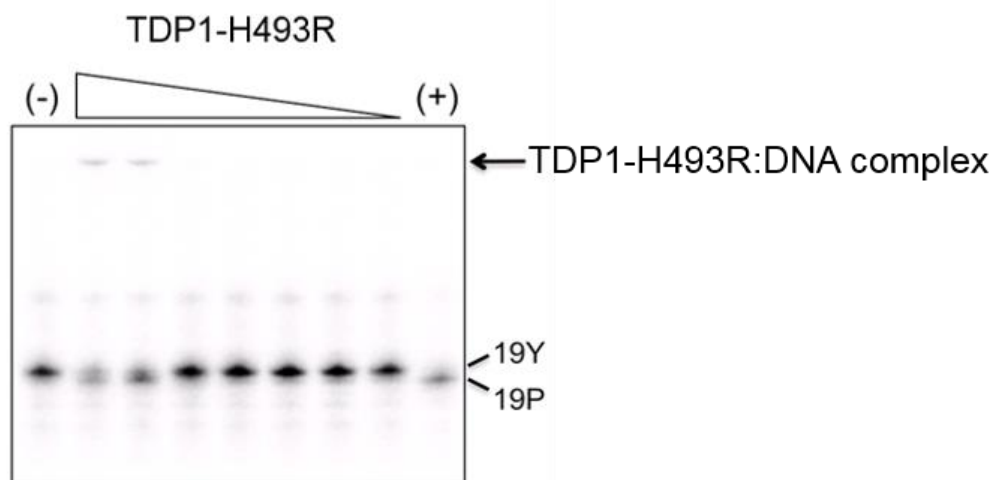


Figure 3-3D-G Enzymatic activity of purified, recombinant TDP1 proteins

Five-fold serial dilutions of the indicated proteins (starting at 0.3  $\mu$ M) were incubated with the substrate for 15 min and products were separated on a 15% denaturing gel. (+) 0.3  $\mu$ M TDP1-WT. Results confirm reports that deletion of the N-terminal domain does not significantly alter catalytic activity, that active site mutant TDP1-H263A is catalytically inactive, and that the SCAN1 mutant TDP1-H493R has reduced activity and forms a covalent TDP1-H493R:DNA complex (arrow).



Figure 3-3H

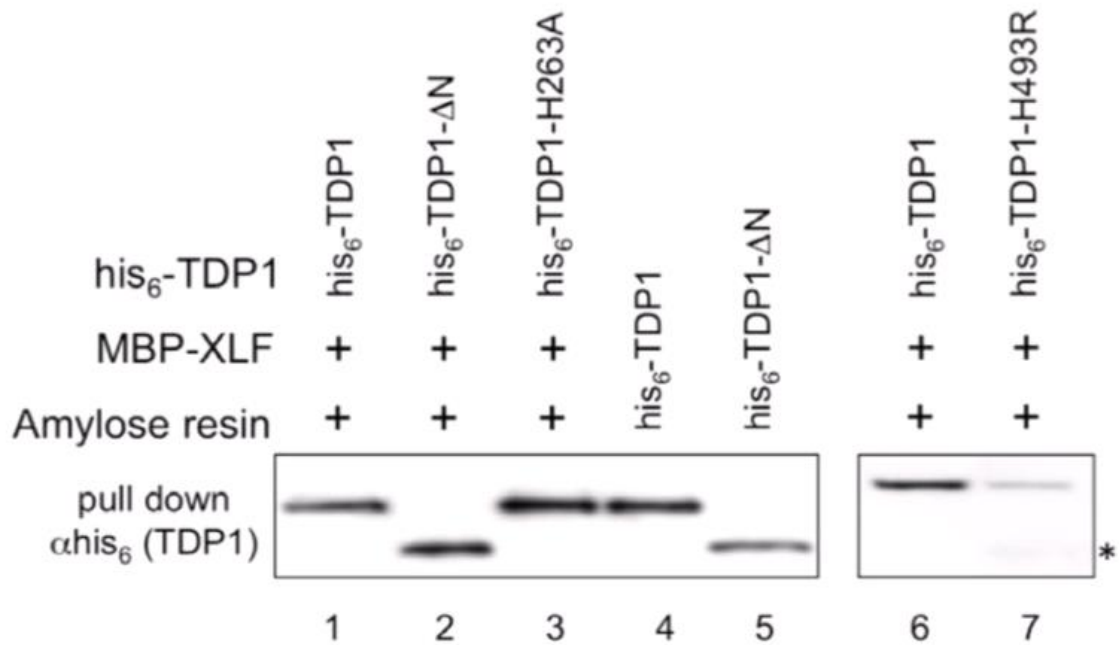


Figure 3-3H Physical interactions between active site and N-terminal deletion mutants of TDP1 and XLF.

Lane 1 and 6, TDP1-WT physically interacts with XLF. Lane 2 and 3, XLF interacts with TDP1-ΔN and TDP1-H263A, respectively. Lanes 4 and 5, his<sub>6</sub>-TDP1 and his<sub>6</sub>-TDP1-ΔN positive controls for Western blot. Lane 7, TDP1-H493R had reduced interaction with XLF. \* indicates C-terminally truncated form of TDP1-H493R that can interact with XLF. Samples were separated by SDS-PAGE, Western transferred and his-tagged TDP1 proteins were detected in the pull-down eluates using anti-his<sub>6</sub> monoclonal antibodies.

### **3-4 The C-terminal domain of XLF is required for interaction with TDP1**

XLF is a homodimer of two identical monomers that are 299 amino acids in length. An XLF monomer is composed of an N-terminal globular head domain that mediates interactions with XRCC4 (residues 1–141) [238], a central coiled-coil domain that mediates homodimerization (residues 142–230), and a C-terminal unstructured domain that facilitates DNA binding (residues 231–299) [239]. David Chen and colleagues showed that the extreme C-terminal residues are required for interaction with Ku and Ku-dependent recruitment to the DSB [36]. This observation suggested that the C-terminal domain might also function as a protein:protein interaction domain. To determine whether the DNA-binding domain of XLF is required for TDP1 interaction, we expressed MBP-XLF- $\Delta$ C (C-terminal deleted XLF - (1-225) in Rosetta2 cells (Figure 3-4A), and used the resulting protein in our affinity capture assay as previously described. We observed that MBP-XLF- $\Delta$ C did not interact with WT his-TDP1 (Figure 3-4B, lane 2). Within the XLF C-terminal domain, lysine 293 (K293) is required for DNA binding, and mutation of K293 to A (XLF-K293A) significantly decreases DNA binding by XLF [138]. To examine the role of XLF DNA binding, or XLF residue K293, in the TDP1:XLF interaction, we expressed MBP-XLF-K293A, which is a XLF mutant was shown lack of DNA binding by electrophoretic mobility shift assay [236], in Rosetta2 cells (Figure 3-4C), and used this mutant XLF to affinity capture WT his-TDP1 on amylose resin. We found that MBP-XLF-K293A reduced TDP1 binding by 2.3 fold relative to binding by XLF-WT

(Figure 3-4D). These data indicates that the C-terminal DNA-binding domain of XLF, and either the DNA-binding activity or K293 of XLF contribute to TDP1:XLF interactions. In addition, these data suggest that the TDP1:XLF interaction might mediated by the DNA binding domain, specifically K293 of XLF, maybe involved in the protein:preprotein interaction.

Figure 3-4A

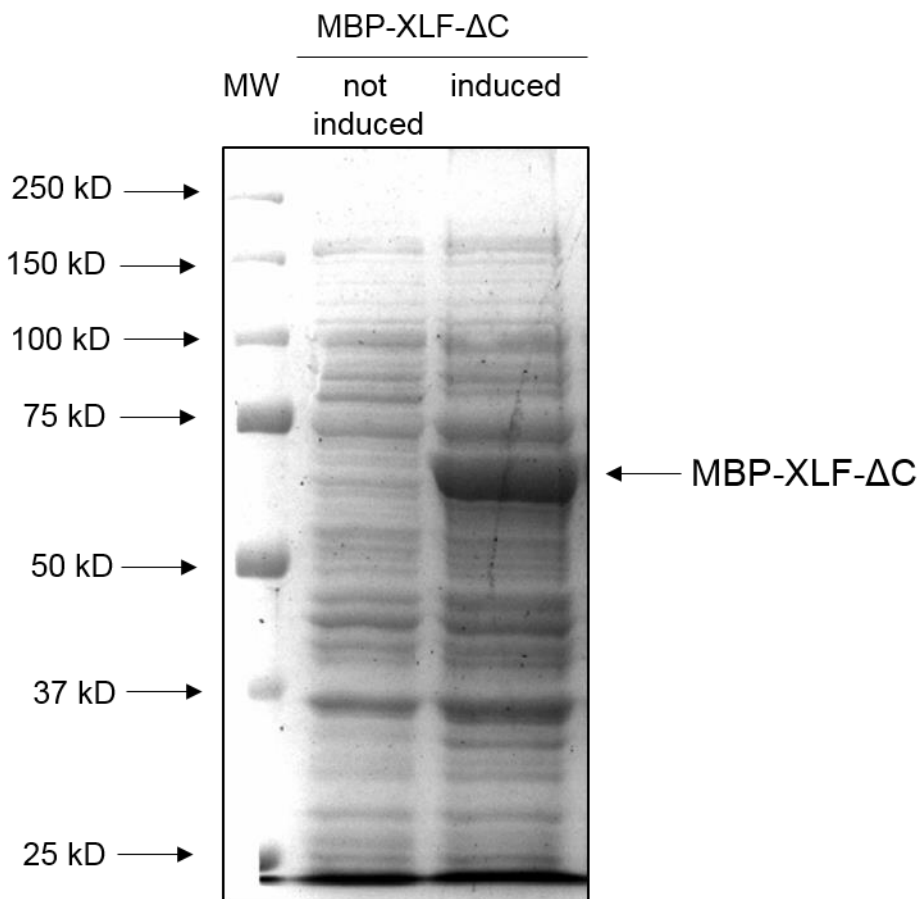


Figure 3-4A C-terminal deleted MBP-XLF lysate used in affinity capture assay

C-terminal deleted MBP-XLF (MBP-XLF-ΔC) was expressed in Rossetta2 cells at 18°C for 16 h. MBP-XLF-ΔC is 67 kD (MBP: 42 kD, XLF-ΔC: 25 kD). Induced sample had significant MBP-XLF-ΔC induction compare to not induced sample. Samples were separated by SDS-PAGE and stained by coomassie brilliant blue.

Figure 3-4B

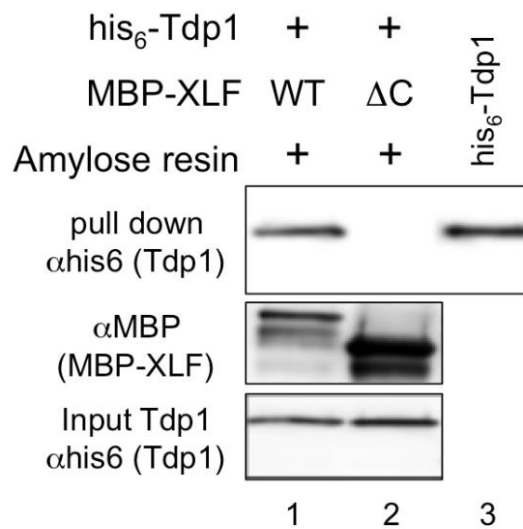


Figure 3-4B The C-terminal domain of XLF is required for interaction with TDP1

MBP-XLF, or XLF-ΔC were used to pull down WT his<sub>6</sub>-TDP1. Samples were separated by SDS-PAGE and Western transferred. His<sub>6</sub>-TDP1 proteins were detected in the pull-down eluates (top) and input (bottom) using anti-his<sub>6</sub> monoclonal antibodies. MBP-XLF proteins were detected with anti-MBP polyclonal antibodies (center).

Figure 3-4C

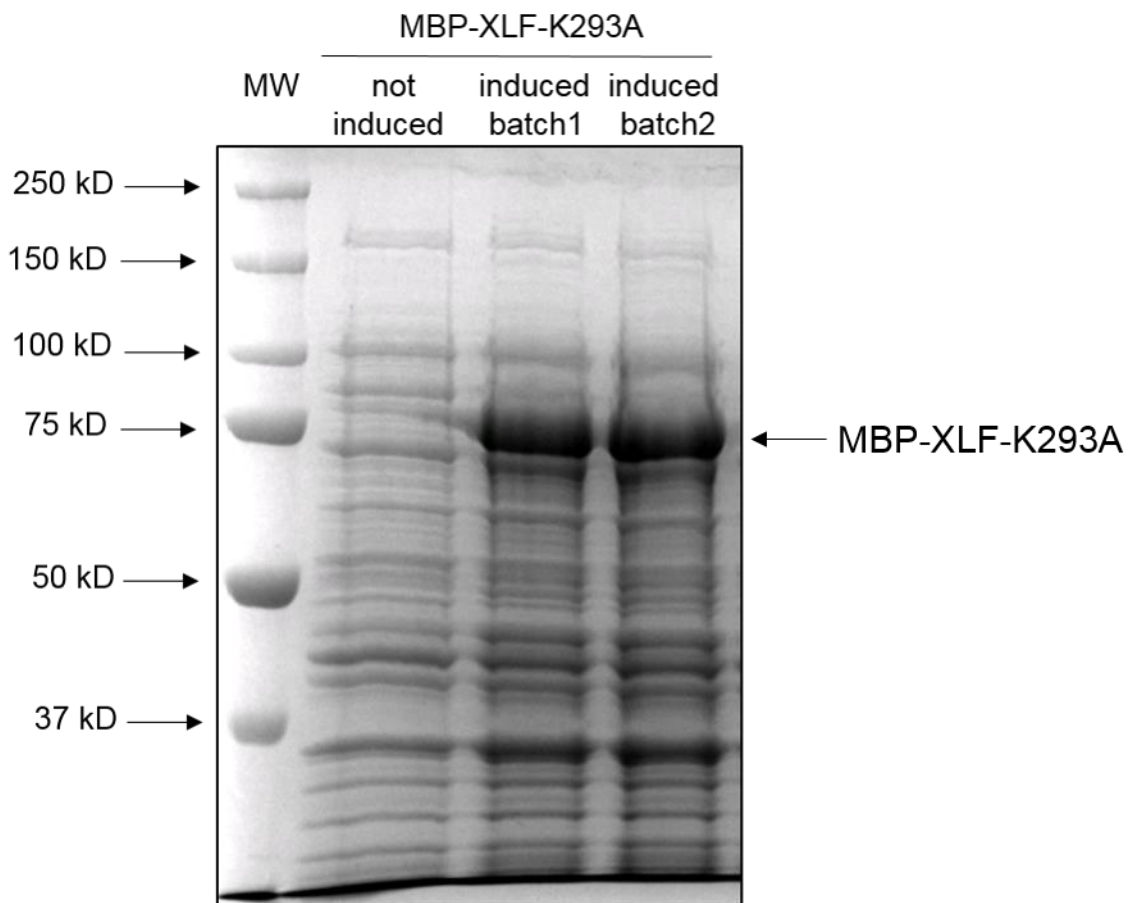


Figure 3-4C MBP-XLF-K293A lysate used in affinity capture assay

MBP-XLF-K293A was expressed in Rossetta2 cells at 18°C for 16 h.

MBP-XLF-K293A is 75 kD (MBP: 42 kD, XLF-K293A: 33 kD). Induced sample had significant MBP-XLF-K293A induction compare to not induced sample. Samples were separated by SDS-PAGE and stained by coomassie brilliant blue.

Figure 3-4D

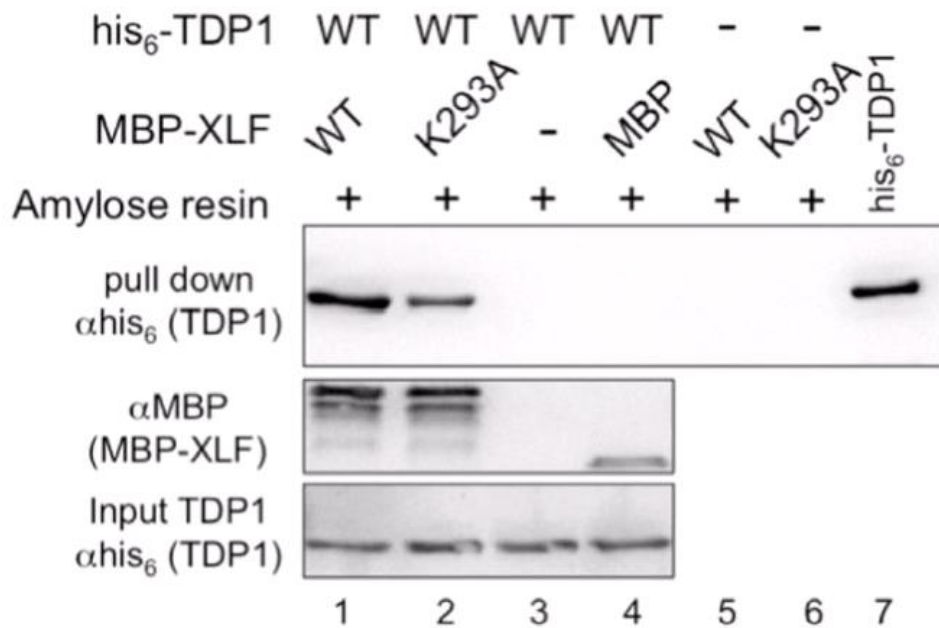


Figure 3-4D XLF-K293A had reduced interaction with TDP1

Samples were separated by SDS-PAGE and Western transferred. His<sub>6</sub>-TDP1 proteins were detected in the pull-down eluates (top) and input (bottom) using anti-his<sub>6</sub> monoclonal antibodies. MBP-XLF proteins were detected with anti-MBP polyclonal antibodies (center).

### **3-5 XLF stimulates TDP1 enzymatic activity on dsDNA, but not on ssDNA**

Having observed a physical interaction between XLF and TDP1, and formation of TDP1:XLF:DNA ternary complexes, we hypothesized that the TDP1:XLF interaction might have biochemical consequences. Specifically, that binding of XLF to TDP1 might affect TDP1 enzymatic activity. To assess the effect of XLF on TDP1 enzymatic activity, we used an oligonucleotide with a 3' biotin, which can be removed by TDP1.

Because both XLF and TDP1 have been described as length-dependent DNA-binding proteins that prefer longer DNA substrates for binding [134, 181, 240, 241], we used longer oligonucleotides than the 19 nucleotide 3' phosphotyrosyl substrates shown in Figure 3-3. For this assay, we employed a previously described 3' biotinylated 61 residue oligonucleotide that was 5' <sup>32</sup>P labeled [182]. We first demonstrated that our purified, recombinant his-TDP1 was able to cleave the 3' biotin and generate the expected product (Figure 3-5A). To visualize the size difference between substrate and product we used a large-format sequencing gel (45 cm x 20 cm) apparatus. TDP1 activity reaction with 19-Y substrate was run on the sequencing gel as a positive control. TDP1 successfully removed the 3' biotin from the 61-mer oligonucleotide and generated a detectable product that could be distinguished from the substrate on the sequencing gel (Figure 3-5B).

Because XLF is a dsDNA binding protein [242], we developed a dsDNA version of the TDP1 substrate by annealing the 5' <sup>32</sup>P-labeled, 3' biotinylated single-stranded



61-mer with a fully complementary bottom strand. As expected, the 3' biotin of the double-strand substrate was removed by TDP1 (Figure 3-5C), and the product was visualized at the same position as single-strand product on the sequencing gel (Figure 3-5D). TDP1 enzymatic activity was tested using single- and double-strand substrates (Figure 3-5D). We found that 50 and 100 ng of TDP1 converted ~50% and ~80%, respectively, of the substrate to product under our assay conditions. Using 50 ng of TDP1 we would be able to determine whether XLF stimulated TDP1 activity, through increased product formation as compared to the same reaction without XLF. Using 100 ng of TDP1, we would be able to determine whether XLF inhibited TDP1 activity, through reduced product formation as compared to the same reaction without XLF. Purified, recombinant XLF used in these TDP1 enzymatic activity assays was his<sub>6</sub>-flag-XLF purified by Ni-NTA column followed by Hi-trap Q column as described in chapter 2 (Figure 3-5E).

We first looked at the effect of XLF on 50 ng TDP1 on single strand DNA by titrating in XLF (0-800 ng, 1:2 dilution steps). Treatment with 800 ng of XLF alone had no effect on the substrate, indicating XLF does not have the ability to cleavage 3'-biotin adduct from DNA end. In addition, this experiment also showed that any impurities that may have co-purified with XLF do not result in a false-positive signal. 800 ng of BSA was used as a negative control to demonstrate the specific effect of XLF effect on TDP1 activity. Compared to the reaction containing TDP1 alone, we saw no effect of XLF on the amount of TDP1 product produced (Figure 3-5F), which indicated that XLF did not affect the

ability of TDP1 to act on a single strand DNA 3' biotin substrate. We then used double strand DNA substrate, with a fixed amount of TDP1 (25 ng or 50 ng), and titrated in XLF to determine whether XLF affect TDP1 enzymatic activity. As compared to the reaction containing TDP1 alone, we observed increased product formation in reactions containing both TDP1 and XLF (Figure 3-5G). In subsequent experiments we used a fixed amount of XLF and titrated TDP1, and clearly observed an increase in TDP1 activity on double strand DNA in the presence of XLF (Figure 3-5H).

In the enzymatic activity assay, we used purified, recombinant flag-his-TDP1 (Figure 3-3B) and his-XLF (Figure 3-5E). We used 60 nM XLF with 4.69, 9.38, 18.75 and 37.5 nM TDP1 on single- and double-stranded DNA substrates. Three independent experiments were carried out using at least two separate batches of purified recombinant proteins, all reactions were done in experimental triplicates (Figure 3-5I). XLF increased TDP1 enzymatic activity on the dsDNA substrate by 2-3 fold, but had no effect on TDP1 activity on the ssDNA substrate. We found that in the absence of XLF, TDP1 had higher enzymatic activity on the ssDNA 3'-biotinylated substrate as compared to the dsDNA 3'-biotinylated substrate, which is consistent with previously published observations [180, 181, 243]. A summary of the data is presented in Figure 3-5J.

Figure 3-5A

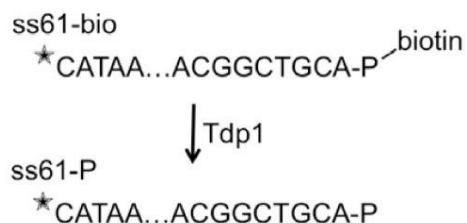


Figure 3-5A Single-strand substrate used in TDP1 enzymatic assay

A 61-mer oligonucleotide was  $^{32}\text{P}$ -labeled at the 5' end with a covalently linked biotin at the 3' end (ss61-bio). TDP1 was able to cleave 3'-biotin, which resulted in a lower molecular weight product ss61-P.  $\star$  Indicates 5'  $^{32}\text{P}$  label.

Figure 3-5B

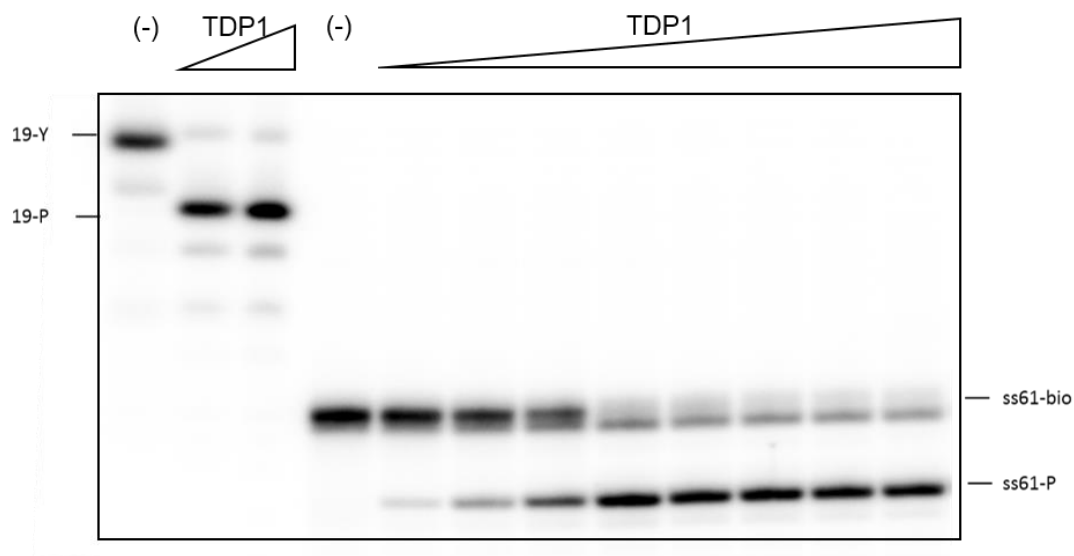


Figure 3-5B Sequencing gel provides suitable separation between ssDNA 3'-biotinylated substrate and the product generated by TDP1

19Y and 19P generated by 8 and 16 ng of TDP1 were used as positive controls for TDP1 enzymatic activity (described in section 3-3). The ssDNA 3'-biotinylated 61-mer (ss61-bio) was incubated with TDP1 (6.25, 12.5, 25, 50, 100, 200, 400 and 800 ng) as described in chapter 2. (-) indicates substrate only (no TDP1 added).

Figure 3-5C

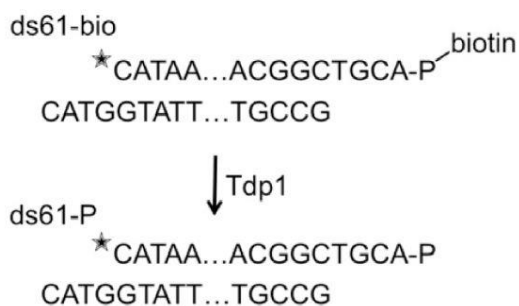


Figure 3-5C Double-strand substrate used in TDP1 enzymatic assay

ss61-bio was annealed with a fully compatible bottom strand to form a dsDNA TDP1 substrate with 3'-biotin. TDP1 was able to cleave 3'-biotin to produce a lower molecular weight product ds61-P. ★ Indicates the <sup>32</sup>P label.

Figure 3-5D

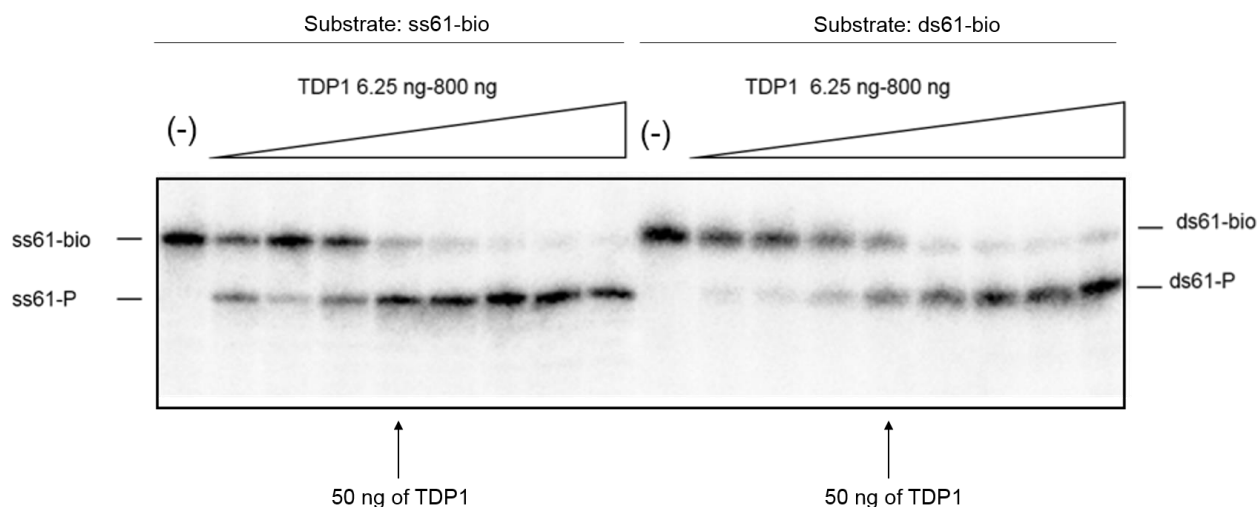
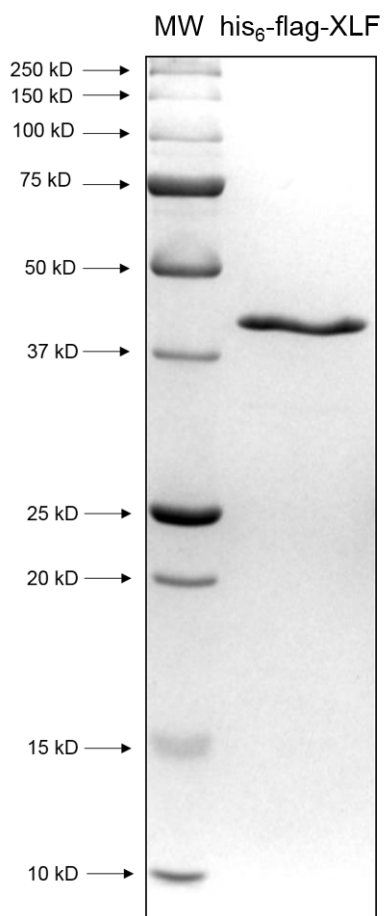


Figure 3-5D Denaturing sequencing gel can separate double strand biotinylated substrate and TDP1 generated product

3'-biotinylated ss- or ds-DNA 61-mer 3'-biotinylated substrates (ss61-bio and ds61-bio) was incubated with TDP1 (6.25, 12.5, 25, 50, 100, 200, 400 and 800 ng). Product generated by TDP1 (ss61-P and ds61-P) is indicated. (-) indicates substrate only (no TDP1). Because we used denaturing gel to separate samples, ds61-bio and ds61-P showed at the same position of ss61-bio and ss61-P, respectively. Arrow: TDP1 amount that chose to use for future experiments.

Figure 3-5E

Figure 3-5E Purified, recombinant his<sub>6</sub>-flag-XLF used in TDP1 activity assay

His<sub>6</sub>-flag-XLF was purified by Ni-NTA column followed by Hi-trap Q column as described in chapter 2.

600 ng of XLF was resolved on 12% SDS-PAGE. Gel was stained with coomassie brilliant blue for detection

Figure 3-5F

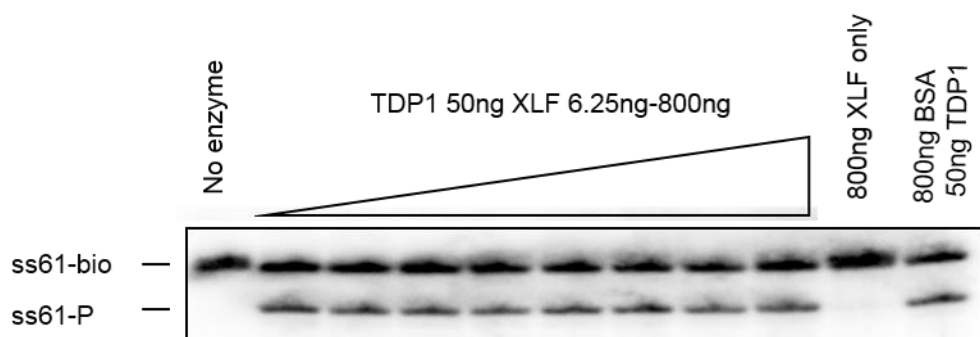


Figure 3-5F XLF has no effect on TDP1 enzymatic activity on ssDNA

TDP1 (50 ng) and XLF (6.25, 12.5, 25, 50, 100, 200, 400 and 800 ng) were incubated with ss61-bio as described in chapter 2. No enzyme: ss61-bio only. 800 ng XLF only: ss61-bio incubated with 800 ng XLF. 800 ng BSA 50 ng TDP1: ss61-bio incubated with 800 ng BSA and 50 ng TDP1.

Figure 3-5G

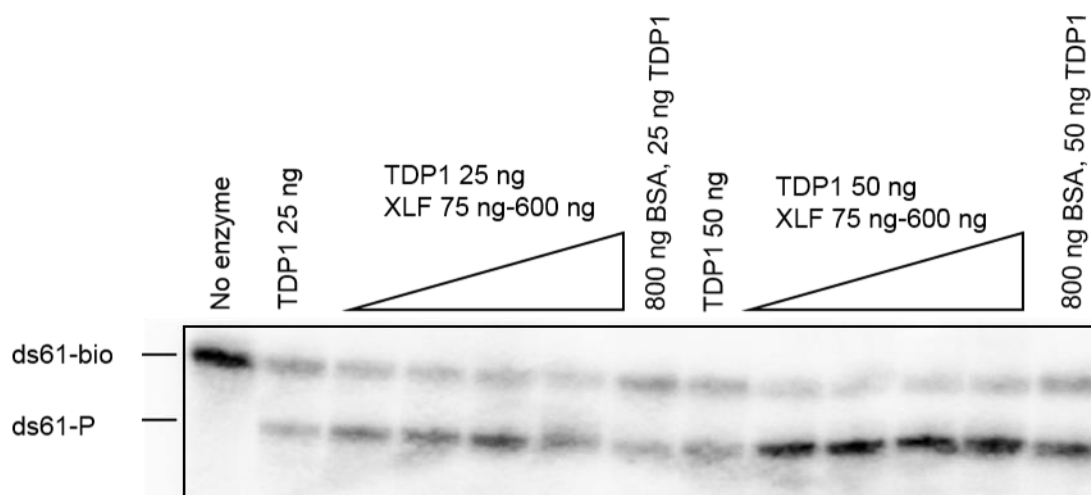


Figure 3-5G XLF increased TDP1 enzymatic activity on dsDNA

TDP1 (25 or 50 ng) and XLF (75, 150, 300 and 600 ng) was incubated with ds61-bio as described in chapter 2. No enzyme: ds61-bio only. 800 ng BSA with 25 or 50 ng TDP1: ds61-bio incubated with 800 ng BSA and 25 or 50 ng TDP1.

Figure 3-5H

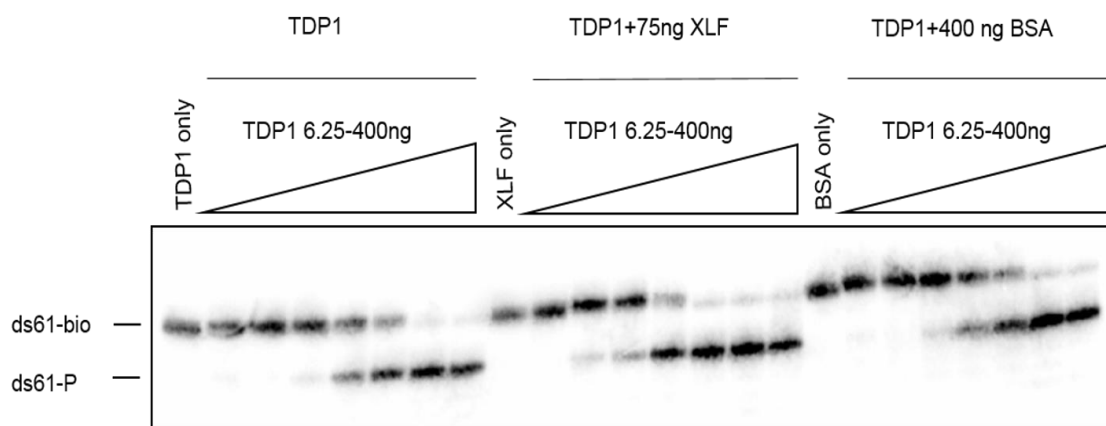


Figure 3-5H XLF increased TDP1 enzymatic activity on dsDNA (TDP1 titration)

ds61-bio was incubated with fixed amount of protein (75 ng XLF or 400 ng BSA) and a variable amount of TDP1 (6.25, 12.5, 25, 50, 100, 200 and 400 ng) as described in chapter 2.

Figure 3-5I

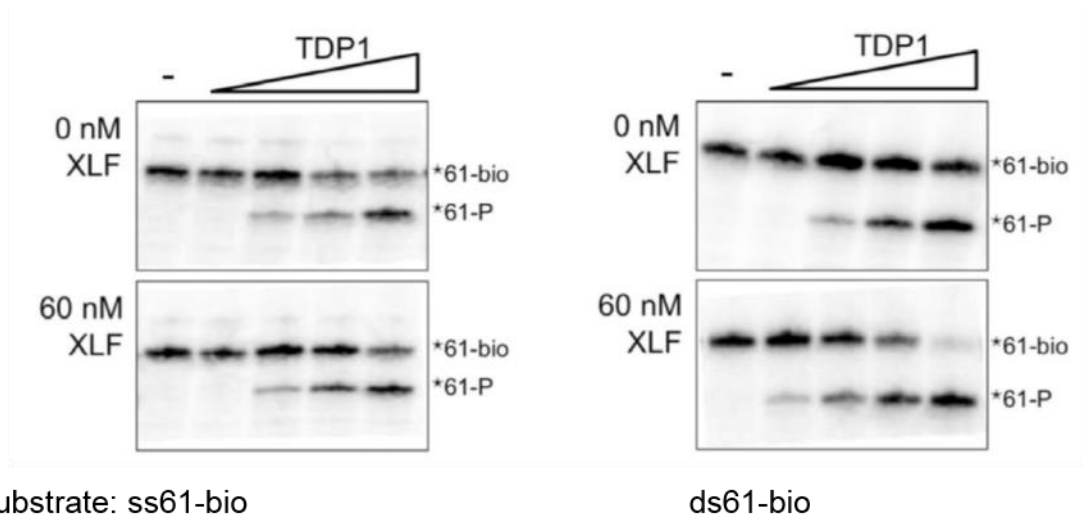


Figure 3-5I XLF increased TDP1 enzymatic activity on dsDNA but not on ssDNA

Left:  $^{32}\text{P}$ -labeled ss61-bio was incubated with TDP1 (4.7, 9.4, 18.75, and 37.5 nM) with 0 or 60 nM XLF.

Right:  $^{32}\text{P}$ -labeled ds61-bio was combined with TDP1 (4.7, 9.4, 18.75, and 37.5 nM) with 0 or 60 nM XLF.



Figure 3-5J

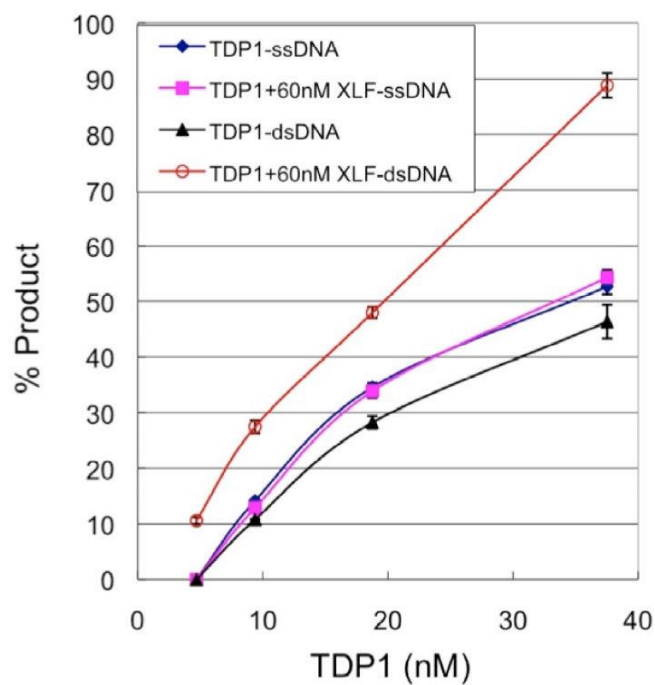


Figure 3-5J Summary of 3 independent TDP1 activity experiments

The intensity of bands (Figure 3-5I) were quantified. % Product: product/ (substrate + product). Graph summarized data from 3 independent experiments with 2 bathes of TDP1 and XLF. Error bars represent standard deviation.

## **Chapter 4**

**TDP1 is required for efficient non-homologous end joining in human cells**

## **Introduction**

Our findings that TDP1 physically interacts XLF and XLF stimulates TDP enzymatic activity on dsDNA *in vitro*. To investigate the role of TDP1 in human cells, we used CRISPR/cas9 technology to knockout TDP1 in 293 human embryonic kidney cells (HEK293). TDP1 knockout (TDP1-KO) cells lacked detectable TDP1 expression, and, as expected, were hypersensitive to topoisomerase poisons and ionizing radiation that resulted in DNA breaks with 3' and 5' terminal adducts. To compare NHEJ efficiency between WT and TDP1-KO cells, we used a chromosomally-integrated end-joining reporter system called EJ5-GFP. In this assay, DSBs with cohesive ends are generated by ectopic expression of the *I-SceI* endonuclease. TDP1-KO cells had 4-5 fold reduced end-joining efficiency as compared with end joining in WT cells. End joining in TDP1-KO cells was largely restored by ectopic expression of wild type TDP1 (TDP1-WT), whereas ectopic expression of the catalytically inactive TDP1-H263A mutant restored only ~60% of end joining. Because the EJ5-GFP system does not discriminate between classical and alternative mechanisms of end joining, we used an *in vitro* NHEJ assay system to compare levels of XRCC4-, and DNA-PK-dependent NHEJ between WT and TDP1-KO cells. Similar to our findings with the EJ5-GFP assay system, extracts prepared from TDP1-KO exhibited only 40% of the *in vitro* NHEJ activity found in extracts from WT cells. To understand the role of TDP1 in error minimization during NHEJ, we used NextGen Sequencing to compare end-joining junctions from the EJ5-GFP reporter in WT and

TDP1-KO cells. The sequencing data showed that while TDP1 deficiency resulted in decreased end joining efficiency, the junctions produced by TDP1-KO cells were overall more accurate than those produced in WT cells. This is likely caused by increased use of microhomology in joining the compatible DNA ends generated by *I-SceI*, which would reflect increased reliance on microhomology-mediated end joining in NHEJ-deficient TDP1-KO cells.

TDP1 was reported to be phosphorylated at serine 81 (S81) by ATM or DNA-PK [223], and this phosphorylation event is thought to regulate interactions with DNA ligase III and XRCC1, and increase accumulation of TDP1 at DNA breaks. We found that ectopic expression of the non-phosphorylatable mutant TDP1-S81A partially restored end-joining efficiency, whereas phosphomimetic mutant TDP1-S81E failed to restore end joining at all. Using affinity capture, we discovered that TDP1-S81A and TDP1-S81E both had reduced XLF binding - TDP1-S81A was reduced by 2-fold, and TDP1-S81E was reduced by 10-fold. These results suggest that: i) TDP1 participation in end joining is likely mediated by interaction with XLF, and ii) that TDP1 participation in NHEJ may be negatively regulated by S81 phosphorylation.

#### **4-1 Generation and characterization of TDP1-knockout cells**

The *in vitro* data suggested a very possible role for TDP1 in NHEJ in living human cells. To assess the role of TDP1 in NHEJ in human cells, we used CRISPR/cas9 to generate TDP1-KO HEK293 cells. HEK293 cell line is stable diploid and only have 2 copy of TDP1 gene (hek293genome.org). The strategy for generating TDP1-KO HEK293 cells is shown in Figure 4-1A. Guide RNAs (gRNAs) designed to target the TDP1 gene right downstream of the start codon in exon 3. Guide RNAs recognizes PAM sequence (NGG) and cleaves at 3-4 nucleotides upstream of the PAM sequence on both strands, that results in DSB. So the knockout was relied on error prone NHEJ to generate in-frame premature stop codon in TDP1 gene. We isolated 12 individual clones. Clones 7D1, 8A3, and 8A5 were picked at random for further investigation, and sequences surrounding the guide RNA targeting site were amplified by PCR and subject to Sanger sequenced (DNA Service Facility in UIC Research Resources Center). We observed that sequences at the target sites in clones 7D1, 8A3, and 8A5 were mutated, resulting in premature in frame stop codons (Figure 4-1B). Western blot with anti-TDP1 antibody showed that 7D1, 8A3 and 8A5 lacked of detectable TDP1 expression (Figure 4-1C).

The role of TDP1 in repair of Top1-mediated DNA damage in response to Top1 poisons is well established [192, 222], so TDP1-KO cells were expected to be hypersensitive to Top1 poisons. Similarly, the role of TDP1 in removal of 3'-phosphoglycolate (3'PG) generated by ionizing radiation has also been reported [189,

190, 229], and we anticipated that TDP1-KO cells would also exhibit increased sensitivity to ionizing radiation. As anticipated, TDP1-KO cell lines 7D1, 8A3, and 8A5 were more sensitive to the Top1 poison camptothecin (CPT) (Figure 4-1D), and to ionizing radiation (Figure 4-1E and F), as compared to WT cells. Ectopic expression of TDP1-WT in TDP1-KO cells restored CPT resistance, which demonstrated that CPT sensitivity was caused by the engineered TDP1 deficiency, and not an off-target effect of CRISPR/cas9 manipulation. As mentioned in Chapter 1, Nitiss and minions showed that TDP1 can cleave a 5' phosphotyrosyl bond, which indicates a probable role for TDP1 in repair of Top2-mediated DNA damage[191]. As predicted by the Nitiss lab findings, we observed that TDP1-KO cells had higher sensitivity to the Top2 poisons etoposide and 4'-(9'-acridinylamino) methanesulfon-m-anisidide (mAMSA) (Figures 4-1G and H). Our findings are consistent with previously published observations made using biochemical assays and cell-free systems, and provide important biological data implicating TDP1 in repair of Top2-mediated DNA damage in human cells. Overall the three TDP1-KO HEK293 cell lines behave in a manner that is consistent with what has been reported for TDP1 deficiency in chicken and murine cells (Table 1). Our drug sensitivity results conclude that they accurately reflect the biological properties of TDP1-deficiency in human cells.

Figure 4-1A

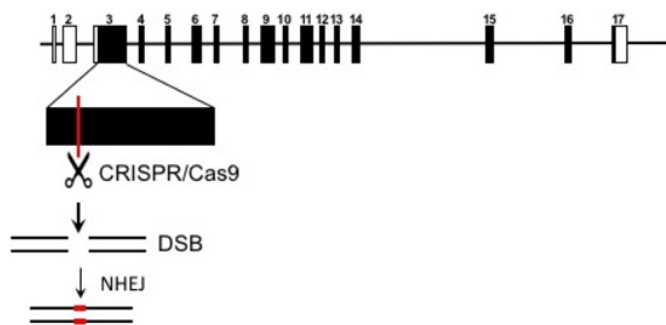


Figure 4-1A Schematic representation of the CRISPR/cas9 strategy used to knockout TDP1 expression

Guide RNAs were designed to target the TDP1 coding sequence 42 bp downstream of the TDP1 start codon, which located on human chromosome 14. Boxes: exons, black boxes: coding sequence, white boxes: 5' and 3' untranslated regions (UTRs). Line: introns.

Figure 4-1B



Figure 4-1B Mutations near CRISPR/Cas9 target site sequences in TDP1-KO cells.

Alignment and comparison of DNA and amino acid sequences surrounding the CRISPR/Cas9 target site comparing TDP1-WT with 3 TDP1-KO cell lines (7D1, 8A3, and 8A5). PAM sequence (red) and CRISPR/cas 9 guide RNA target site (blue) are highlighted.



Figure 4-1C

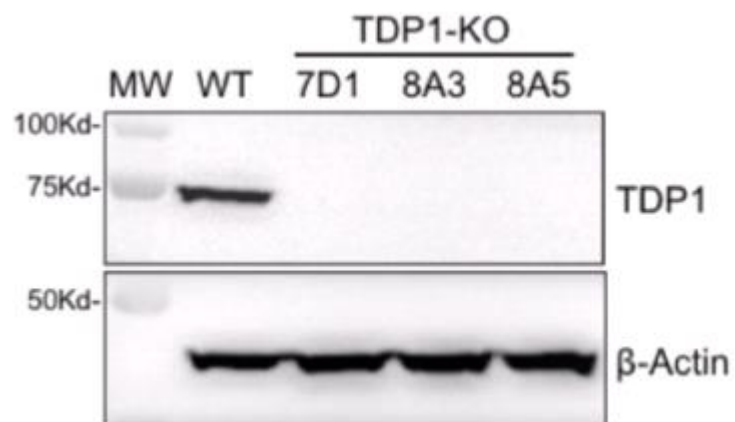


Figure 4-1C TDP1-KO cells lack detectable TDP1 expression.

Western blot analysis was used to detect TDP1 expression in 40  $\mu$ g of whole cell extracts prepared from wild type HEK293 cells (WT) and TDP1-KO clones 7D1, 8A3, and 8A5. Detection of beta-actin ( $\beta$ -actin) is used as a loading control.

Figure 4-1D

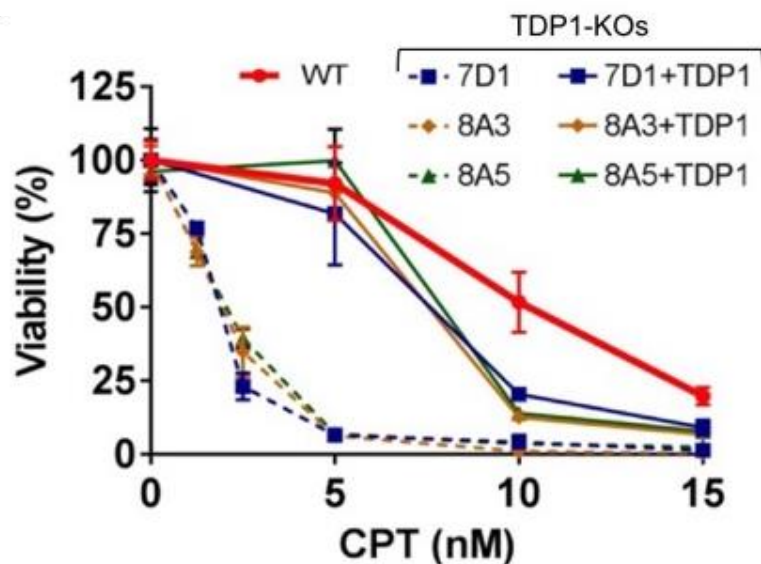


Figure 4-1D TDP1-deficiency dramatically increases camptothecin (CPT) sensitivity in TDP1-KO cells 7D1, 8A3 and 8A5.

WT, TDP1-KO, and TDP1-KO cells ectopically expressing TDP1-WT were treated with CPT at the indicated concentrations (0 nM, 1.25 nM, 2.5 nM, 5 nM, 10 nM, 15 nM) for 72 h. WT (*red*). TDP-KOs (dashed lines): 7D1 (*blue*), 8A3 (*yellow*), and 8A5 (*green*). TDP1-KOs ectopically expressing TDP1 (solid lines): (*blue*), 8A3 (*yellow*), 8A5 (*green*). Cell viability was determined by WST-1 as described in chapter 2.

Figure 4-1E

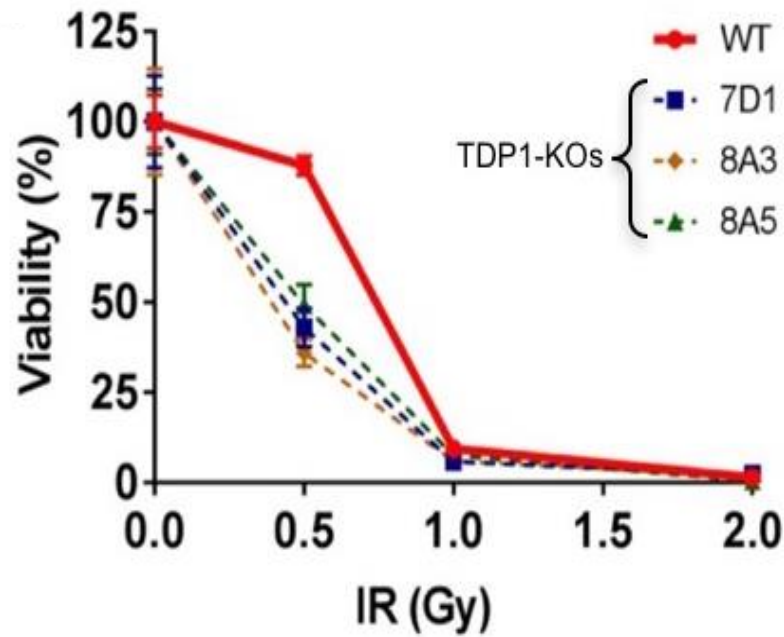


Figure 4-1E TDP1-KO cells 7D1, 8A3, and 8A5 are sensitive to ionizing radiation (IR) as compared to WT cells.

WT and TDP1-KO cells 7D1, 8A3, and 8A5 were exposed to IR as indicated (0 Gy, 0.5 Gy, 1 Gy, 2 Gy) and viability was determined by clonogenic survival. WT (*red*). TDP-KOs (dashed lines): 7D1 (*blue*), 8A3 (*yellow*), and 8A5 (*green*).

#### **4-2 TDP1-knockout cells have reduced end-joining efficiency**

To determine how TDP1 deficiency affects end-joining efficiency, we used the chromosomally-integrated EJ5-GFP end-joining reporter assay. Specifically, this system contains a GFP cDNA that is separated from the promoter by a puromycin-resistance marker (puro), which is flanked by two *I-SceI* meganuclease sites. Cleavage by *I-SceI* will excise the puro marker, leaving a DSB with compatible 3' extensions that will be repaired by homology-independent end joining. Repair will result in GFP expression (Figure 4-2A), and GFP-positive cells can be counted by fluorescence activated cell sorting (FACS) to provide a measure of end joining efficiency (Figure 4-2B).

Cell lines used in the reporter assays are WT-EJ5 and TDP1-KO-EJ5 (TDP1-7D1-EJ5, TDP1-8A3-EJ5, TDP1-8A5-EJ5) which were stably integrated with EJ5-GFP reporter in their chromosomal DNA. We transiently expressed *I-SceI* in WT-EJ5 and the three TDP1-KO-EJ5 cell lines, incubated for 3 days, harvested cells and performed FACS analysis as described in Chapter 2. As shown in Figure 4-2C, TDP1-KO-EJ5 cells had significantly reduced (4-5 fold) end joining efficiency as compared to WT cells. Ectopic expression of TDP1-WT in TDP1-KO-EJ5 cells restored end joining efficiency to near-wild type levels. The XLF-KO-EJ5 cells, which should lack NHEJ, showed around 6% of end joining efficiency. These results indicate that TDP1 is required for efficient end joining in human cells.

We also wanted assessed the effects of enzymatic activity and SCAN1 mutation of TDP1 on end joining efficiency. So we ectopically expressed TDP1-H293A and TDP1-H493R in TDP1-KO cells and then measured the end joining efficiency (Figure 4-2D). Compare to TDP1-KO cells that were ectopic expressed with TDP1-WT, we observed that TDP1 loss of TDP1 enzymatic activity (H263A) rescued some end joining efficiency but SCAN1 mutation (H493R) failed to do so. This experiment suggested that enzymatic activity of TDP1 was not absolute required for end joining, however, same as TDP1 deficiency, TDP1 SCAN1 mutant, which could lead to DNA-TDP1 covalent binding, resulted in reducing end joining efficiency.

Figure 4-2A

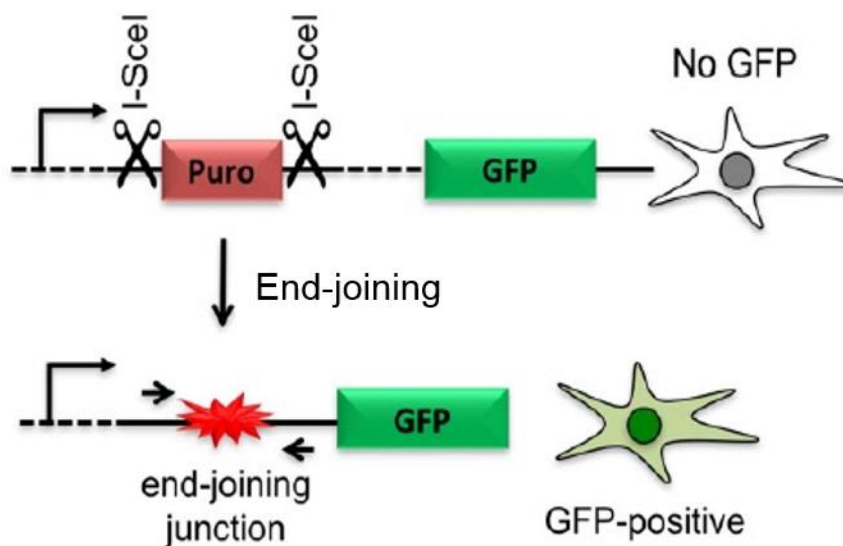


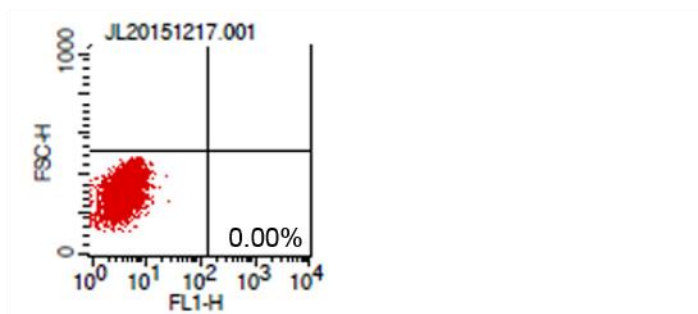
Figure 4-2A Schematic diagram for the EJ5-GFP end-joining reporter system.

EJ5-GFP is shown along with products of end-joining between the DSB ends that restores the GFP expression cassette.

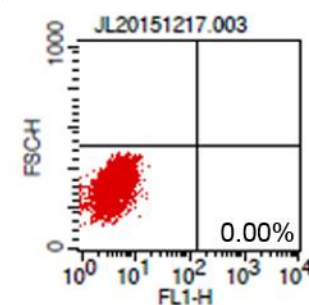
Arrows ( $\rightarrow$   $\leftarrow$ ) indicate PCR primers used to amplify EJ5 end-joining junctions for DNA sequence analysis.

Figure 4-2B

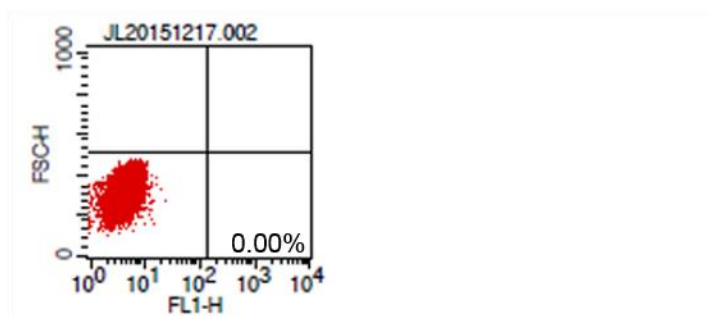
Cell line: HEK293 WT  
Plasmid: No plasmid



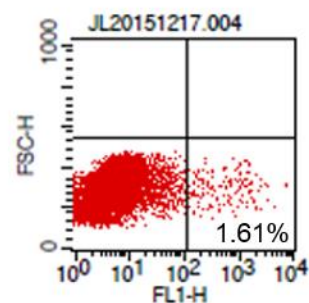
Cell line: HEK293 WT  
Plasmid: I-SceI



Cell line: HEK293 WT-EJ5  
Plasmid: No plasmid



Cell line: HEK293 WT-EJ5  
Plasmid: I-SceI



Cell line: HEK293 WT-EJ5  
Plasmid: EGFP

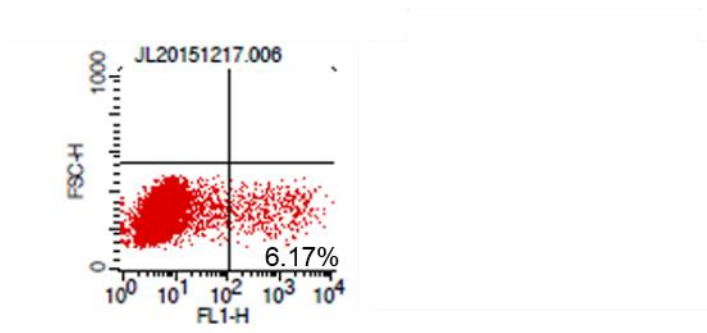


Figure 4-2B Representative FACS analysis of WT HEK293 cells with EJ5-GFP end joining reporter system

Cell line and transfected plasmid are indicated above the FACS analysis graph of each sample. GFP positive cells and GFP cell percentage of each sample are indicated in bottom right quadrant.

Figure 4-2C

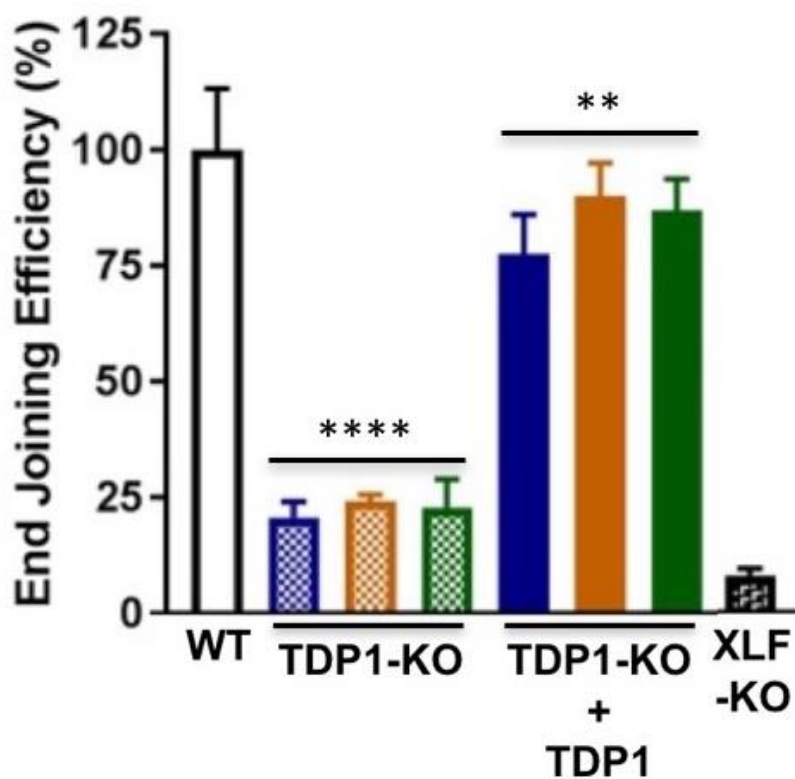


Figure 4-2C TDP1-KO cells have reduced end-joining efficiency.

WT, TDP1-KO (7D1, 8A3, and 8A5) and XLF-KO cells carrying the chromosomally integrated EJ5 end-joining reporter were transiently transfected with the *I-SceI* expression vector, incubated for 72 h, after which the fraction of cells expressing GFP was determined by FACS. Where indicated, TDP1-KO-EJ5 cells were transiently transfected with a TDP1-WT expression construct 24 h prior to transfection for *I-SceI* expression. Data are normalized to GFP expression in WT cells.

WT: solid bar (white). TDP1-KO cells: checkered colored bars (7D1 (blue), 8A3 (brown) 8A5 (green)). TDP1-KO cells ectopically expressing TDP1-WT: solid colored bars (7D1 (blue), 8A3 (brown) 8A5 (green)). XLF-KO: checkered bar. \*\*\*\*,  $p < 0.0001$ . \*\*,  $p = 0.095$



Figure 4-2D

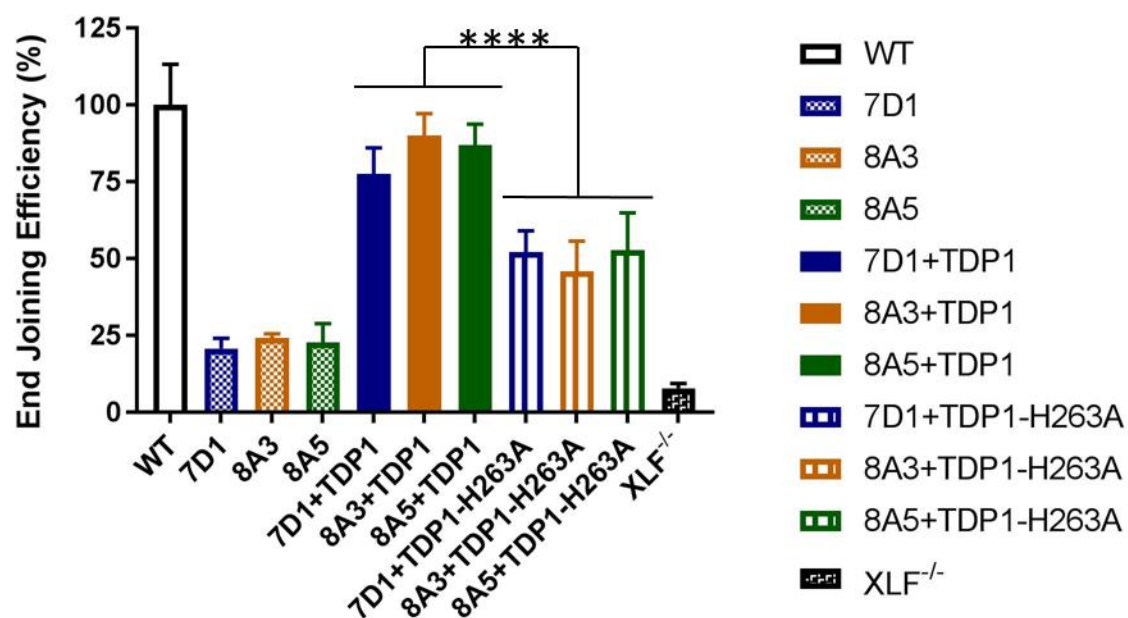


Figure 4-2D Ectopic expression of catalytic inactive TDP1 in TDP1-KO cells partially restored end joining efficiency.

WT, TDP1-KO (7D1, 8A3, and 8A5) and XLF-KO cells carrying the chromosomally integrated EJ5 end-joining reporter were transiently transfected with the *I-SceI* expression vector, incubated for 72 h, after which the fraction of cells expressing GFP was determined by FACS. Where indicated, TDP1-KO-EJ5 cells were transiently transfected with TDP1-WT or TDP1-H263A expression construct 24 h prior to transfection for *I-SceI* expression. \*\*\*\*,  $p < 0.0001$ .

Figure 4-2E

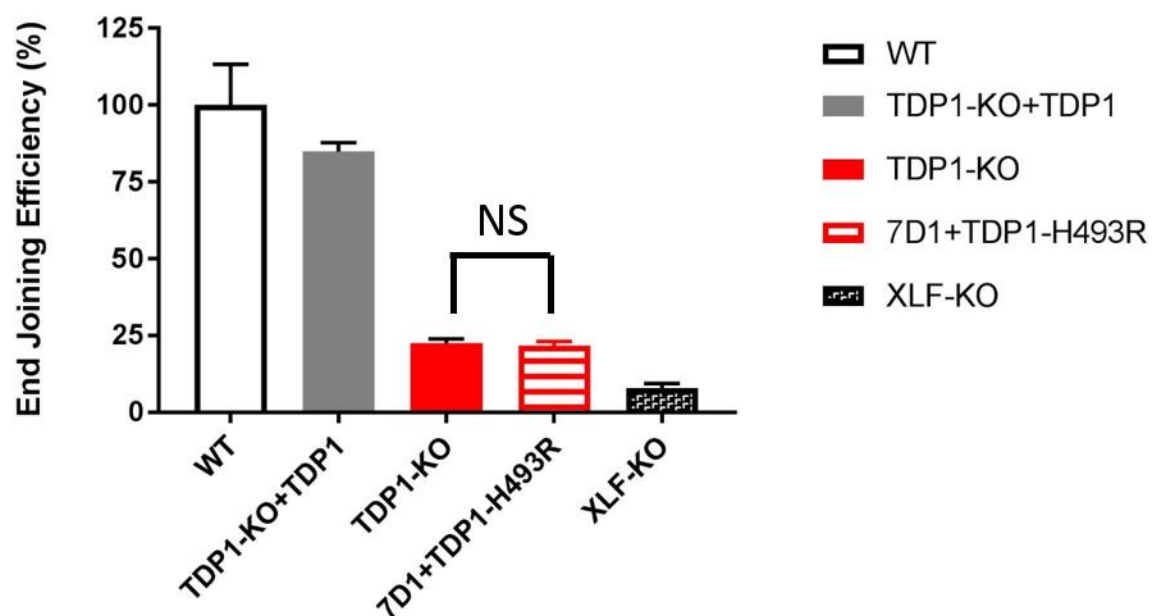


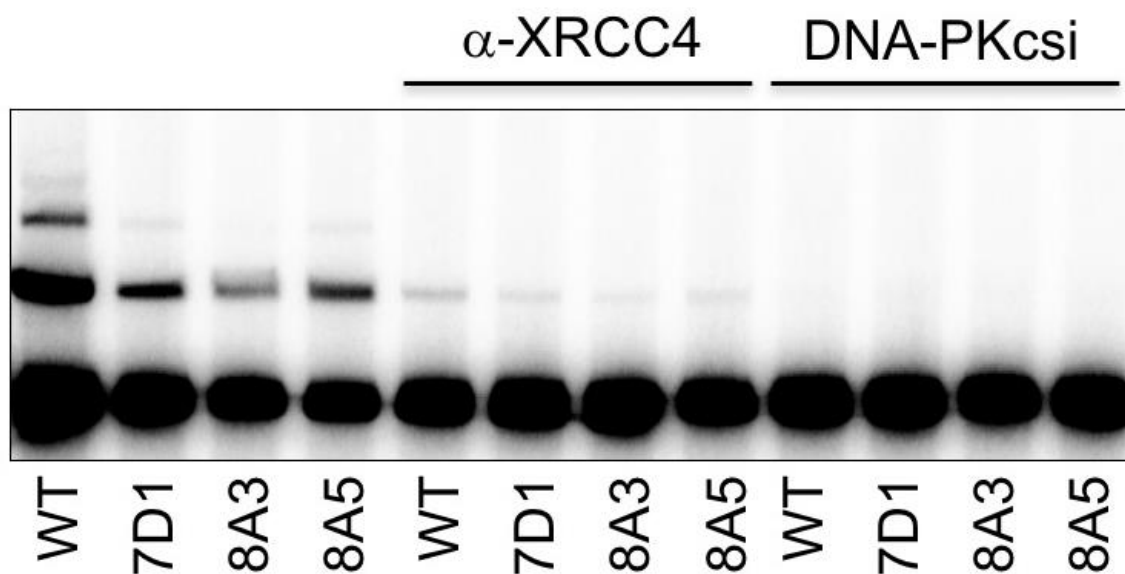
Figure 4-2E Ectopic expression of SCAN1 mutant TDP1 in TDP1-KO cells failed to restore end joining efficiency.

WT, TDP1-KO (7D1, 8A3, and 8A5) and XLF-KO cells carrying the chromosomally integrated EJ5 end-joining reporter were transiently transfected with the *I-SceI* expression vector, incubated for 72 h, after which the fraction of cells expressing GFP was determined by FACS. Where indicated, TDP1-KO-EJ5 cells were transiently transfected with TDP1-WT or TDP1-H493R expression construct 24 h prior to transfection for *I-SceI* expression. ns, not significant,  $p=0.7218$ .

### **4-3 TDP1 is required for efficient NHEJ in vitro**

To determine whether the reduced end joining efficiency in EJ5-GFP system also represented classic NHEJ, we used an *in vitro* NHEJ assay, which required XRCC4 and DNA-PK (Figure 4-3A), with WT and TDP1-KO cells. As shown in Figure 4-3B, all TDP1-KO cell extracts had reduced NHEJ efficiency as compared to cell extract from WT cells. Figure 4-3B is the representative figure for the agarose gel image. The graph showed in Figure 4-3C is the quantification of four independent experiments. To demonstrate the reduced NHEJ efficiency in TDP1-KO extract was not caused by reduce or loss of NHEJ factors, we used western blot to evaluate the NHEJ factors expression. In TDP1-KO extract, NHEJ factors Ku70, Ku80, XLF, ligase IV, DNA-PKcs and XRCC4 were equally expressed as compared to WT cell extract (Figure 4-3D).

Figure 4-3A

Figure 4-3A NHEJ *in vitro* assay is XRCC4 and DNA-PKcs dependent.

Lysate from HEK-WT and TDP-KOs cells are used to join  $^{32}\text{P}$  labeled DNA substrate. Reaction is described in methods section.

$\alpha$ -XRCC4: anti-XRCC4 antibodies (1:500), DNA-PKcsi: DNA-PKcs inhibitor Nu7024 (50  $\mu\text{M}$ ).

Figure 4-3B

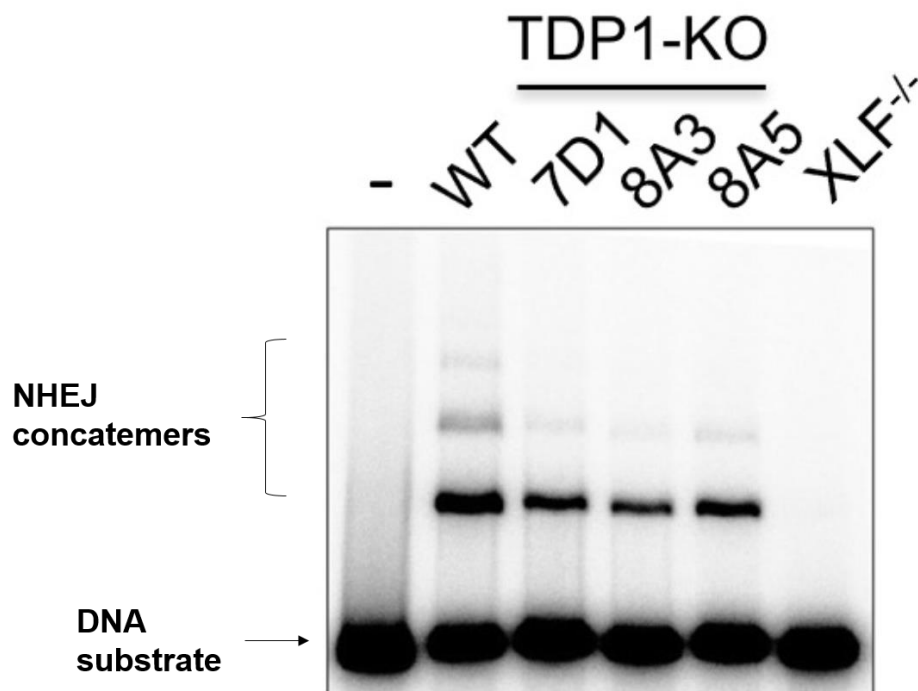


Figure 4-3B Extracts prepared from TDP1-KO cells have reduced NHEJ efficiency *in vitro*.

Lysate from HEK-WT, TDP-KOs and XLF deficient cells are incubate with <sup>32</sup>P labeled DNA substrate. Reaction is described in methods section.

<sup>32</sup>P labeled DNA substrate and NHEJ products (concatemers) are indicated.

Figure 4-3C

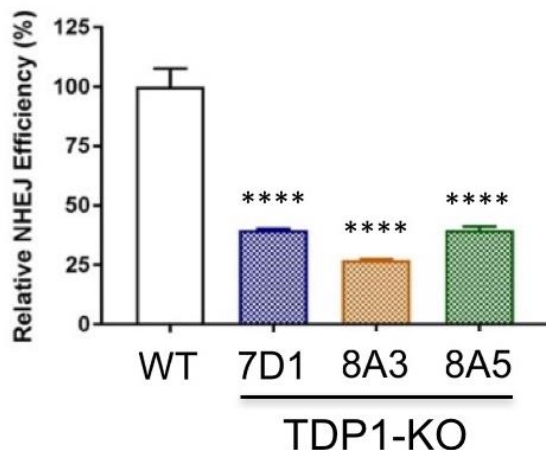


Figure 4-3C Summary of 4 independent NHEJ experiments

Results are the average of 12 individual measurements from 4 independent experiments, with all measurements made in technical triplicate (N=4, n=12). \*\*\*\*, p < 0.0001.

Figure 4-3D

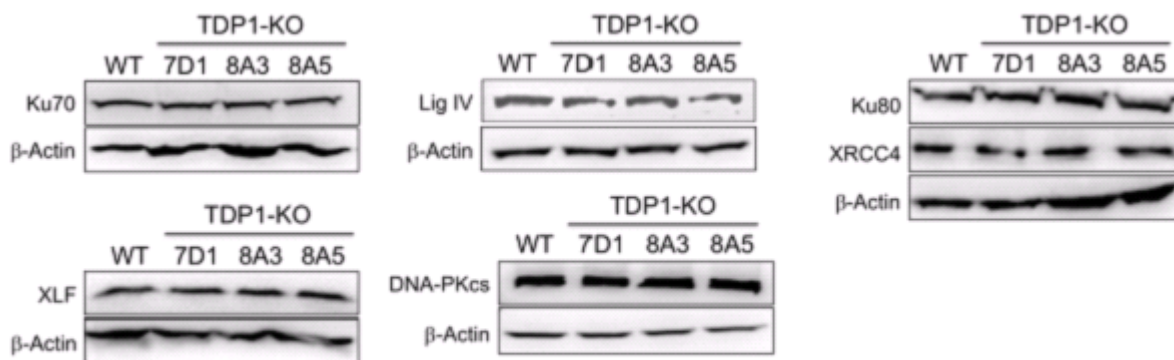


Figure 4-3D NHEJ factors (Ku70, Ku80, ligase IV, XLF, XRCC4 and DNA-PKcs) in TDP-KO cells were equally expressed as compared to WT cells.

#### **4-4 TDP1-knockout cells have different end joining accuracy**

Bahmed and colleagues showed that NHEJ fidelity in TDP1 deficient yeast was changed on compatible DNA ends with 5' extension but not 3' extension. To determine whether TDP1 affects NHEJ fidelity in human cells, we used PCR to amplified end joining junctions of sorted GFP positive TDP1-KO cells and WT cells generated from EJ5-GFP assay. NextGen sequencing was used to determine the sequences of the junctions. Since the DSBs generated by I-SceI have compatible 3' extension, repair of the DSBs by end joining will potentially restore an I-SceI site and considered to be "perfect joining". Whereas "inaccurate joining" includes insertion, single nucleotide mutation and deletion that could also generated by end joining and fail to restore the I-SceI site. When we compared the accuracy between WT and TDP1-KO cells, we observed that TDP1-KO cells showed higher "perfect joining" as compared to WT cells (Figure 4-4A). In these analysis, we only collected sequences showed more than 0.1% frequency among all the sequences detected by NextGen sequencing (9900 and 12,306 junctions from WT and TDP1-KO cell respectively). The detailed sequences and their frequency from WT and TDP1-KO cells were showed in Figure 4-4B. TDP1-KO cells only produced single nucleotide substitution (1.62%) as inaccurate junctions. In 11.94% inaccurate junctions generated from WT cells, we observed 1.34% single nucleotide substitution, 2.65% insertion and 7.95% deletions.

Figure 4-4A

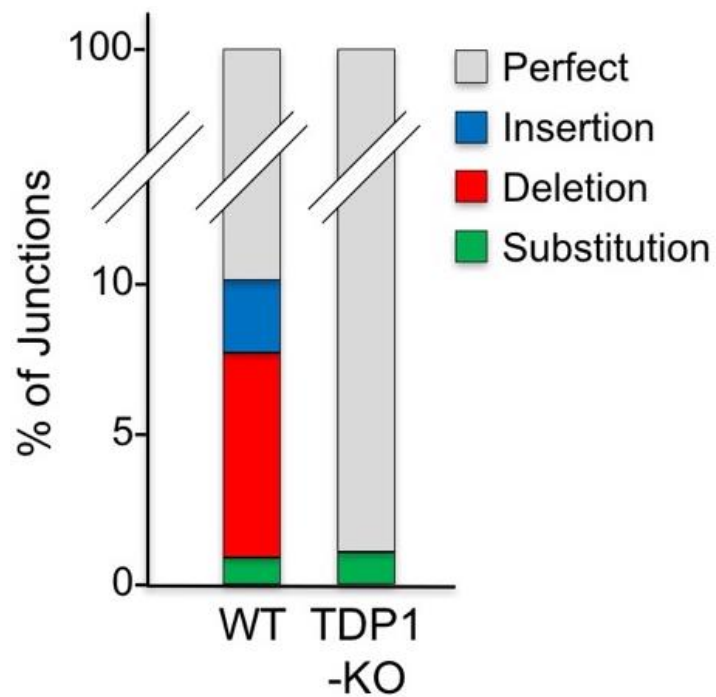


Figure 4-4A TDP1 affected end joining junctions in EJ5-GFP assay

EJ5 end-joining junctions from WT and TDP1-KO 7D1 cells were PCR amplified and subject to NextGen Sequencing. Perfect: *I-SceI* recognition site restored.



Figure 4-4B

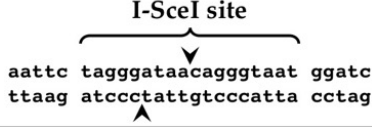
<p style="text-align: center;"> <b>I-SceI site</b>   </p>		
<b>EJ5 junctions from wild type cells</b>		
<b>Perfect</b>	aattc tagggataacagggtaat ggatc	88.06%
<b>Substitution</b>	.....G.....	0.30%
	.....C.....	0.25%
	.....C.....	0.23%
	.....G.....	0.21%
	.....G.....	0.18%
	.....G.....	0.17%
<b>Insertion</b>	tagggataa( <b>INS</b> )cagggtaat	
	tagggataa( <b>AA</b> )cagggtaat	1.13%
	tagggataa( <b>GGCAGTGGAGTCTCCATCTTCTACTATCC CACAGCCCTGTTTGTAA</b> )cagggtaat	0.96%
	tagggataa( <b>GTCCAAGAATGCACTCGCAGCTGAATGGC GCTTACACAGTTCAATCTCTCAGGTCCTAAGGTGGGGTC TCAGCACCCACAGATGCATAA</b> )cagggtaat	0.56%
<b>Deletion</b>	aattc tagggataacagggtaat ggatc	
	aattc -----taat ggatc	1.51%
	aattc taggg-----atc	1.40%
	aattc ta----taacagggtaat ggatc	1.07%
	aattc taggg-----taat ggatc	0.69%
	aattc tagg-----ggatc	0.67%
	aattc ta----aacagggtaat ggatc	0.61%
	aattc tagg-ataacagggtaat ggatc	0.51%
	aattc taggg--aacagggtaat ggatc	0.42%
	aattc taggg-----Ataat ggatc	0.38%
	aattc taggg-taacagggtaat ggatc	0.32%
	aattc ta----taacagggtaat ggatc	0.22%
	aattc <u>ta</u> -----at ggatc	0.15%
<b>EJ5 junctions from TDP1-KO cells</b>		
<b>Perfect</b>	aattc tagggataacagggtaat ggatc	98.38%
<b>Substitution</b>	.....G.....	0.41%
	.....G..	0.24%
	.....A.....	0.23%
	.....C.....	0.16%
	.....G.....	0.15%
	.....G.....	0.15%
	.....C.....	0.14%
	.....G.....	0.14%
<b>Insertion</b>		<b>0%</b>
<b>Deletion</b>		<b>0%</b>

Figure 4-4B Detail of junction sequences from WT-EJ5-GFP and TDP1-KO-EJ5-GFP cells.

Substitutions: homologous bases are shown as dots (.) and substitutions are shown in caps. Insertions: Top line shows parental sequence and highlights the site of insertions, which are shown in bold caps. Deletions: Top line shows parental sequence, retained sequences are shown in lower case, deleted bases are marked with dashes (-), microhomologies are shown as bold, italic, underline. Right column shows the percent of total junctions with the indicated sequence.

#### **4-5 Phosphorylation of TDP1 at serine-81 regulates TDP1 participation in NHEJ**

Previous studies showed TDP1 can be phosphorylated at serine 81 by DSB repair protein kinases ATM or DNA-PK. The phosphorylation of TDP1 increased TDP1 accumulation at DNA breaks, regulated TDP1 stability and mediated interaction with ligase III and XRCC1, which are well known for their roles in base excision repair (BER). In addition, like ligase III and XRCC1, TDP1 is also well studied in the area of base excision repair. Our data suggested an unexpected role of TDP1 in NHEJ. So it is interesting to investigate that how does TDP1 regulate its participation in different DNA repair pathways. In EJ5-GFP assay, we observed only 23% end joining efficiency in TDP-KO cells as compared to WT cells. Ectopic express of phosphomimetic TDP1 (TDP1-S81E) failed to rescue end joining efficiency in TDP1-KO cells. However ectopic expression of non-phosphorylatable TDP1 (TDP1-S81A) in TDP1-KO cells raised up end joining efficiency to 56% (Figure 4-5A). Because TDP1-S81 phosphorylation affected its stability, we showed that in this assay, TDP1-WT, TDP1-S81A and TDP1-S81E were equally expressed (Figure 4-5B).

To study the role of TDP1-S81A and S81E in DNA repair, we ectopic expressed these TDP1 mutants in TDP1-KO cells but either of them significantly affected cell sensitivity to CPT (Figure 4-5C). We also assessed the catalytic activity of TDP1-S81A and S81E by using oligonucleotide with 3' tyrosine and we observed that neither of them showed significant activity difference. However, the affinity capture assay showed interaction of

XLF was reduced by 2 fold and 10 fold by TDP1-S81A and TDP1-S81E respectively (Figure 4-5D). This observation of TDP1:XLF interaction was correlated with the ability to retain end joining efficiency in EJ5-GFP assay. These data suggested that TDP1 participation in NHEJ was mediated by interaction with XLF that might be regulated by TDP1-S81 phosphorylation.

Figure 4-5A

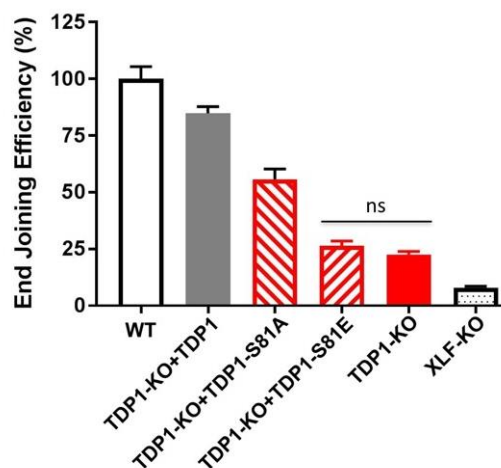


Figure 4-5A Ectopic expression of phosphomimetic TDP1 in TDP1-KO cells failed to restore end joining efficiency.

WT, TDP1-KO and XLF-KO cells carrying the chromosomally integrated EJ5 end-joining reporter were transiently transfected with the *I-SceI* expression vector, incubated for 72 h, after which the fraction of cells expressing GFP was determined by FACS. Where indicated, TDP1-KO-EJ5 cells were transiently transfected with TDP1-WT, non-phosphorylatable TDP1 (TDP1-S81A) or phosphomimetic TDP1 (TDP1-S81E) expression construct 24 h prior to transfection for *I-SceI* expression. ns, not significant,  $p=0.8671$ .

Figure 4-5B

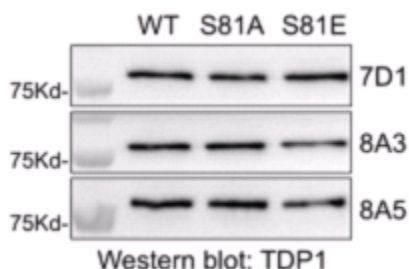


Figure 4-5B Ectopic expression of TDP1-WT, TDP1-S81A and TDP1-S81E proteins results in equal amounts of TDP1 proteins in TDP1-KO cells.

TDP1-KO 7D1, 8A3, and 8A5 cells were transiently transfected with constructs expressing WT or non-phosphorylatable TDP1 (TDP1-S81A) or phosphomimetic TDP1 (TDP1-S81E). After 72 h, whole cell extracts were prepared and TDP1 proteins were detected by western blot analysis.

Figure 4-5C

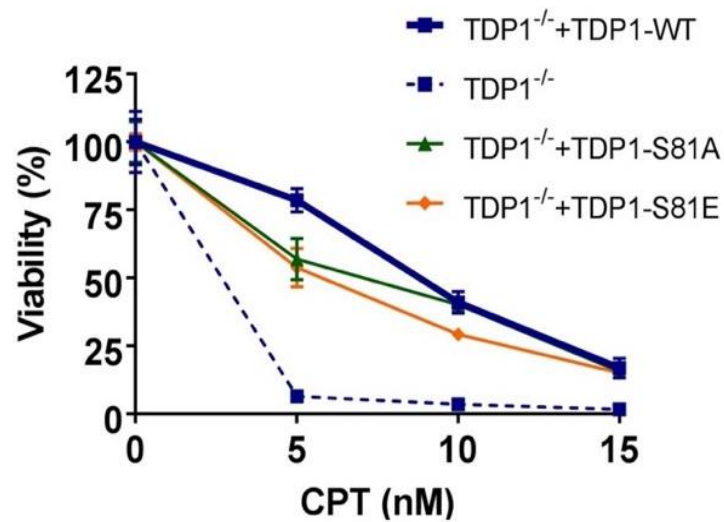


Figure 4-5C Effect of TDP1- S81 mutation on CPT resistance in TDP1-KO cells.

TDP1-KO 7D1 cells were exposed to CPT at the concentrations indicated for 72 h. Where indicated cells were transiently transfected with constructs expressing WT, S81A and S81E TDP1 proteins, and incubated for 24 h prior to CPT treatment.

Figure 4-5D

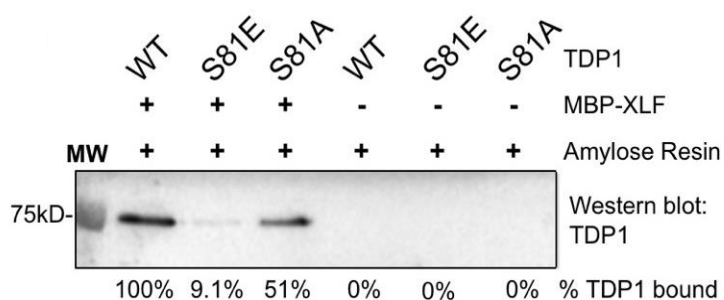


Figure 4-5D Mutation of TDP1-S81 reduces interaction with XLF.

Interaction of TDP1-WT:MBP-XLF is normalized to 100%. Affinity capture assay used to determine protein-protein recombinant MBP-XLF and TDP1 mutants was described in chapter 3.

## **Chapter 5**

### **Discussion**



**5-1 Biochemical evidence for TDP1 participation in human NHEJ: TDP1 physically interacts with NHEJ required factor XLF, and XLF stimulates TDP1 enzymatic activity on dsDNA but not on ssDNA**

NHEJ is capable of joining DNA ends with little or no template, which allows NHEJ to repair DSBs throughout the whole cell cycle [244]. Because of the independence from needing template, NHEJ is considered to be an error prone pathway that can result in mutations at the site of repair or join inaccurate DNA strands to cause translocations [3, 164]. However, NHEJ can still join ends accurately in a lot of cases [7, 245]. This raises questions about how error is minimized during NHEJ in human cells. Yeast studies showed that TDP1 contributes to accurate NHEJ on cohesive DSBs with 3' extension [12]. Our hypothesis is that TDP1 participates in NHEJ in human cells.

Deficiency of required NHEJ factors including: Ku70, Ku80, XRCC4 or DNA ligase IV, completely impairs V(D)J recombination in mice. So factors that might play a role in NHEJ are expected to contribute to immunodeficiency when they are absent. However, XLF is required in NHEJ, but XLF deficient mice are not immunodeficient. These observations argue against that NHEJ defect is not always correlated to immunodeficiency, and no detectable immunodeficiency in TDP1-deficient mice does not rule out TDP1 participation in NHEJ.

Our affinity capture assay showed that human TDP1 can physically interact with XLF, which is an NHEJ required factor [236], suggesting TDP1 participates in mammalian

NHEJ. The majority of DSBs generated by environmental DNA damaging agents have damaged DNA ends that need to be removed before DNA repair. TDP1 is one of the DNA end processing factors and is able to cleave 3'-and 5'-DNA damages [182]. Our data showed that XLF stimulates TDP1 enzymatic activity to cleave 3'-DNA damage on dsDNA but not on ssDNA. This stimulation of TDP1 is likely mediated by the TDP1:XLF interaction, which was observed in the affinity capture assay. TDP1 was found to preferentially bind ssDNA and blunt ends over dsDNA with extensions [205, 243]. In our TDP1 enzymatic activity assay, we observed the similar preference of TDP1 on ssDNA over dsDNA with 3'-biotin. However, when we had XLF in the reaction, TDP1 showed preference of dsDNA. Because XLF is a dsDNA binding protein, we assume interaction with XLF forced TDP1 to favor dsDNA damage instead of ssDNA. Postdoc Dr. Heo in our lab detected a TDP1:XLF:DNA ternary complex by using electrophoresis mobility shift assay. He also showed TDP1 can enhance DNA binding by Ku and stimulates DNA-PKcs protein kinase activity. Together, these biochemical experiments first detected a TDP1 interaction with an NHEJ factor and indicated TDP1 might participate in NHEJ.

## **5-2 Biological evidence for TDP1 participation in human NHEJ: TDP1 is required for efficient NHEJ in human cells**

TDP1 was well known for its role to process damaged DNA ends such as damage generated by ionizing radiation and CPT [182, 246]. In our study, as expected, human

TDP1-KO cell also showed higher sensitivity to CPT and ionizing radiation. Ectopic expression of inactive TDP1-H263A failed to restore CPT resistance, suggesting catalytic activity of TDP1 is required for TDP1 to participate in DNA repair of damaged DNA ends. However, TDP1 is not an enzyme that exclusively removing DNA damage [182]. Yeast studies showed that the 3' nucleosidase activity of TDP1 allowed end processing on undamaged DNA ends generated by restriction endonucleases [12]. This study presented a model that TDP1 cleaves 3' DNA ends and results in a 3' phosphate which is not a substrate for polymerases, and therefore prevents polymerase-dependent insertion before appropriate DNA end alignment and recruitment of the other NHEJ factors. TDP1 is protecting the accuracy of NHEJ by temporarily preventing polymerization. This yeast study first identified TDP1 as the factor to regulate NHEJ fidelity.

Correlating to the yeast study, our end joining efficiency assay in human cells showed that TDP1 participates in end joining by helping repair DSBs with undamaged DNA ends generated by restriction endonuclease I-SceI. We observed that TDP1 was required for efficient end joining on 3'-extensions. This is different from the yeast study showing that TDP1 deficiency had no impact on NHEJ efficiency on DSBs with 3'- or 5'-extension generated by Pst1 and HindIII respectively [12], while blunt ends generated by SmaI had increased repair in TDP1-deficient yeast. The yeast study also found that catalytic activity of TDP1 is required for TDP1 to promote NHEJ fidelity on DSBs with 5' overhang polarity. However, our study showed that on DSBs with 3' overhang polarity,

enzymatic inactive TDP1 still retained 60% end joining efficiency whereas TDP1-KO cells only had 23% end joining on average. In this study, TDP1 mutants were overexpressed in TDP1-KO cells by using transient transfection and may affect our observations. To further optimize this assay, we are planning to use CRISPR/cas9 to knock-in TDP1 mutants (at least TDP1-H293A) so we can assess the effect of these mutants on NHEJ at endogenous levels. Our study in human cells suggest that although TDP1 is conserved through species, the role of TDP1 in NHEJ might differ from what is observed in yeast. One important difference in NHEJ between human and yeast is that DNA-PK is required for NHEJ in mammals but is not present in *S. cerevisiae* [247, 248]. These data suggests that TDP1, in humans, might have DNA-PK dependent activity that is not identical to TDP1 activity in yeast.

### **5-3 TDP1-deficiency changes the spectrum of end joining products:**

#### **TDP1-knockout cells have different spectrum of end joining junctions**

Our NGS data showed that TDP1-KO cells had more accurate junction as compared to WT cells. This observation is the opposite of the result in the yeast study examining TDP1 deficiency in NHEJ showing that TDP1-deficient yeast exhibited more insertions when repairing DSBs by NHEJ. Our data, including TDP1:XLFI interaction and TDP1 requirement in end joining, indicates that TDP1 contributes to efficient NHEJ. Therefore, deficiency of TDP1 might result in more alternative end joining for DSB repair. However,

alternative end joining is generally an error prone DNA repair pathway, so the increased accurate junctions in TDP1 deficient cells cannot be explained by increased use of alternative NHEJ. The substrate for end joining in the EJ5-GFP assay are DSBs with complementary ends. These ends can be joined efficiently and accurately in NHEJ-deficient cells, so we think the increased accuracy in TDP1 deficient cells can be caused by using microhomologies present in the cohesive ends generated by I-SceI and mediated by MMEJ. To avoid an intrinsic disadvantage that can lead to bias toward end joining by MMEJ, we should assess TDP1 effect on NHEJ accuracy by using substrates with different types of ends, such as incompatible ends, 5' overhangs and blunt ends.

#### **5-4 Role of TDP1 in NHEJ**

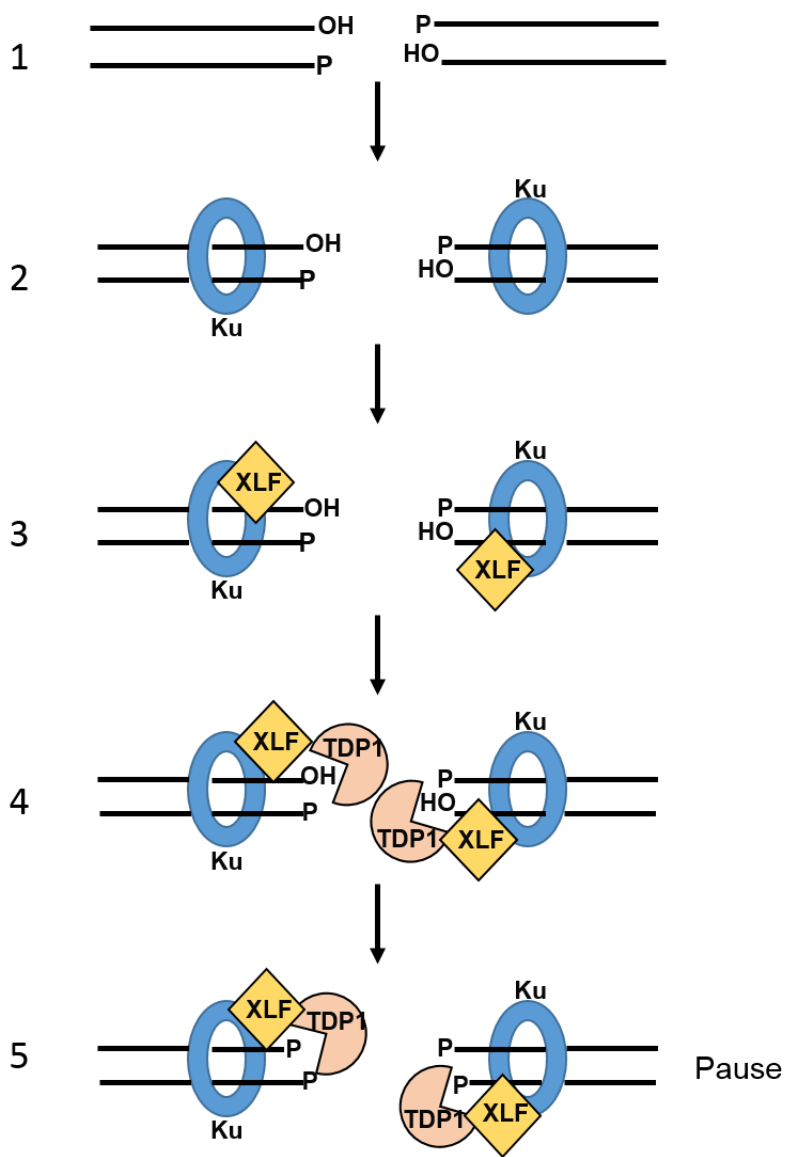
As mentioned in Chapter 1, Ku is very abundant and is the first required factor to bind to DSBs to initiate NHEJ [37]. Before ligation, how and when NHEJ required factors assemble is not well understood.

Here, we propose a model of the NHEJ mechanism involving TDP1 via our TDP1:XLF interaction as earlier described (Figure 5). XLF was shown to be recruited by Ku to the DNA ends within 5 seconds, suggesting XLF binds to the DSBs at the very early stage of NHEJ [35]. We have shown that TDP1, through interaction with XLF, forms

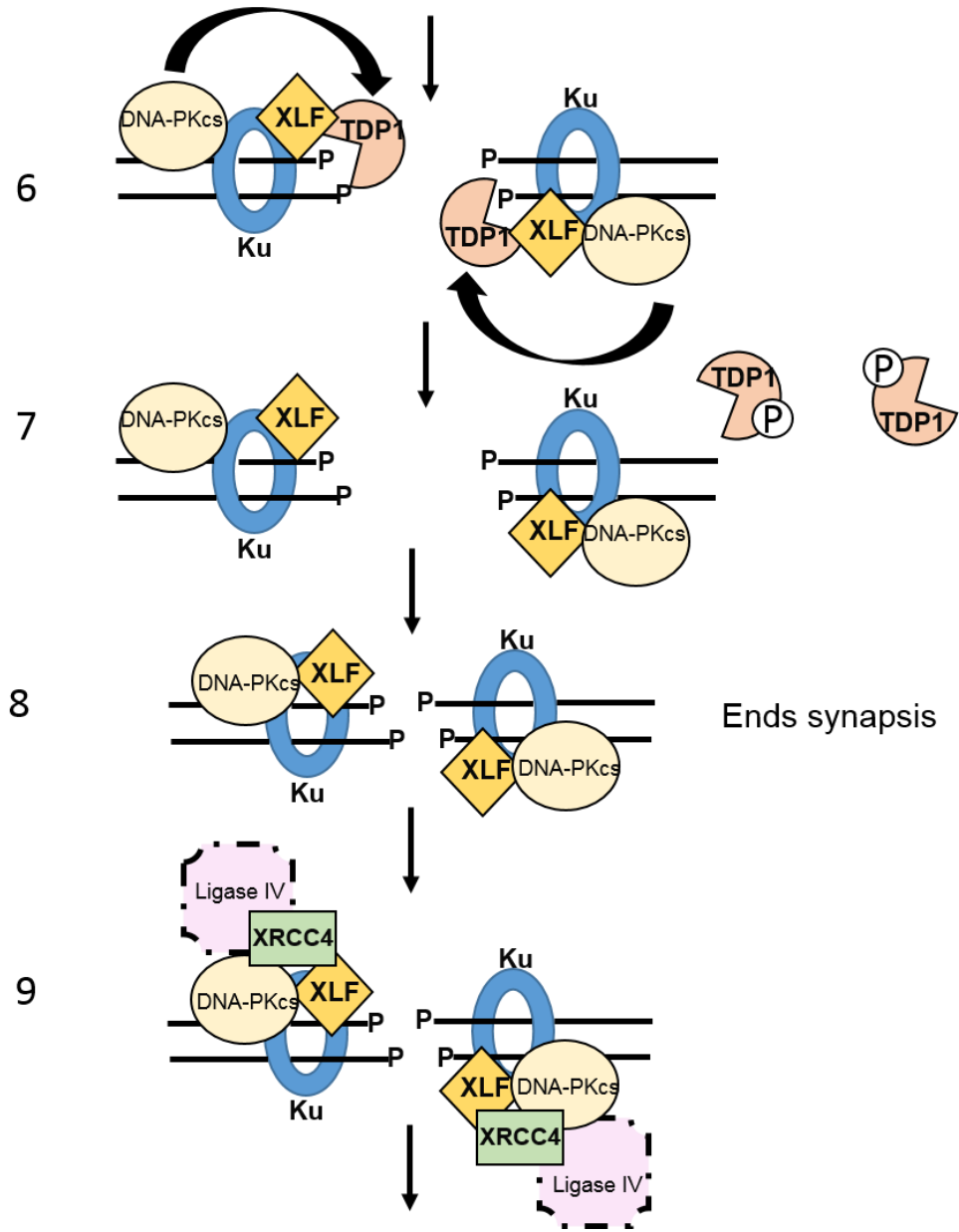
complex with XLF and DNA [236]. So we hypothesize that TDP1 can act on DSBs by interacting with XLF. TDP1 can then remove a single nucleoside by using its 3' nucleosidase activity, and leave a 3' phosphate at the DNA end [182]. Nitiss and colleagues suggested that 3' phosphates have the potential to temporarily stop the repair from subsequent gap filling by polymerases, such as pol  $\mu$  or pol  $\lambda$  [12]. Povirk and colleagues showed that, in human cell extract, XLF is required for gap filling by polymerase  $\lambda$  and  $\mu$  in NHEJ [233]. Besides the 3' phosphate, interaction between TDP1 and XLF may also impair XLF interaction with pol  $\mu$  or  $\lambda$  that can promote gap filling. DNA-PKcs, which is recruited by Ku, can phosphorylate TDP1 at S81 [223]. We have shown that phosphomimetic TDP1 lacked interaction with XLF. We hypothesize that this phosphorylation can facilitate TDP1 release from XLF and the DSB. Recruitment of DNA-PKcs and subsequent autophosphorylation promotes DNA strand synapsis [83]. The temporary stop generated by TDP1 gives NHEJ time to recruit other required factors, such as XRCC4. XRCC4 was observed to interact with polynucleotide kinase phosphatase (PNKP) and is required for PNKP recruitment [124]. We hypothesize that XRCC4 recruits PNKP that results in removal of the 3' phosphate and then restores the ligatable 3' hydroxyl end. XRCC4 can exist in cells as homodimer, homotetramer and ligase IV-XRCC4 complex [109, 121, 249]. We are not sure about which form of XRCC4 is recruited at this step, therefore, we are not sure whether DNA ligase IV is present, but XRCC4 is required to recruit PNKP to remove 3' phosphate. Polymerase  $\mu$  or  $\lambda$  may be

recruited by XLF at this step to fill the gap generated by TDP1. The DSB, at this point, is ligatable and close enough to be ligated by ligase IV through recruitment of XRCC4-ligase IV complex. Our model suggests a novel role of TDP1 in NHEJ regulated by TDP1 phosphorylation at Serine 81 and contributes to our understanding of the NHEJ mechanism.

Figure 5







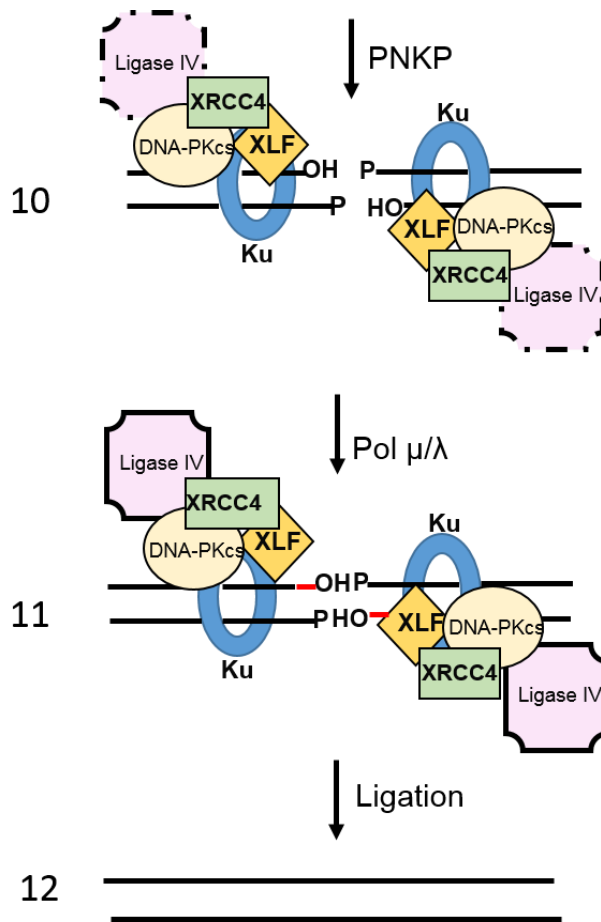


Figure 5 Role of TDP1 in NHEJ

- 1 and 2. Ku recognizes and binds to DSB
3. XLF is recruited by Ku in the early stage of NHEJ.
4. TDP1 acts on DSB through interaction with XLF and form TDP1:XLF:DNA complex.
5. TDP1 then removes one nucleoside and leaves 3' phosphate at DNA end, which is not a substrate for polymerase or ligase.
6. Ku recruits DNA-PKcs, which can phosphorylate TDP1.
7. Phosphorylated TDP1 reduces its affinity to XLF, result in TDP1 released from NHEJ apparatus.
8. Autophosphorylation of DNA-PKcs results in DNA end synapsis
9. XRCC4 or ligase IV-XRCC4 complex may then be recruited to DSB by Ku.
10. XRCC4 recruits PNKP to the DSB to removes 3' phosphate and restore 3' hydroxyl.
11. The gap generated by TDP1, is filled by pol  $\mu$  and  $\lambda$  via interaction with XLF.

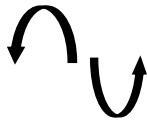
12. At this point, ligase IV is required to ligate the DSB and finish NHEJ.



Phosphorylated TDP1.



Insertions by gap filling.



DNA-PKcs phosphorylates TDP1



Ligase IV may or may not present

## CITED LITERATURE

1. Rich, T., R.L. Allen, and A.H. Wyllie, *Defying death after DNA damage*. Nature, 2000. **407**(6805): p. 777-83.
2. Branzei, D. and M. Foiani, *Regulation of DNA repair throughout the cell cycle*. Nat Rev Mol Cell Biol, 2008. **9**(4): p. 297-308.
3. Nambiar, M. and S.C. Raghavan, *How does DNA break during chromosomal translocations?* Nucleic Acids Res, 2011. **39**(14): p. 5813-25.
4. Haber, J.E., *Partners and pathways repairing a double-strand break*. Trends Genet, 2000. **16**(6): p. 259-64.
5. Chang, H.H.Y., et al., *Non-homologous DNA end joining and alternative pathways to double-strand break repair*. Nat Rev Mol Cell Biol, 2017.
6. Davis, A.J. and D.J. Chen, *DNA double strand break repair via non-homologous end-joining*. Transl Cancer Res, 2013. **2**(3): p. 130-143.
7. Dubois, E., et al., *Transposon Invasion of the Paramecium Germline Genome Countered by a Domesticated PiggyBac Transposase and the NHEJ Pathway*. Int J Evol Biol, 2012. **2012**: p. 436196.
8. Feldmann, E., et al., *DNA double-strand break repair in cell-free extracts from Ku80-deficient cells: implications for Ku serving as an alignment factor in non-homologous DNA end joining*. Nucleic Acids Res, 2000. **28**(13): p. 2585-96.
9. Kabotyanski, E.B., et al., *Double-strand break repair in Ku86- and XRCC4-deficient cells*. Nucleic Acids Res, 1998. **26**(23): p. 5333-42.
10. Smith, J., et al., *The influence of DNA double-strand break structure on end-joining in human cells*. Nucleic Acids Res, 2001. **29**(23): p. 4783-92.
11. Smith, J., et al., *Impact of DNA ligase IV on the fidelity of end joining in human cells*. Nucleic Acids Res, 2003. **31**(8): p. 2157-67.

12. Bahmed, K., K.C. Nitiss, and J.L. Nitiss, *Yeast Tdp1 regulates the fidelity of nonhomologous end joining*. Proc Natl Acad Sci U S A, 2010. **107**(9): p. 4057-62.
13. Arnaudeau, C., C. Lundin, and T. Helleday, *DNA double-strand breaks associated with replication forks are predominantly repaired by homologous recombination involving an exchange mechanism in mammalian cells*. J Mol Biol, 2001. **307**(5): p. 1235-45.
14. Murakami, H. and S. Keeney, *Regulating the formation of DNA double-strand breaks in meiosis*. Genes Dev, 2008. **22**(3): p. 286-92.
15. Karanjawala, Z.E., et al., *Oxygen metabolism causes chromosome breaks and is associated with the neuronal apoptosis observed in DNA double-strand break repair mutants*. Curr Biol, 2002. **12**(5): p. 397-402.
16. Karanjawala, Z.E., et al., *The nonhomologous DNA end joining pathway is important for chromosome stability in primary fibroblasts*. Curr Biol, 1999. **9**(24): p. 1501-4.
17. Ciccia, A. and S.J. Elledge, *The DNA damage response: making it safe to play with knives*. Mol Cell, 2010. **40**(2): p. 179-204.
18. Zhou, B.B. and S.J. Elledge, *The DNA damage response: putting checkpoints in perspective*. Nature, 2000. **408**(6811): p. 433-9.
19. Lovejoy, C.A. and D. Cortez, *Common mechanisms of PIKK regulation*. DNA Repair (Amst), 2009. **8**(9): p. 1004-8.
20. Lempiainen, H. and T.D. Halazonetis, *Emerging common themes in regulation of PIKKs and PI3Ks*. EMBO J, 2009. **28**(20): p. 3067-73.
21. Marechal, A. and L. Zou, *DNA damage sensing by the ATM and ATR kinases*. Cold Spring Harb Perspect Biol, 2013. **5**(9).
22. Uziel, T., et al., *Requirement of the MRN complex for ATM activation by DNA damage*. EMBO J, 2003. **22**(20): p. 5612-21.

23. Meier, A., et al., *Spreading of mammalian DNA-damage response factors studied by ChIP-chip at damaged telomeres*. EMBO J, 2007. **26**(11): p. 2707-18.
24. Heyer, W.D., K.T. Ehmsen, and J. Liu, *Regulation of homologous recombination in eukaryotes*. Annu Rev Genet, 2010. **44**: p. 113-39.
25. Symington, L.S. and J. Gautier, *Double-strand break end resection and repair pathway choice*. Annu Rev Genet, 2011. **45**: p. 247-71.
26. Renkawitz, J., C.A. Lademann, and S. Jentsch, *Mechanisms and principles of homology search during recombination*. Nat Rev Mol Cell Biol, 2014. **15**(6): p. 369-83.
27. Zelensky, A., R. Kanaar, and C. Wyman, *Mediators of homologous DNA pairing*. Cold Spring Harb Perspect Biol, 2014. **6**(12): p. a016451.
28. Chapman, J.R., M.R. Taylor, and S.J. Boulton, *Playing the end game: DNA double-strand break repair pathway choice*. Mol Cell, 2012. **47**(4): p. 497-510.
29. Wilson, J.H., P.B. Berget, and J.M. Pipas, *Somatic cells efficiently join unrelated DNA segments end-to-end*. Mol Cell Biol, 1982. **2**(10): p. 1258-69.
30. Malyarchuk, S., et al., *Expression of Mycobacterium tuberculosis Ku and Ligase D in Escherichia coli results in RecA and RecB-independent DNA end-joining at regions of microhomology*. DNA Repair (Amst), 2007. **6**(10): p. 1413-24.
31. Leber, R., et al., *The XRCC4 gene product is a target for and interacts with the DNA-dependent protein kinase*. J Biol Chem, 1998. **273**(3): p. 1794-801.
32. Hsu, H.L., S.M. Yannone, and D.J. Chen, *Defining interactions between DNA-PK and ligase IV/XRCC4*. DNA Repair (Amst), 2002. **1**(3): p. 225-35.
33. Mari, P.O., et al., *Dynamic assembly of end-joining complexes requires interaction between Ku70/80 and XRCC4*. Proc Natl Acad Sci U S A, 2006. **103**(49): p. 18597-602.

34. Costantini, S., et al., *Interaction of the Ku heterodimer with the DNA ligase IV/Xrcc4 complex and its regulation by DNA-PK*. DNA Repair (Amst), 2007. **6**(6): p. 712-22.
35. Yano, K. and D.J. Chen, *Live cell imaging of XLF and XRCC4 reveals a novel view of protein assembly in the non-homologous end-joining pathway*. Cell Cycle, 2008. **7**(10): p. 1321-5.
36. Yano, K., et al., *Ku recruits XLF to DNA double-strand breaks*. EMBO Rep, 2008. **9**(1): p. 91-6.
37. Lieber, M.R., *The mechanism of double-strand DNA break repair by the nonhomologous DNA end-joining pathway*. Annu Rev Biochem, 2010. **79**: p. 181-211.
38. Yano, K., et al., *Functional significance of the interaction with Ku in DNA double-strand break recognition of XLF*. FEBS Lett, 2011. **585**(6): p. 841-6.
39. Chiruvella, K.K., Z. Liang, and T.E. Wilson, *Repair of double-strand breaks by end joining*. Cold Spring Harb Perspect Biol, 2013. **5**(5): p. a012757.
40. Shuman, S. and M.S. Glickman, *Bacterial DNA repair by non-homologous end joining*. Nat Rev Microbiol, 2007. **5**(11): p. 852-61.
41. Malu, S., et al., *Role of non-homologous end joining in V(D)J recombination*. Immunol Res, 2012. **54**(1-3): p. 233-46.
42. Tonegawa, S., *Somatic generation of antibody diversity*. Nature, 1983. **302**(5909): p. 575-81.
43. de Villartay, J.P., A. Fischer, and A. Durandy, *The mechanisms of immune diversification and their disorders*. Nat Rev Immunol, 2003. **3**(12): p. 962-72.
44. Schuler, W., et al., *Rearrangement of antigen receptor genes is defective in mice with severe combined immune deficiency*. Cell, 1986. **46**(7): p. 963-72.

45. Bosma, G.C., R.P. Custer, and M.J. Bosma, *A severe combined immunodeficiency mutation in the mouse*. Nature, 1983. **301**(5900): p. 527-30.
46. Fulop, G.M. and R.A. Phillips, *The scid mutation in mice causes a general defect in DNA repair*. Nature, 1990. **347**(6292): p. 479-82.
47. Biedermann, K.A., et al., *scid mutation in mice confers hypersensitivity to ionizing radiation and a deficiency in DNA double-strand break repair*. Proc Natl Acad Sci U S A, 1991. **88**(4): p. 1394-7.
48. Wang, C. and S.P. Lees-Miller, *Detection and repair of ionizing radiation-induced DNA double strand breaks: new developments in nonhomologous end joining*. Int J Radiat Oncol Biol Phys, 2013. **86**(3): p. 440-9.
49. Shibata, A. and P.A. Jeggo, *DNA double-strand break repair in a cellular context*. Clin Oncol (R Coll Radiol), 2014. **26**(5): p. 243-9.
50. Paillard, S. and F. Strauss, *Analysis of the mechanism of interaction of simian Ku protein with DNA*. Nucleic Acids Res, 1991. **19**(20): p. 5619-24.
51. Blier, P.R., et al., *Binding of Ku protein to DNA. Measurement of affinity for ends and demonstration of binding to nicks*. J Biol Chem, 1993. **268**(10): p. 7594-601.
52. Walker, J.R., R.A. Corpina, and J. Goldberg, *Structure of the Ku heterodimer bound to DNA and its implications for double-strand break repair*. Nature, 2001. **412**(6847): p. 607-14.
53. Kragelund, B.B., et al., *The Ku70/80 ring in Non-Homologous End-Joining: easy to slip on, hard to remove*. Front Biosci (Landmark Ed), 2016. **21**: p. 514-27.
54. Postow, L., et al., *Ku80 removal from DNA through double strand break-induced ubiquitylation*. J Cell Biol, 2008. **182**(3): p. 467-79.
55. Gell, D. and S.P. Jackson, *Mapping of protein-protein interactions within the DNA-dependent protein kinase complex*. Nucleic Acids Res, 1999. **27**(17): p. 3494-502.



56. Dynan, W.S. and S. Yoo, *Interaction of Ku protein and DNA-dependent protein kinase catalytic subunit with nucleic acids*. Nucleic Acids Res, 1998. **26**(7): p. 1551-9.
57. Roberts, S.A., et al., *Ku is a 5'-dRP/AP lyase that excises nucleotide damage near broken ends*. Nature, 2010. **464**(7292): p. 1214-7.
58. Grundy, G.J., et al., *APLF promotes the assembly and activity of non-homologous end joining protein complexes*. EMBO J, 2013. **32**(1): p. 112-25.
59. Aravind, L. and E.V. Koonin, *SAP - a putative DNA-binding motif involved in chromosomal organization*. Trends Biochem Sci, 2000. **25**(3): p. 112-4.
60. Falck, J., J. Coates, and S.P. Jackson, *Conserved modes of recruitment of ATM, ATR and DNA-PKcs to sites of DNA damage*. Nature, 2005. **434**(7033): p. 605-11.
61. Singleton, B.K., et al., *The C terminus of Ku80 activates the DNA-dependent protein kinase catalytic subunit*. Mol Cell Biol, 1999. **19**(5): p. 3267-77.
62. Nussenzweig, A., et al., *Hypersensitivity of Ku80-deficient cell lines and mice to DNA damage: the effects of ionizing radiation on growth, survival, and development*. Proc Natl Acad Sci U S A, 1997. **94**(25): p. 13588-93.
63. Gu, Y., et al., *Growth retardation and leaky SCID phenotype of Ku70-deficient mice*. Immunity, 1997. **7**(5): p. 653-65.
64. Ouyang, H., et al., *Ku70 is required for DNA repair but not for T cell antigen receptor gene recombination In vivo*. J Exp Med, 1997. **186**(6): p. 921-9.
65. Manis, J.P., et al., *Ku70 is required for late B cell development and immunoglobulin heavy chain class switching*. J Exp Med, 1998. **187**(12): p. 2081-9.
66. Strande, N., et al., *Specificity of the dRP/AP lyase of Ku promotes nonhomologous end joining (NHEJ) fidelity at damaged ends*. J Biol Chem, 2012. **287**(17): p. 13686-93.

67. Hanakahi, L.A., et al., *Binding of inositol phosphate to DNA-PK and stimulation of double-strand break repair*. Cell, 2000. **102**(6): p. 721-9.
68. Hanakahi, L.A. and S.C. West, *Specific interaction of IP6 with human Ku70/80, the DNA-binding subunit of DNA-PK*. EMBO J, 2002. **21**(8): p. 2038-44.
69. Cheung, J.C., B. Salerno, and L.A. Hanakahi, *Evidence for an inositol hexakisphosphate-dependent role for Ku in mammalian nonhomologous end joining that is independent of its role in the DNA-dependent protein kinase*. Nucleic Acids Res, 2008. **36**(17): p. 5713-26.
70. Fell, V.L. and C. Schild-Poulter, *Ku regulates signaling to DNA damage response pathways through the Ku70 von Willebrand A domain*. Mol Cell Biol, 2012. **32**(1): p. 76-87.
71. Amsel, A.D., et al., *Regulation of the proapoptotic factor Bax by Ku70-dependent deubiquitylation*. Proc Natl Acad Sci U S A, 2008. **105**(13): p. 5117-22.
72. Sawada, M., et al., *Ku70 suppresses the apoptotic translocation of Bax to mitochondria*. Nat Cell Biol, 2003. **5**(4): p. 320-9.
73. Maciejowski, J. and T. de Lange, *Telomeres in cancer: tumour suppression and genome instability*. Nat Rev Mol Cell Biol, 2017. **18**(3): p. 175-186.
74. Porter, S.E., et al., *The DNA-binding protein Hdf1p (a putative Ku homologue) is required for maintaining normal telomere length in Saccharomyces cerevisiae*. Nucleic Acids Res, 1996. **24**(4): p. 582-5.
75. Boulton, S.J. and S.P. Jackson, *Identification of a Saccharomyces cerevisiae Ku80 homologue: roles in DNA double strand break rejoining and in telomeric maintenance*. Nucleic Acids Res, 1996. **24**(23): p. 4639-48.
76. Gravel, S., et al., *Yeast Ku as a regulator of chromosomal DNA end structure*. Science, 1998. **280**(5364): p. 741-4.

77. Samper, E., et al., *Mammalian Ku86 protein prevents telomeric fusions independently of the length of TTAGGG repeats and the G-strand overhang*. EMBO Rep, 2000. **1**(3): p. 244-52.
78. Espejel, S., et al., *Mammalian Ku86 mediates chromosomal fusions and apoptosis caused by critically short telomeres*. EMBO J, 2002. **21**(9): p. 2207-19.
79. Teo, S.H. and S.P. Jackson, *Identification of Saccharomyces cerevisiae DNA ligase IV: involvement in DNA double-strand break repair*. EMBO J, 1997. **16**(15): p. 4788-95.
80. Gottlieb, T.M. and S.P. Jackson, *The DNA-dependent protein kinase: requirement for DNA ends and association with Ku antigen*. Cell, 1993. **72**(1): p. 131-42.
81. Yaneva, M., T. Kowalewski, and M.R. Lieber, *Interaction of DNA-dependent protein kinase with DNA and with Ku: biochemical and atomic-force microscopy studies*. EMBO J, 1997. **16**(16): p. 5098-112.
82. Yoo, S. and W.S. Dynan, *Geometry of a complex formed by double strand break repair proteins at a single DNA end: recruitment of DNA-PKcs induces inward translocation of Ku protein*. Nucleic Acids Res, 1999. **27**(24): p. 4679-86.
83. Weterings, E., et al., *The role of DNA dependent protein kinase in synapsis of DNA ends*. Nucleic Acids Res, 2003. **31**(24): p. 7238-46.
84. DeFazio, L.G., et al., *Synapsis of DNA ends by DNA-dependent protein kinase*. EMBO J, 2002. **21**(12): p. 3192-200.
85. Reddy, Y.V., et al., *Non-homologous end joining requires that the DNA-PK complex undergo an autophosphorylation-dependent rearrangement at DNA ends*. J Biol Chem, 2004. **279**(38): p. 39408-13.
86. Jette, N. and S.P. Lees-Miller, *The DNA-dependent protein kinase: A multifunctional protein kinase with roles in DNA double strand break repair and mitosis*. Prog Biophys Mol Biol, 2015. **117**(2-3): p. 194-205.

87. Weterings, E. and D.J. Chen, *DNA-dependent protein kinase in nonhomologous end joining: a lock with multiple keys?* J Cell Biol, 2007. **179**(2): p. 183-6.
88. Neal, J.A. and K. Meek, *Choosing the right path: does DNA-PK help make the decision?* Mutat Res, 2011. **711**(1-2): p. 73-86.
89. Chan, D.W., et al., *DNA-dependent protein kinase phosphorylation sites in Ku 70/80 heterodimer.* Biochemistry, 1999. **38**(6): p. 1819-28.
90. Douglas, P., et al., *DNA-PK-dependent phosphorylation of Ku70/80 is not required for non-homologous end joining.* DNA Repair (Amst), 2005. **4**(9): p. 1006-18.
91. Yu, Y., et al., *DNA-PK and ATM phosphorylation sites in XLF/Cernunnos are not required for repair of DNA double strand breaks.* DNA Repair (Amst), 2008. **7**(10): p. 1680-92.
92. Yu, Y., et al., *DNA-PK phosphorylation sites in XRCC4 are not required for survival after radiation or for V(D)J recombination.* DNA Repair (Amst), 2003. **2**(11): p. 1239-52.
93. Dobbs, T.A., J.A. Tainer, and S.P. Lees-Miller, *A structural model for regulation of NHEJ by DNA-PKcs autophosphorylation.* DNA Repair (Amst), 2010. **9**(12): p. 1307-14.
94. Douglas, P., et al., *Identification of in vitro and in vivo phosphorylation sites in the catalytic subunit of the DNA-dependent protein kinase.* Biochem J, 2002. **368**(Pt 1): p. 243-51.
95. Merkle, D., et al., *The DNA-dependent protein kinase interacts with DNA to form a protein-DNA complex that is disrupted by phosphorylation.* Biochemistry, 2002. **41**(42): p. 12706-14.
96. Meek, K., et al., *trans Autophosphorylation at DNA-dependent protein kinase's two major autophosphorylation site clusters facilitates end processing but not end joining.* Mol Cell Biol, 2007. **27**(10): p. 3881-90.

97. Lees-Miller, S.P., et al., *Absence of p350 subunit of DNA-activated protein kinase from a radiosensitive human cell line*. Science, 1995. **267**(5201): p. 1183-5.
98. Jeggo, P.A., S.P. Jackson, and G.E. Taccioli, *Identification of the catalytic subunit of DNA dependent protein kinase as the product of the mouse scid gene*. Curr Top Microbiol Immunol, 1996. **217**: p. 79-89.
99. Kienker, L.J., E.K. Shin, and K. Meek, *Both V(D)J recombination and radioresistance require DNA-PK kinase activity, though minimal levels suffice for V(D)J recombination*. Nucleic Acids Res, 2000. **28**(14): p. 2752-61.
100. Sibanda, B.L., D.Y. Chirgadze, and T.L. Blundell, *Crystal structure of DNA-PKcs reveals a large open-ring cradle comprised of HEAT repeats*. Nature, 2010. **463**(7277): p. 118-21.
101. Williams, D.R., et al., *Cryo-EM structure of the DNA-dependent protein kinase catalytic subunit at subnanometer resolution reveals alpha helices and insight into DNA binding*. Structure, 2008. **16**(3): p. 468-77.
102. Spagnolo, L., et al., *Three-dimensional structure of the human DNA-PKcs/Ku70/Ku80 complex assembled on DNA and its implications for DNA DSB repair*. Mol Cell, 2006. **22**(4): p. 511-9.
103. Weterings, E. and D.C. van Gent, *The mechanism of non-homologous end-joining: a synopsis of synopsis*. DNA Repair (Amst), 2004. **3**(11): p. 1425-35.
104. Grawunder, U., et al., *Activity of DNA ligase IV stimulated by complex formation with XRCC4 protein in mammalian cells*. Nature, 1997. **388**(6641): p. 492-5.
105. Chen, L., et al., *Interactions of the DNA ligase IV-XRCC4 complex with DNA ends and the DNA-dependent protein kinase*. J Biol Chem, 2000. **275**(34): p. 26196-205.
106. Nick McElhinny, S.A., et al., *Ku recruits the XRCC4-ligase IV complex to DNA ends*. Mol Cell Biol, 2000. **20**(9): p. 2996-3003.

107. Calsou, P., et al., *Coordinated assembly of Ku and p460 subunits of the DNA-dependent protein kinase on DNA ends is necessary for XRCC4-ligase IV recruitment*. J Mol Biol, 2003. **326**(1): p. 93-103.
108. Ellenberger, T. and A.E. Tomkinson, *Eukaryotic DNA ligases: structural and functional insights*. Annu Rev Biochem, 2008. **77**: p. 313-38.
109. Sibanda, B.L., et al., *Crystal structure of an Xrcc4-DNA ligase IV complex*. Nat Struct Biol, 2001. **8**(12): p. 1015-9.
110. Wu, P.Y., et al., *Structural and functional interaction between the human DNA repair proteins DNA ligase IV and XRCC4*. Mol Cell Biol, 2009. **29**(11): p. 3163-72.
111. Frank, K.M., et al., *Late embryonic lethality and impaired V(D)J recombination in mice lacking DNA ligase IV*. Nature, 1998. **396**(6707): p. 173-7.
112. Barnes, D.E., et al., *Targeted disruption of the gene encoding DNA ligase IV leads to lethality in embryonic mice*. Curr Biol, 1998. **8**(25): p. 1395-8.
113. Gao, Y., et al., *A critical role for DNA end-joining proteins in both lymphogenesis and neurogenesis*. Cell, 1998. **95**(7): p. 891-902.
114. Frank, K.M., et al., *DNA ligase IV deficiency in mice leads to defective neurogenesis and embryonic lethality via the p53 pathway*. Mol Cell, 2000. **5**(6): p. 993-1002.
115. Sekiguchi, J., et al., *Genetic interactions between ATM and the nonhomologous end-joining factors in genomic stability and development*. Proc Natl Acad Sci U S A, 2001. **98**(6): p. 3243-8.
116. Ochi, T., X. Gu, and T.L. Blundell, *Structure of the catalytic region of DNA ligase IV in complex with an Artemis fragment sheds light on double-strand break repair*. Structure, 2013. **21**(4): p. 672-9.
117. Tomkinson, A.E. and A. Sallmyr, *Structure and function of the DNA ligases encoded by the mammalian LIG3 gene*. Gene, 2013. **531**(2): p. 150-7.

118. Tomkinson, A.E. and Z.B. Mackey, *Structure and function of mammalian DNA ligases*. Mutat Res, 1998. **407**(1): p. 1-9.
119. Grawunder, U., D. Zimmer, and M.R. Lieber, *DNA ligase IV binds to XRCC4 via a motif located between rather than within its BRCT domains*. Curr Biol, 1998. **8**(15): p. 873-6.
120. Modesti, M., et al., *Tetramerization and DNA ligase IV interaction of the DNA double-strand break repair protein XRCC4 are mutually exclusive*. J Mol Biol, 2003. **334**(2): p. 215-28.
121. Junop, M.S., et al., *Crystal structure of the Xrcc4 DNA repair protein and implications for end joining*. EMBO J, 2000. **19**(22): p. 5962-70.
122. Hammel, M., et al., *XLF regulates filament architecture of the XRCC4.ligase IV complex*. Structure, 2010. **18**(11): p. 1431-42.
123. Critchlow, S.E., R.P. Bowater, and S.P. Jackson, *Mammalian DNA double-strand break repair protein XRCC4 interacts with DNA ligase IV*. Curr Biol, 1997. **7**(8): p. 588-98.
124. Mani, R.S., et al., *Dual modes of interaction between XRCC4 and polynucleotide kinase/phosphatase: implications for nonhomologous end joining*. J Biol Chem, 2010. **285**(48): p. 37619-29.
125. Modesti, M., J.E. Hesse, and M. Gellert, *DNA binding of Xrcc4 protein is associated with V(D)J recombination but not with stimulation of DNA ligase IV activity*. EMBO J, 1999. **18**(7): p. 2008-18.
126. Buck, D., et al., *Cernunnos, a novel nonhomologous end-joining factor, is mutated in human immunodeficiency with microcephaly*. Cell, 2006. **124**(2): p. 287-99.
127. Ahnesorg, P., P. Smith, and S.P. Jackson, *XLF interacts with the XRCC4-DNA ligase IV complex to promote DNA nonhomologous end-joining*. Cell, 2006. **124**(2): p. 301-13.

128. Andres, S.N., et al., *Crystal structure of human XLF: a twist in nonhomologous DNA end-joining*. Mol Cell, 2007. **28**(6): p. 1093-101.
129. Li, G., et al., *Lymphocyte-specific compensation for XLF/cernunnos end-joining functions in V(D)J recombination*. Mol Cell, 2008. **31**(5): p. 631-40.
130. Gu, J., et al., *Single-stranded DNA ligation and XLF-stimulated incompatible DNA end ligation by the XRCC4-DNA ligase IV complex: influence of terminal DNA sequence*. Nucleic Acids Res, 2007. **35**(17): p. 5755-62.
131. Yano, K., K. Morotomi-Yano, and H. Akiyama, *Cernunnos/XLF: a new player in DNA double-strand break repair*. Int J Biochem Cell Biol, 2009. **41**(6): p. 1237-40.
132. Hentges, P., et al., *Evolutionary and functional conservation of the DNA non-homologous end-joining protein, XLF/Cernunnos*. J Biol Chem, 2006. **281**(49): p. 37517-26.
133. Gu, J., et al., *XRCC4:DNA ligase IV can ligate incompatible DNA ends and can ligate across gaps*. EMBO J, 2007. **26**(4): p. 1010-23.
134. Lu, H., et al., *Length-dependent binding of human XLF to DNA and stimulation of XRCC4.DNA ligase IV activity*. J Biol Chem, 2007. **282**(15): p. 11155-62.
135. Hammel, M., et al., *XRCC4 protein interactions with XRCC4-like factor (XLF) create an extended grooved scaffold for DNA ligation and double strand break repair*. J Biol Chem, 2011. **286**(37): p. 32638-50.
136. Ropars, V., et al., *Structural characterization of filaments formed by human Xrcc4-Cernunnos/XLF complex involved in nonhomologous DNA end-joining*. Proc Natl Acad Sci U S A, 2011. **108**(31): p. 12663-8.
137. Wu, Q., et al., *Non-homologous end-joining partners in a helical dance: structural studies of XLF-XRCC4 interactions*. Biochem Soc Trans, 2011. **39**(5): p. 1387-92, suppl 2 p following 1392.



138. Andres, S.N., et al., *A human XRCC4-XLF complex bridges DNA*. Nucleic Acids Res, 2012. **40**(4): p. 1868-78.
139. Dai, Y., et al., *Nonhomologous end joining and V(D)J recombination require an additional factor*. Proc Natl Acad Sci U S A, 2003. **100**(5): p. 2462-7.
140. Ochi, T., et al., *DNA repair. PAXX, a paralog of XRCC4 and XLF, interacts with Ku to promote DNA double-strand break repair*. Science, 2015. **347**(6218): p. 185-8.
141. Xing, M., et al., *Interactome analysis identifies a new paralogue of XRCC4 in non-homologous end joining DNA repair pathway*. Nat Commun, 2015. **6**: p. 6233.
142. Balmus, G., et al., *Synthetic lethality between PAXX and XLF in mammalian development*. Genes Dev, 2016. **30**(19): p. 2152-2157.
143. Zha, S., et al., *ATM damage response and XLF repair factor are functionally redundant in joining DNA breaks*. Nature, 2011. **469**(7329): p. 250-4.
144. Waters, C.A., et al., *Nonhomologous end joining: a good solution for bad ends*. DNA Repair (Amst), 2014. **17**: p. 39-51.
145. Lohman, G.J., L. Chen, and T.C. Evans, Jr., *Kinetic characterization of single strand break ligation in duplex DNA by T4 DNA ligase*. J Biol Chem, 2011. **286**(51): p. 44187-96.
146. Downs, J.A. and S.P. Jackson, *A means to a DNA end: the many roles of Ku*. Nat Rev Mol Cell Biol, 2004. **5**(5): p. 367-78.
147. Uematsu, N., et al., *Autophosphorylation of DNA-PKCS regulates its dynamics at DNA double-strand breaks*. J Cell Biol, 2007. **177**(2): p. 219-29.
148. Reynolds, P., et al., *The dynamics of Ku70/80 and DNA-PKcs at DSBs induced by ionizing radiation is dependent on the complexity of damage*. Nucleic Acids Res, 2012. **40**(21): p. 10821-31.

149. Menon, V. and L.F. Povirk, *End-processing nucleases and phosphodiesterases: An elite supporting cast for the non-homologous end joining pathway of DNA double-strand break repair*. DNA Repair (Amst), 2016. **43**: p. 57-68.
150. Bahmed, K., et al., *End-processing during non-homologous end-joining: a role for exonuclease 1*. Nucleic Acids Res, 2011. **39**(3): p. 970-8.
151. Xie, A., A. Kwok, and R. Scully, *Role of mammalian Mre11 in classical and alternative nonhomologous end joining*. Nat Struct Mol Biol, 2009. **16**(8): p. 814-8.
152. Weterings, E., et al., *The Ku80 carboxy terminus stimulates joining and artemis-mediated processing of DNA ends*. Mol Cell Biol, 2009. **29**(5): p. 1134-42.
153. Rass, U., I. Ahel, and S.C. West, *Molecular mechanism of DNA deadenylation by the neurological disease protein aprataxin*. J Biol Chem, 2008. **283**(49): p. 33994-4001.
154. Kusumoto, R., et al., *Werner protein cooperates with the XRCC4-DNA ligase IV complex in end-processing*. Biochemistry, 2008. **47**(28): p. 7548-56.
155. Nick McElhinny, S.A., et al., *A gradient of template dependence defines distinct biological roles for family X polymerases in nonhomologous end joining*. Mol Cell, 2005. **19**(3): p. 357-66.
156. Lee, J.W., et al., *Implication of DNA polymerase lambda in alignment-based gap filling for nonhomologous DNA end joining in human nuclear extracts*. J Biol Chem, 2004. **279**(1): p. 805-11.
157. Ma, Y., et al., *A biochemically defined system for mammalian nonhomologous DNA end joining*. Mol Cell, 2004. **16**(5): p. 701-13.
158. Mahajan, K.N., et al., *Association of DNA polymerase mu (pol mu) with Ku and ligase IV: role for pol mu in end-joining double-strand break repair*. Mol Cell Biol, 2002. **22**(14): p. 5194-202.

159. Boulton, S.J. and S.P. Jackson, *Saccharomyces cerevisiae Ku70 potentiates illegitimate DNA double-strand break repair and serves as a barrier to error-prone DNA repair pathways*. EMBO J, 1996. **15**(18): p. 5093-103.
160. Liang, F. and M. Jasin, *Ku80-deficient cells exhibit excess degradation of extrachromosomal DNA*. J Biol Chem, 1996. **271**(24): p. 14405-11.
161. Bennardo, N., et al., *Alternative-NHEJ is a mechanistically distinct pathway of mammalian chromosome break repair*. PLoS Genet, 2008. **4**(6): p. e1000110.
162. Zhu, C., et al., *Unrepaired DNA breaks in p53-deficient cells lead to oncogenic gene amplification subsequent to translocations*. Cell, 2002. **109**(7): p. 811-21.
163. Guirouilh-Barbat, J., et al., *Defects in XRCC4 and KU80 differentially affect the joining of distal nonhomologous ends*. Proc Natl Acad Sci U S A, 2007. **104**(52): p. 20902-7.
164. Simsek, D. and M. Jasin, *Alternative end-joining is suppressed by the canonical NHEJ component Xrcc4-ligase IV during chromosomal translocation formation*. Nat Struct Mol Biol, 2010. **17**(4): p. 410-6.
165. Decottignies, A., *Microhomology-mediated end joining in fission yeast is repressed by pku70 and relies on genes involved in homologous recombination*. Genetics, 2007. **176**(3): p. 1403-15.
166. Wang, H. and X. Xu, *Microhomology-mediated end joining: new players join the team*. Cell Biosci, 2017. **7**: p. 6.
167. Pommier, Y., et al., *Roles of eukaryotic topoisomerases in transcription, replication and genomic stability*. Nat Rev Mol Cell Biol, 2016. **17**(11): p. 703-721.
168. Watson, J.D. and F.H. Crick, *Genetical implications of the structure of deoxyribonucleic acid*. Nature, 1953. **171**(4361): p. 964-7.
169. Wang, J.C., *Cellular roles of DNA topoisomerases: a molecular perspective*. Nat Rev Mol Cell Biol, 2002. **3**(6): p. 430-40.

170. Lanza, A., et al., *Human DNA topoisomerase I-mediated cleavages stimulated by ultraviolet light-induced DNA damage*. J Biol Chem, 1996. **271**(12): p. 6978-86.
171. Pourquier, P., et al., *Effects of uracil incorporation, DNA mismatches, and abasic sites on cleavage and religation activities of mammalian topoisomerase I*. J Biol Chem, 1997. **272**(12): p. 7792-6.
172. Subramanian, D., B.S. Rosenstein, and M.T. Muller, *Ultraviolet-induced DNA damage stimulates topoisomerase I-DNA complex formation in vivo: possible relationship with DNA repair*. Cancer Res, 1998. **58**(5): p. 976-84.
173. Pourquier, P. and Y. Pommier, *Topoisomerase I-mediated DNA damage*. Adv Cancer Res, 2001. **80**: p. 189-216.
174. Leshar, D.T., et al., *8-Oxoguanine rearranges the active site of human topoisomerase I*. Proc Natl Acad Sci U S A, 2002. **99**(19): p. 12102-7.
175. Nitiss, J. and J.C. Wang, *DNA topoisomerase-targeting antitumor drugs can be studied in yeast*. Proc Natl Acad Sci U S A, 1988. **85**(20): p. 7501-5.
176. Bjornsti, M.A., et al., *Expression of human DNA topoisomerase I in yeast cells lacking yeast DNA topoisomerase I: restoration of sensitivity of the cells to the antitumor drug camptothecin*. Cancer Res, 1989. **49**(22): p. 6318-23.
177. Pommier, Y., *Topoisomerase I inhibitors: camptothecins and beyond*. Nat Rev Cancer, 2006. **6**(10): p. 789-802.
178. Yang, S.W., et al., *A eukaryotic enzyme that can disjoin dead-end covalent complexes between DNA and type I topoisomerases*. Proc Natl Acad Sci U S A, 1996. **93**(21): p. 11534-9.
179. Pouliot, J.J., et al., *Yeast gene for a Tyr-DNA phosphodiesterase that repairs topoisomerase I complexes*. Science, 1999. **286**(5439): p. 552-5.

180. Pouliot, J.J., C.A. Robertson, and H.A. Nash, *Pathways for repair of topoisomerase I covalent complexes in Saccharomyces cerevisiae*. Genes Cells, 2001. **6**(8): p. 677-87.
181. Debethune, L., et al., *Processing of nucleopeptides mimicking the topoisomerase I-DNA covalent complex by tyrosyl-DNA phosphodiesterase*. Nucleic Acids Res, 2002. **30**(5): p. 1198-204.
182. Interthal, H., H.J. Chen, and J.J. Champoux, *Human Tdp1 cleaves a broad spectrum of substrates, including phosphoamide linkages*. J Biol Chem, 2005. **280**(43): p. 36518-28.
183. Interthal, H., J.J. Pouliot, and J.J. Champoux, *The tyrosyl-DNA phosphodiesterase Tdp1 is a member of the phospholipase D superfamily*. Proc Natl Acad Sci U S A, 2001. **98**(21): p. 12009-14.
184. Davies, D.R., et al., *The crystal structure of human tyrosyl-DNA phosphodiesterase, Tdp1*. Structure, 2002. **10**(2): p. 237-48.
185. Plo, I., et al., *Association of XRCC1 and tyrosyl DNA phosphodiesterase (Tdp1) for the repair of topoisomerase I-mediated DNA lesions*. DNA Repair (Amst), 2003. **2**(10): p. 1087-100.
186. Davies, D.R., et al., *Crystal structure of a transition state mimic for Tdp1 assembled from vanadate, DNA, and a topoisomerase I-derived peptide*. Chem Biol, 2003. **10**(2): p. 139-47.
187. Porter, S.E. and J.J. Champoux, *Mapping in vivo topoisomerase I sites on simian virus 40 DNA: asymmetric distribution of sites on replicating molecules*. Mol Cell Biol, 1989. **9**(2): p. 541-50.
188. Jaxel, C., et al., *Effect of local DNA sequence on topoisomerase I cleavage in the presence or absence of camptothecin*. J Biol Chem, 1991. **266**(30): p. 20418-23.

189. Inamdar, K.V., et al., *Conversion of phosphoglycolate to phosphate termini on 3' overhangs of DNA double strand breaks by the human tyrosyl-DNA phosphodiesterase hTdp1*. J Biol Chem, 2002. **277**(30): p. 27162-8.
190. Zhou, T., et al., *Deficiency in 3'-phosphoglycolate processing in human cells with a hereditary mutation in tyrosyl-DNA phosphodiesterase (TDP1)*. Nucleic Acids Res, 2005. **33**(1): p. 289-97.
191. Nitiss, K.C., et al., *Tyrosyl-DNA phosphodiesterase (Tdp1) participates in the repair of Top2-mediated DNA damage*. Proc Natl Acad Sci U S A, 2006. **103**(24): p. 8953-8.
192. Murai, J., et al., *Tyrosyl-DNA phosphodiesterase 1 (TDP1) repairs DNA damage induced by topoisomerases I and II and base alkylation in vertebrate cells*. J Biol Chem, 2012. **287**(16): p. 12848-57.
193. Huang, S.Y., et al., *TDP1 repairs nuclear and mitochondrial DNA damage induced by chain-terminating anticancer and antiviral nucleoside analogs*. Nucleic Acids Res, 2013. **41**(16): p. 7793-803.
194. Alagoz, M., O.S. Wells, and S.F. El-Khamisy, *TDP1 deficiency sensitizes human cells to base damage via distinct topoisomerase I and PARP mechanisms with potential applications for cancer therapy*. Nucleic Acids Res, 2014. **42**(5): p. 3089-103.
195. Lebedeva, N.A., et al., *Tyrosyl-DNA phosphodiesterase 1 initiates repair of apurinic/apyrimidinic sites*. Biochimie, 2012. **94**(8): p. 1749-53.
196. Thomson, G.J., et al., *A fluorescence-based assay for the apurinic/apyrimidinic-site cleavage activity of human tyrosyl-DNA phosphodiesterase 1*. Anal Biochem, 2013. **440**(1): p. 1-5.
197. Lebedeva, N.A., et al., *The mechanism of human tyrosyl-DNA phosphodiesterase 1 in the cleavage of AP site and its synthetic analogs*. DNA Repair (Amst), 2013. **12**(12): p. 1037-42.

198. Prasad, R., et al., *Mammalian Base Excision Repair: Functional Partnership between PARP-1 and APE1 in AP-Site Repair*. PLoS One, 2015. **10**(5): p. e0124269.
199. Lebedeva, N.A., et al., *Poly(ADP-ribose)polymerase 1 stimulates the AP-site cleavage activity of tyrosyl-DNA phosphodiesterase 1*. Biosci Rep, 2015. **35**(4).
200. Rechkunova, N.I., N.A. Lebedeva, and O.I. Lavrik, *[Tyrosyl-DNA Phosphodiesterase 1 Is a New Player in Repair of Apurinic/Apyrimidinic Sites]*. Bioorg Khim, 2015. **41**(5): p. 531-8.
201. Kuznetsov, N.A., et al., *Pre-steady state kinetics of DNA binding and abasic site hydrolysis by tyrosyl-DNA phosphodiesterase 1*. J Biomol Struct Dyn, 2016: p. 1-14.
202. Das, B.B., et al., *Role of tyrosyl-DNA phosphodiesterase (TDP1) in mitochondria*. Proc Natl Acad Sci U S A, 2010. **107**(46): p. 19790-5.
203. El-Khamisy, S.F., *To live or to die: a matter of processing damaged DNA termini in neurons*. EMBO Mol Med, 2011. **3**(2): p. 78-88.
204. Chen, S., et al., *Accurate in vitro end joining of a DNA double strand break with partially cohesive 3'-overhangs and 3'-phosphoglycolate termini: effect of Ku on repair fidelity*. J Biol Chem, 2001. **276**(26): p. 24323-30.
205. Zhou, T., et al., *Tyrosyl-DNA phosphodiesterase and the repair of 3'-phosphoglycolate-terminated DNA double-strand breaks*. DNA Repair (Amst), 2009. **8**(8): p. 901-11.
206. Dedon, P.C. and I.H. Goldberg, *Free-radical mechanisms involved in the formation of sequence-dependent bistranded DNA lesions by the antitumor antibiotics bleomycin, neocarzinostatin, and calicheamicin*. Chem Res Toxicol, 1992. **5**(3): p. 311-32.

207. El-Khamisy, S.F., et al., *Synergistic decrease of DNA single-strand break repair rates in mouse neural cells lacking both Tdp1 and aprataxin*. DNA Repair (Amst), 2009. **8**(6): p. 760-6.
208. Chiang, S.C., J. Carroll, and S.F. El-Khamisy, *TDP1 serine 81 promotes interaction with DNA ligase IIIalpha and facilitates cell survival following DNA damage*. Cell Cycle, 2010. **9**(3): p. 588-595.
209. Takashima, H., et al., *Mutation of TDP1, encoding a topoisomerase I-dependent DNA damage repair enzyme, in spinocerebellar ataxia with axonal neuropathy*. Nat Genet, 2002. **32**(2): p. 267-72.
210. Fam, H.K., et al., *Spinocerebellar Ataxia with Axonal Neuropathy, Autosomal Recessive*, in *GeneReviews(R)*, R.A. Pagon, et al., Editors. 1993: Seattle (WA).
211. He, X., et al., *Mutation of a conserved active site residue converts tyrosyl-DNA phosphodiesterase I into a DNA topoisomerase I-dependent poison*. J Mol Biol, 2007. **372**(4): p. 1070-81.
212. El-Khamisy, S.F., et al., *Defective DNA single-strand break repair in spinocerebellar ataxia with axonal neuropathy-1*. Nature, 2005. **434**(7029): p. 108-13.
213. Gajewski, S., et al., *Analysis of the active-site mechanism of tyrosyl-DNA phosphodiesterase I: a member of the phospholipase D superfamily*. J Mol Biol, 2012. **415**(4): p. 741-58.
214. Interthal, H., et al., *SCAN1 mutant Tdp1 accumulates the enzyme--DNA intermediate and causes camptothecin hypersensitivity*. EMBO J, 2005. **24**(12): p. 2224-33.
215. Comeaux, E.Q., et al., *Tyrosyl-DNA phosphodiesterase I catalytic mutants reveal an alternative nucleophile that can catalyze substrate cleavage*. J Biol Chem, 2015. **290**(10): p. 6203-14.



216. Fam, H.K., et al., *TDP1 and PARP1 deficiency are cytotoxic to rhabdomyosarcoma cells*. Mol Cancer Res, 2013. **11**(10): p. 1179-92.
217. McKinnon, P.J., *Maintaining genome stability in the nervous system*. Nat Neurosci, 2013. **16**(11): p. 1523-9.
218. Katyal, S., et al., *Aberrant topoisomerase-1 DNA lesions are pathogenic in neurodegenerative genome instability syndromes*. Nat Neurosci, 2014. **17**(6): p. 813-21.
219. el-Khamisy, S.F. and K.W. Caldecott, *DNA single-strand break repair and spinocerebellar ataxia with axonal neuropathy-1*. Neuroscience, 2007. **145**(4): p. 1260-6.
220. Caldecott, K.W., *DNA single-strand break repair and spinocerebellar ataxia*. Cell, 2003. **112**(1): p. 7-10.
221. El-Khamisy, S.F. and K.W. Caldecott, *TDP1-dependent DNA single-strand break repair and neurodegeneration*. Mutagenesis, 2006. **21**(4): p. 219-24.
222. Pommier, Y., et al., *Tyrosyl-DNA-phosphodiesterases (TDP1 and TDP2)*. DNA Repair (Amst), 2014. **19**: p. 114-29.
223. Das, B.B., et al., *Optimal function of the DNA repair enzyme TDP1 requires its phosphorylation by ATM and/or DNA-PK*. EMBO J, 2009. **28**(23): p. 3667-80.
224. Das, B.B., et al., *PARP1-TDP1 coupling for the repair of topoisomerase I-induced DNA damage*. Nucleic Acids Res, 2014. **42**(7): p. 4435-49.
225. Caldecott, K.W., *Single-strand break repair and genetic disease*. Nat Rev Genet, 2008. **9**(8): p. 619-31.
226. Hawkins, A.J., et al., *In vitro complementation of Tdp1 deficiency indicates a stabilized enzyme-DNA adduct from tyrosyl but not glycolate lesions as a consequence of the SCAN1 mutation*. DNA Repair (Amst), 2009. **8**(5): p. 654-63.

227. Katyal, S., et al., *TDP1 facilitates chromosomal single-strand break repair in neurons and is neuroprotective in vivo*. EMBO J, 2007. **26**(22): p. 4720-31.
228. Guo, D., et al., *Neuroprotection and repair of 3'-blocking DNA ends by glaikit (gkt) encoding Drosophila tyrosyl-DNA phosphodiesterase 1 (TDP1)*. Proc Natl Acad Sci U S A, 2014. **111**(44): p. 15816-20.
229. Akopiants, K., et al., *Tracking the processing of damaged DNA double-strand break ends by ligation-mediated PCR: increased persistence of 3'-phosphoglycolate termini in SCAN1 cells*. Nucleic Acids Res, 2014. **42**(5): p. 3125-37.
230. Hanakahi, L.A., *2-Step purification of the Ku DNA repair protein expressed in Escherichia coli*. Protein Expr Purif, 2007. **52**(1): p. 139-45.
231. Hanakahi, L., *Effect of the inositol polyphosphate InsP(6) on DNA-PK-dependent phosphorylation*. Mol Cancer Res, 2011. **9**(10): p. 1366-76.
232. Zhang, J., et al., *PEAR: a fast and accurate Illumina Paired-End reAd mergeR*. Bioinformatics, 2014. **30**(5): p. 614-20.
233. Akopiants, K., et al., *Requirement for XLF/Cernunnos in alignment-based gap filling by DNA polymerases lambda and mu for nonhomologous end joining in human whole-cell extracts*. Nucleic Acids Res, 2009. **37**(12): p. 4055-62.
234. Lai, J.S. and W. Herr, *Ethidium bromide provides a simple tool for identifying genuine DNA-independent protein associations*. Proc Natl Acad Sci U S A, 1992. **89**(15): p. 6958-62.
235. Nguyen, T.N. and J.A. Goodrich, *Protein-protein interaction assays: eliminating false positive interactions*. Nat Methods, 2006. **3**(2): p. 135-9.
236. Heo, J., et al., *TDP1 promotes assembly of non-homologous end joining protein complexes on DNA*. DNA Repair (Amst), 2015. **30**: p. 28-37.

237. Hudson, J.J., et al., *SUMO modification of the neuroprotective protein TDP1 facilitates chromosomal single-strand break repair*. Nat Commun, 2012. **3**: p. 733.
238. Malivert, L., et al., *Delineation of the Xrcc4-interacting region in the globular head domain of cernunnos/XLF*. J Biol Chem, 2010. **285**(34): p. 26475-83.
239. Roy, S., et al., *XRCC4's interaction with XLF is required for coding (but not signal) end joining*. Nucleic Acids Res, 2012. **40**(4): p. 1684-94.
240. Dexheimer, T.S., et al., *The DNA binding and 3'-end preferential activity of human tyrosyl-DNA phosphodiesterase*. Nucleic Acids Res, 2010. **38**(7): p. 2444-52.
241. Interthal, H. and J.J. Champoux, *Effects of DNA and protein size on substrate cleavage by human tyrosyl-DNA phosphodiesterase 1*. Biochem J, 2011. **436**(3): p. 559-66.
242. Brouwer, I., et al., *Sliding sleeves of XRCC4-XLF bridge DNA and connect fragments of broken DNA*. Nature, 2016. **535**(7613): p. 566-9.
243. Raymond, A.C., B.L. Staker, and A.B. Burgin, Jr., *Substrate specificity of tyrosyl-DNA phosphodiesterase I (Tdp1)*. J Biol Chem, 2005. **280**(23): p. 22029-35.
244. Deriano, L. and D.B. Roth, *Modernizing the nonhomologous end-joining repertoire: alternative and classical NHEJ share the stage*. Annu Rev Genet, 2013. **47**: p. 433-55.
245. Betermier, M., P. Bertrand, and B.S. Lopez, *Is non-homologous end-joining really an inherently error-prone process?* PLoS Genet, 2014. **10**(1): p. e1004086.
246. Barthelmes, H.U., et al., *TDP1 overexpression in human cells counteracts DNA damage mediated by topoisomerases I and II*. J Biol Chem, 2004. **279**(53): p. 55618-25.
247. Critchlow, S.E. and S.P. Jackson, *DNA end-joining: from yeast to man*. Trends Biochem Sci, 1998. **23**(10): p. 394-8.

- 248. Featherstone, C. and S.P. Jackson, *DNA double-strand break repair*. Curr Biol, 1999. **9**(20): p. R759-61.
  
- 249. Li, Y., et al., *Crystal structure of human XLF/Cernunnos reveals unexpected differences from XRCC4 with implications for NHEJ*. EMBO J, 2008. **27**(1): p. 290-300.

**VITA**

**NAME:** Jing Li

**EDUCATION:** B.A., Pharmacology, China Pharmaceutical University, Nanjing, Jiangsu, China, 2010  
PhD., Medicinal Chemistry and Pharmacognosy, University of Illinois at Chicago, Rockford, Illinois, United States, 2017 (expected)

**HONORS:** Second Place of Poster Award. 19th Annual Midwest DNA Repair Symposium. 2017

Student Travel Award. Environmental Mutagenesis and Genomic Society 47<sup>th</sup> Annual Meeting. 2016

Honorable Poster Award in Biology: Molecular and Cell Biology; Mechanisms of Action category. UIC College of Pharmacy Research Day. 2016

Outstanding Poster Award of UIC Cancer Center Forum UIC. Cancer Center Research Forum. 2015

Second Place of Poster Award. 17th Annual Midwest DNA Repair Symposium. 2015

Outstanding Poster Award. UIC College of Pharmacy Research Day. 2013

**PROFESSIONAL MEMBERSHIP:** Environmental Mutagenesis and Genomic Society

**PUBLICATIONS:** Heo, J., et al., TDP1 promotes assembly of non-homologous end joining protein complexes on DNA. DNA Repair (Amst), 2015. 30: p. 28-37. (Co-first author)

Li, J., et al., TDP1 is required for efficient non-homologous end joining in human cells. DNA Repair (Amst), 2017 (submitted)